conceptual error often made is to assume that elastic behavior is *always* linear; the rubber example shows very clearly that there are notable exceptions. However, for metals, the stress and strain can be assumed to be proportional in the elastic regimen; these materials are known as Hookean solids. For polymers, viscoelastic effects are very important. Viscoelasticity results in different trajectories for loading and unloading, with the formation of a hysteresis loop. The area of the hysteresis loop is the energy lost per unit volume in the entire deformation cycle. Metals also exhibit some viscoelasticity, but it is most often neglected. Viscoelasticity is attributed to time-dependent microscopic processes accompanying deformation. An analogy that applies well is the attachment of a spring and dashpot. The spring represents the elastic portion of the material, the dashpot the viscoelastic portion.

In 1678, Robert Hooke performed experiments that demonstrated the proportionality between stress and strain. He proposed his law as an anagram – "ceiiinosssttuv," which rearranged, forms the Latin *Ut tensio sic vis*. The meaning is "As the tension goes, so does the stretch." In its most simplified form, we express this law as

$$E = \frac{\sigma}{\varepsilon}, \tag{2.3}$$

where E is Young's modulus. For metals and ceramics, E has a very high value – for example, 210 GPa for iron. Chapter 4 devotes some effort to the derivation of E for materials from first principles. E depends mainly on the composition, crystallographic structure, and nature of the bonding of elements. Heat and mechanical treatments have little effect on E, as long as they do not affect the former parameters. Hence, annealed and cold-rolled steel should have the same Young's modulus; there are, of course, small differences due to the formation of the cold-rolling texture. E decreases slightly with increases in temperature.

In monocrystals, E shows different values for different crystallographic orientations. In polycrystalline aggregates that do not exhibit any texture, E is isotropic: It has the same value in all directions. The values of E given in tables (e.g., Tables 2.3–2.5 later in this chapter) are usually obtained by dynamic methods involving the propagation of elastic waves, not from conventional stress–strain tests. An elastic wave is passed through a sample; the velocities of the longitudinal and shear waves, V_ℓ and V_s, respectively, are related to the elastic constants by means of the following mathematical expressions (ρ is the density, E is Young's modulus, and G is the shear modulus):[1]

$$\boxed{V_\ell = \sqrt{\frac{E}{\rho}} \qquad V_s = \sqrt{\frac{G}{\rho}}.}$$

[1] For more details, see M. A. Meyers, *Dynamic Behavior of Materials* (New York: Wiley, 1994).

Example 2.1

Calculate the material properties E, G, and ν of SiC, given the graphs of the longitudinal and shear sound velocities obtained using ultrasonic equipment. (See Figure E2.1). Here, $\rho = 3.18 \times 10^3$ kg/m^3 and the length of specimen is $L = 4$ mm.

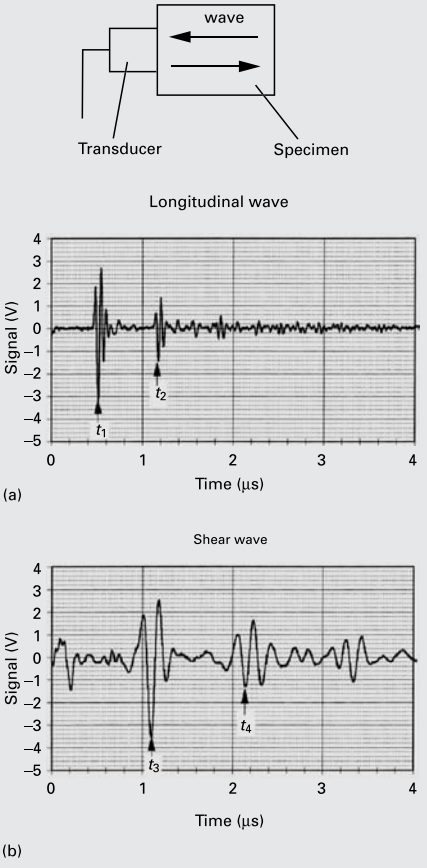

Fig. E2.1

Solution: We take equivalent peaks, marked by arrows, in sequential signal packets. We must remember that the pulse reflects at the free surface, and therefore, we have to take twice the length of the pulse. We have

$$V_\ell = \frac{2L}{t_2 - t_1} = \frac{2 \times 4 \times 10^{-3}}{(1.16 - 0.52) \times 10^{-6}} = 12.5 \times 10^3 \text{ m/s},$$

$$V_\ell = \sqrt{\frac{E}{\rho}},$$

$$E = \rho V_\ell^2 = 3.18 \times 10^3 \times (12.5 \times 10^3)^2 = 496.9 \times 10^9 \text{ Pa} = 496.9 \text{ GPa},$$

$$V_s = \frac{2L}{t_4 - t_3} = \frac{2 \times 4 \times 10^{-3}}{(2.15 - 1.10) \times 10^{-6}} = 7.62 \times 10^3 \text{ m/s}$$

$$V_s = \sqrt{\frac{G}{\rho}},$$

$$G = \rho V_s^2 = 3.18 \times 10^3 \times (7.62 \times 10^3)^2 = 184.6 \times 10^9 \text{ Pa} = 184.6 \text{ GPa}.$$

Since, according to Table 2.2,

$$G = \frac{E}{2(1+\nu)},$$

where ν is Poisson's ratio, as explained in Section 2.4, it follows that

$$\nu = \frac{E}{2G} - 1 = \frac{496.9}{2 \times 184.6} - 1 = 0.346.$$

(*Note:* The preceding calculations were conducted assuming uniaxial stress and without the dispersion correction; hence, the results are only approximate.)

A correct equation for the elastic modulus would be

$$V_\ell = \sqrt{\frac{\bar{E}}{\rho}}, \quad \bar{E} = \frac{(1-\nu)}{(1+\nu)(1-2\nu)} E\,.$$

This is because the length of the pulse is much shorter than the lateral dimension of the specimen, and therefore, the specimen is stressed in uniaxial strain.[2]

2.3 Strain Energy (or Deformation Energy) Density

When work is done on a body, its dimensions change. The work done (W) is converted into heat (Q) and an increase in internal energy (U) of the body. We can write as per the first law of thermodynamics

$$\mathrm{d}U = \mathrm{d}Q - \mathrm{d}W.$$

For most solids, the elastic work produces an insignificant amount of heat. Hence, the work done on a body during deformation is converted into internal energy, which is stored in the deformed material and we call it strain energy or strain energy density when referring to the stored strain energy per unit volume. In elastic springs the energy is stored, while in a damping element the energy is dissipated as heat. Quite frequently, in mechanics, we use the principle of minimization of energy to arrive at useful expression.

Consider an elemental cube under uniaxial tension, σ_{11}, as shown in Fig. 2.3(a). The work done is given by product of force and change in length. Figure 2.3(b) shows the plot of tensile force vs. displacement, where we have converted the stress into force and strain into

[2] The interested student can obtain more information in M. A. Meyers, *Dynamic Behavior of Materials* (New York: Wiley, 1994).

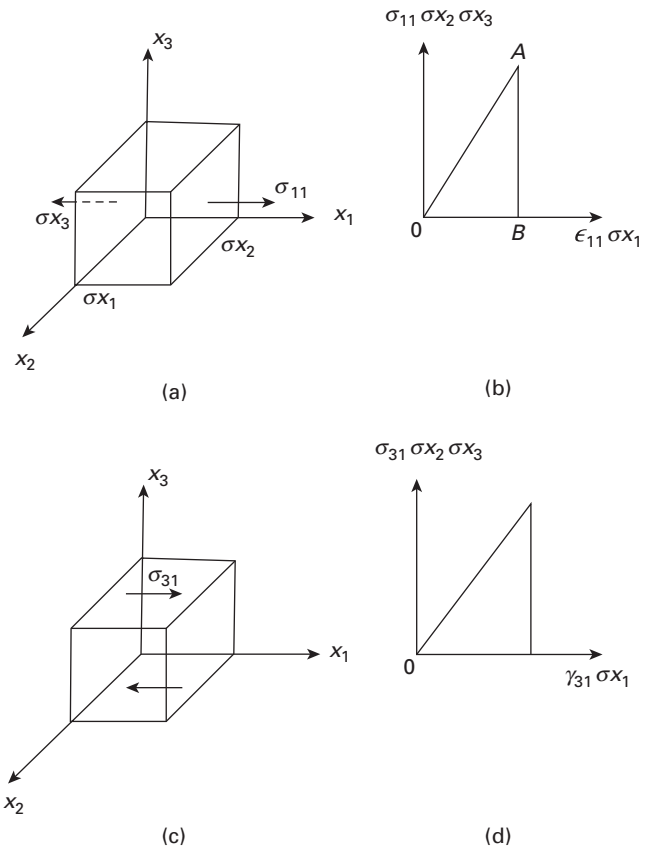

Fig. 2.3 (a) Cube under a tensile stress, σ_{11}. (b) Tensile force vs. displacement. (c) Cube under a shear stress, σ_{31}. (d) Shear force vs. displacement.

displacement. The work done is the area under the force vs. displacement curve:

$$\text{Total work done} = \frac{1}{2}[\sigma_{11}(\sigma x_2 \sigma x_3)\varepsilon_{11}\sigma x_1] = \frac{1}{2}[\sigma_{11}\varepsilon_{11}(\sigma x_1 \sigma x_2 \sigma x_3)],$$

where σ_{11} is the tensile stress component in direction 1, ε_{11} is the corresponding tensile strain, σx_1, σx_2 and σx_3 are the lengths of side of the cube.

The work done per unit volume is

$$W_{11} = \frac{1}{2}\sigma_{11}\varepsilon_{11}.$$

We can obtain similar expressions for the work done by other stress components. The reader can show that for the shear stress, σ_{31}, the work done per unit volume (see Figure 2.3(c) and (d)) is given by

$$W_{31} = \frac{1}{2}\sigma_{31}\gamma_{31},$$

where σ_{31} and γ_{31} are the shear stress and shear strain components, respectively, acting in direction 3.

Using the principle of superposition, i.e., combining the results for two or more stresses (or strains), we can write for the total work done per unit volume or the strain energy density as

$$W = \frac{1}{2}(\sigma_{11}\varepsilon_{11} + \sigma_{22}\varepsilon_{22} + \sigma_{33}\varepsilon_{33} + 2\sigma_{12}\gamma_{12} + 2\sigma_{23}\gamma_{23} + 2\sigma_{31}\gamma_{31}).$$

In more compact indicial notation, we can write

$$U = W = \frac{1}{2}\sigma_{ij}\varepsilon_{ij},$$

where the subscripts i and j represent the plane normal on which the stress is acting and the direction in which the stress is acting, respectively. This notation is explained in Section 2.9. The units of strain energy density are J/m^3 or N $\cdot$ m/m^3, or N/m^2. The last one is the same as the units of stress. It should not cause any confusion if the reader will recall that the strain is a dimensionless quantity. Note that strain energy density is a scalar quantity, hence no indexes.

For a linearly elastic solid under a uniaxial stress we can use the Hooke's law ($\sigma_{ij} = E\,\varepsilon_{ij}$) to obtain an alternate expression for the strain energy density:

$$U = W = \frac{1}{2}\sigma_{ij}\varepsilon_{ij} = \frac{1}{2}E\,\varepsilon_{ij}^2 = \frac{1}{2E}\sigma_{ij}^2.$$

One can extend the concept of elastic strain energy density to region of inelastic behavior by defining the strain energy density as the area under the stress–strain curve of a material. Sometimes, we take this area under the stress–strain curve as a measure of the toughness of a material.

Example 2.2

A bar of a material with Young's modulus, E, length, L, and cross-sectional area, A, is subjected to an axial load, P. Derive an expression for strain energy stored in the bar.

Solution: In order to determine the total elastic strain energy stored in a body under a general stress, σ, we need to integrate the elastic strain energy density over the original volume of the material. Thus, the total elastic strain energy for a material of volume V, can be written as

$$U_{\text{total}} = \int_V \frac{\sigma^2}{2E}\,\mathrm{d}V.$$

For the simple case of a tensile force P acting on an area, A, we can write this as

$$U_{\text{total}} = \int_0^L \frac{P^2}{2EA^2}\,\mathrm{d}x = \frac{P^2 L}{2EA^2}.$$

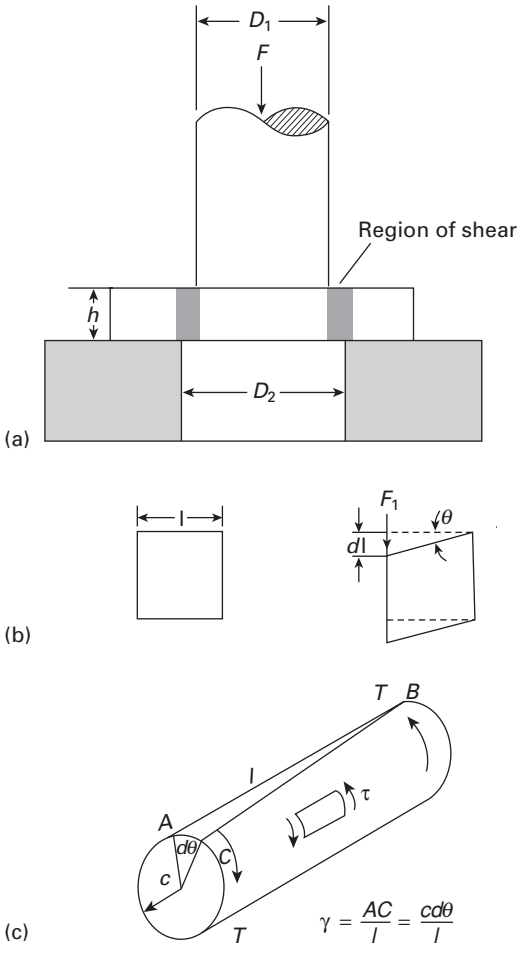

Fig. 2.4 (a) Specimen subjected to shear force. (b) Strain undergone by small cube in shear region. (c) Specimen (cylinder) subjected to torsion by a torque T.

2.4 Shear Stress and Strain

Imagine the loading arrangement shown in Figure 2.4(a). The specimen is placed between a punch and a base having a cylindrical orifice; the punch compresses the specimen. The internal resistance to the external forces now has the nature of a shear. The small cube in Figure 2.4(b) was removed from the region being sheared (between punch and base). It is distorted in such a way that the perpendicularity of the faces is lost. The shear stresses and strains are defined as

$$\tau = \frac{F}{A}, \quad \gamma = \frac{dl}{l} = \tan\theta \cong \theta. \tag{2.4}$$

The sign convention for shear stresses is given in Section 2.6. The area of the surface that undergoes shear is

$$A \cong \pi \left(\frac{D_1 + D_2}{2} \right) h.$$

The average of the two diameters is taken because D_2 is slightly larger than D_1.

A mechanical test commonly used to find shear stresses and strains is the torsion test. The equations that give the shear stresses and strains in terms of the torque are given in texts on the mechanics of materials. Figure 2.4(c) shows a cylindrical specimen subjected to a torque T. The relationship between the torque and the shear stresses that are generated is given by[3]

$$\tau_{\max} = \frac{T\,c}{J},$$

where c is the radius of the cylinder and $J = \pi c^4/2$ is the polar moment of inertia. Tubular specimens are preferred over solid cylinders because the shear stress can be approximated as constant over the cross section of the cylinder. For a hollow cylinder with b and c as inner and outer radii, respectively, we subtract out (the hollow part to obtain)

$$J = \frac{\pi c^4}{2} - \frac{\pi b^4}{2}.$$

For metals, ceramics, and certain polymers (the Hookean solids), the proportionality between τ and γ is observed in the elastic regimen. In analogy with Young's modulus, a transverse elasticity, called, the *rigidity*, or *shear modulus*, is defined as

$$G = \frac{\tau}{\gamma}. \tag{2.5}$$

G, which is numerically less than E, is related to E by Poisson's ratio, discussed in Section 2.5. Values of G for different materials are given in Table 2.5; it can be seen that G varies between one-third and one-half of E.

Example 2.3

A cylindrical steel specimen (length = 200 mm, diameter = 5 mm), is subjected to a torque equal to 40 N · m.

(a) What is the deflection of the specimen end, if one end is fixed?
(b) Will the specimen undergo plastic deformation?

Given:

$E = 210$ GPa,
$\nu = 0.3$,
$\sigma_y = 300$ MPa (tensile yield stress).

[3] See E. P. Popov, *Engineering Mechanics of Solids* (Englewood Cliffs, NJ: Prentice Hall, 1990).

Solution:

(a) $$\tau_{\max} = \frac{T \cdot c}{J}. \tag{1}$$

Given

$$T = 40 \text{ N·m}, \quad c = \frac{d}{2} = 2.5 \text{ mm}.$$

To calculate $\tau_{\max}$, we need to know J:

$$J = \pi \frac{c^4}{2}. \tag{2}$$

Substitute (2) into (1).

$$\tau_{\max} = \frac{T \cdot c}{\pi\left(\frac{c^4}{2}\right)} = \frac{2T}{\pi c^3} = \frac{2 \cdot 40}{\pi \cdot (2.5)^3} \frac{\text{N·m}}{\text{mm}^3}$$

$$= 1630 \text{ MPa}$$

$$= 1.63 \text{ GPa}.$$

Shear stress and shear strain are related as

$$\tau = G\gamma.$$

G can be calculated from E and ν.

$$G = \frac{E}{2(1+\nu)} = \frac{210}{2(1+0.3)} = 81 \text{ GPa},$$

$$\gamma = \frac{\tau_{\max}}{G} = \frac{1.63}{81} = 0.02.$$

But,

$$\gamma = \frac{c\theta}{L},$$

where θ is the angle of rotation.

$$\text{Torsional deflection} = \text{angle of rotation}$$

$$= \frac{\gamma L}{c}$$

$$= \frac{0.02 \times 200}{2.5} = 1.6 \text{ radians}.$$

(b) $\tau_{\max} = 1.63$ GPa.

The shear stress required to cause permanent deformation is related to the yield stress as follows:

$$\tau_y = \frac{\sigma_y}{2}.$$

When the stress is σ_y,

$$\tau_y = \frac{300}{2} = 150 \text{ MPa}.$$

But from (a), $\tau_{\max} = 1.63$ GPa > 150 MPa. Therefore, the specimen will undergo plastic deformation.

Example 2.4

What is the strain energy density in a low-carbon steel sample loaded to its elastic limit of 500 MPa?

Solution: Take E for a low-carbon steel to be 210 GPa. For such a material under a stress σ, we have a strain energy density given by

$$U = \frac{1}{2}\frac{\sigma^2}{E} = \frac{1}{2}\frac{(500 \times 10^6)^2}{210 \times 10^9}$$
$$= 595\,\text{kJ/m}^3.$$

2.5 Poisson's Ratio

A body, upon being pulled in tension, tends to contract laterally. The cube shown in Figure 2.5 exhibits this behavior. The stresses are now defined in a tridimensional body, and they have two indices. The first indicates the plane (or the normal to the plane) on which they are acting; the second indicates the direction in which they are pointing. These stresses are schematically shown acting on three faces of a unit cube in Figure 2.5(a). The normal stresses have two identical subscripts: σ_{11}, σ_{22}, σ_{33}. The shear stresses have two different subscripts: σ_{12}, σ_{13}, σ_{23}. These subscripts refer to the reference system $Ox_1x_2x_3$. If this notation is used, both normal and shear stresses are designated by the same letter, lower case sigma. On the other hand, in more simplified cases where we are dealing with only one normal and one shear stress component, σ and τ will be used, respectively; this notation will be maintained throughout the text. In Figure 2.5, the stress σ_{33} generates strains ε_{11}, ε_{22}, ε_{33}. (The same convention is used for stresses and strains.) Since the initial dimensions of the cube are equal to 1, the changes in length are equal to the strains. Poisson's ratio is defined as the ratio between the lateral and the longitudinal strains. Both ε_{11} and ε_{22} are negative (signifying a decrease in length), and ε_{33} is positive. In order for Poisson's ratio to be positive, the negative sign is used. Hence,

$$\nu = -\frac{\varepsilon_{11}}{\varepsilon_{33}} = -\frac{\varepsilon_{22}}{\varepsilon_{33}}. \tag{2.6}$$

In an isotropic material, ε_{11} is equal to ε_{22}. We can calculate the value of ν for two extreme cases: (1) when the volume remains constant and (2) when there is no lateral contraction. When the volume is constant, the initial and final volumes, V_0 and V, respectively, are equal to

$$V_0 = 1,$$
$$V = (1 + \varepsilon_{11})\,(1 + \varepsilon_{22})\,(1 + \varepsilon_{33}).$$

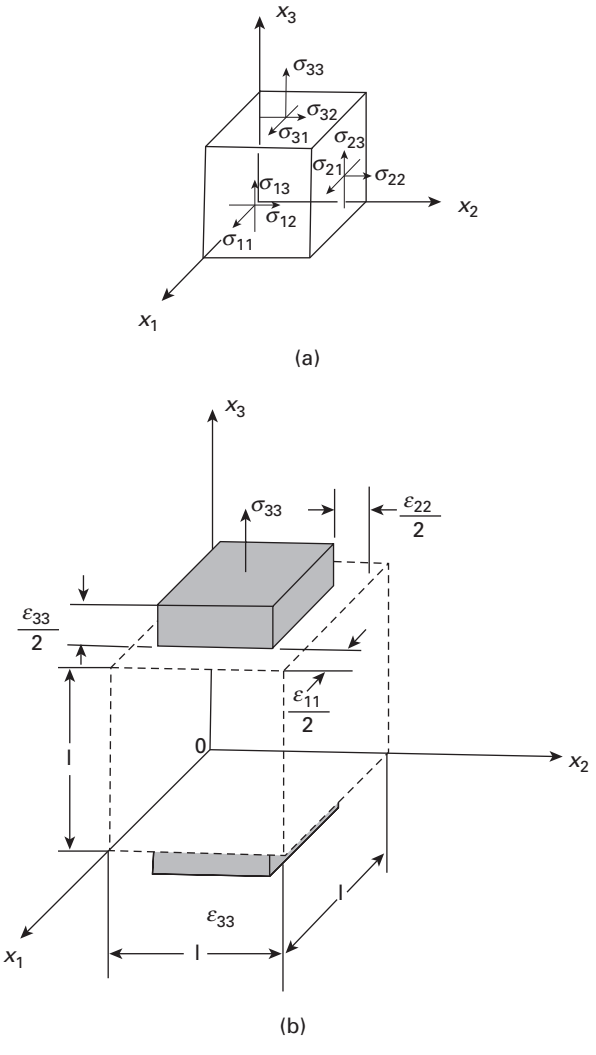

Fig. 2.5 (a) Unit cube in body subjected to tridimensional stress; only stresses on the three exposed faces of the cube are shown. (b) Unit cube being extended in direction Ox_3.

Neglecting the cross products of the strains, because they are orders of magnitude smaller than the strains themselves, we have

$$V = 1 + \varepsilon_{11} + \varepsilon_{22} + \varepsilon_{33}.$$

Since $V = V_0$,

$$\varepsilon_{11} + \varepsilon_{22} + \varepsilon_{33} = 0.$$

For the isotropic case, the two lateral contractions are the same ($\varepsilon_{11} = \varepsilon_{22}$). Hence,

$$2\varepsilon_{11} = -\varepsilon_{33}. \tag{2.7}$$

Substituting Equation 2.7 into Equation 2.6, we arrive at

$$\nu = 0.5.$$

For the case in which there is no lateral contraction, ν is equal to zero. Poisson's ratio for metals is usually around 0.3. (See Table 2.5.) The values given in the table apply to the elastic regimen; in the plastic regimen, ν increases to 0.5, since the volume remains constant during plastic deformation.

Poisson's ratio for cork (and other cellular materials) is about 0.2, which means that we can push cork into a glass bottle without expanding the bottle. The student should try to do this with a *rubber* stopper ($\nu \sim 0.5$)!

It is possible to establish the maximum and minimum for Poisson's ratio. We know that G and E are positive. This is a consequence of the positiveness and definiteness of the strain energy function (a subject that we will not treat here – in simple words, the unloaded state of the body is the lowest energy state).

In the equation below:

$$G = \frac{E}{2(1+\upsilon)}$$

we set:

$$E, G \geq 0.$$

Thus:

$$\frac{G}{E} = \frac{1}{2(1+\upsilon)} \geq 0$$

This leads to:

$$\upsilon \geq -1.$$

The lower bound for Poisson's ratio is obtained by deforming a body and assuming that its volume remains constant, as was done earlier in this section. Thus:

$$0.5 \geq \upsilon \geq -1.$$

2.6 More Complex States of Stress

The relationships between stress and strain described in sections 2.2 and 2.4 are unidimensional or uniaxial stress states, and do not apply to bidimensional and tridimensional states of stress. The most general state of stress can be represented by the unit cube of Figure 2.5(a). The generalized Hooke's law (as the set of equations relating tridimensional stresses and strains is called) is derived next, for an isotropic solid. It is assumed that shear stresses can generate *only* shear strains. Thus, the longitudinal strains are produced exclusively by the normal stresses. σ_{11} generates the following strain:

$$\varepsilon_{11} = \frac{\sigma_{11}}{E}. \tag{2.8}$$

Since $\nu = -\varepsilon_{22}/\varepsilon_{11} = -\varepsilon_{33}/\varepsilon_{11}$ for stress σ_{11}, we also have

$$\varepsilon_{22} = \varepsilon_{33} = -\frac{\nu\sigma_{11}}{E}.$$

The stress σ_{22}, in its turn, generates the following strains:

$$\varepsilon_{22} = \frac{\sigma_{22}}{E} \quad \text{and} \quad \varepsilon_{11} = \varepsilon_{33} = -\frac{\nu\sigma_{22}}{E}. \tag{2.9}$$

For σ_{33},

$$\varepsilon_{33} = \frac{\sigma_{33}}{E} \quad \text{and} \quad \varepsilon_{11} = \varepsilon_{22} = -\frac{\nu\sigma_{33}}{E}. \tag{2.10}$$

In this treatment, the shear stresses generate only shear strains:

$$\gamma_{12} = \frac{\sigma_{12}}{G}, \quad \gamma_{13} = \frac{\sigma_{13}}{G}, \quad \gamma_{23} = \frac{\sigma_{23}}{G}.$$

The second simplifying assumption is called the "principle of superposition." The total strain in one direction is considered to be equal to the sum of the strains generated by the various stresses along that direction. Hence, the total ε_{11} is the sum of ε_{11} produced by σ_{11}, σ_{22}, and σ_{33}. Adding strains from Equations 2.8 through 2.10, we obtain the generalized Hooke's law:

$$\boxed{\begin{aligned}
\varepsilon_{11} &= \frac{1}{E}\,[\sigma_{11} - \nu\,(\sigma_{22} + \sigma_{33})].\\
\varepsilon_{22} &= \frac{1}{E}\,[\sigma_{22} - \nu\,(\sigma_{11} + \sigma_{33})].\\
\varepsilon_{33} &= \frac{1}{E}\,[\sigma_{33} - \nu\,(\sigma_{11} + \sigma_{22})].\\
\gamma_{12} &= \frac{\sigma_{12}}{G}, \quad \gamma_{13} = \frac{\sigma_{13}}{G}, \quad \gamma_{23} = \frac{\sigma_{23}}{G}.
\end{aligned}} \tag{2.11}$$

Applying these equations to a hydrostatic stress situation ($\sigma_{11} = \sigma_{22} = \sigma_{33} = -p$), we can see perfectly that there are no distortions in the cube ($\gamma_{12} = \gamma_{13} = \gamma_{23} = 0$) and that $\varepsilon_{11} = \varepsilon_{22} = \varepsilon_{33}$.

The triaxial state of stress is difficult to treat in elasticity (and even more difficult in plasticity). In the great majority of cases, we try to assume a more simplified state of stress that resembles the tridimensional stress. This is often justified by the geometry of the body and by the loading configuration. The example discussed in Section 2.2 is the simplest state (uniaxial stress). It occurs when beams are axially loaded (in tension or compression). In sheets and plates (where one dimension can be neglected with respect to the other two), the state of stress can be assumed to be bidimensional. This state of stress is also known as *plane stress*, because normal stresses (normal to the surface) are zero at the surface, as are shear stresses (parallel to the surface) at the surface. In Figure 2.5(a), one would be left with σ_{11}, σ_{12}, σ_{22} if Ox_1x_2 were the plane of the sheet. Since the sheet is thin, there is no space for buildup of the stresses that are zero at the surface. The

solution to this problem is approached graphically in Section 2.7. The opposite case, in which one of the dimensions is infinite with respect to the other two, is treated under the assumption of plane strain. If one dimension is infinite, strain in it is constrained; hence, one has two dimensions left. This state is called *bidimensional* or, more commonly, *plane strain*. It also occurs when strain is constrained in one direction by some other means. A long dam is an example in which deformation in the direction of the dam is constrained. Yet another state of stress is pure shear, when there are no normal stresses.

Example 2.5

Consider a plate under uniaxial tension that is prevented from contracting in the transverse direction. Find the effective modulus along the loading direction under this condition of plane strain.

Solution: Take

$$E = \text{Young's modulus}, \quad \nu = \text{Poisson's ratio}$$

Let the loading and transverse directions be 1 and 2, respectively. There is no stress normal to the free surface, i.e., $\sigma_3 = 0$. Although the applied stress is uniaxial, the constraint on contraction in direction 2 results in a stress in that direction also. The strain in direction 2 can be written in terms of Hooke's law as

$$\varepsilon_2 = 0 = (1/E)[\sigma_2 - \nu\sigma_1].$$

Thus, $\sigma_2 = \nu\sigma_1$.

In direction 1, we can write, for the strain,

$$\begin{aligned}\varepsilon_{11} &= (1/E)[\sigma_1 - \nu\sigma_2] = (1/E)[\sigma_1 - \nu^2\sigma_1] \\ &= (\sigma_1/E)(1 - \nu^2).\end{aligned}$$

Hence, the plane strain modulus in direction 1 is

$$E' = (\sigma_1/\varepsilon_1) = E/(1 - \nu^2).$$

If we take $\nu = 0.33$, then the plane strain modulus $E' = 1.12E$.

Example 2.6

An isotropic, linear, elastic material is compressed by a force P by means of a punch in a rigid die. The material has a Young's modulus E and a Poisson's ratio ν. The displacement of the material is Δ, and the cavity has a height h and a square base of side a. (See Figure E2.6.)

Determine the stress and strain components. Also, determine the relationship between P and the displacement Δ of the material.

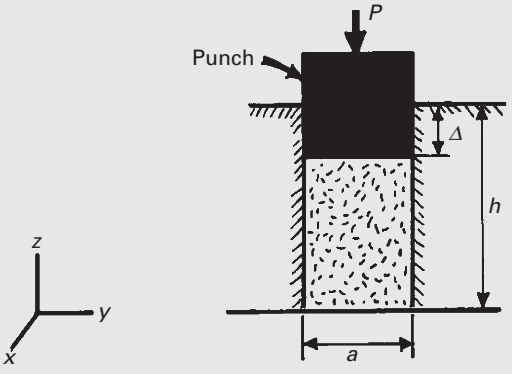

Fig. E2.6

Solution: This is a three-dimensional problem. There are no shear strains, and the only nonzero normal strain component is ε_z, the strain in the z-direction. The normal strains in the x- and y-directions are zero, because the rigid die does not allow deformation in these directions. However, the stress components in these directions are not zero. We use the generalized Hooke's law to obtain the three stress components. We can write, for the strain components,

$$\varepsilon_z = -\Delta/h, \quad \varepsilon_x = \varepsilon_y = \varepsilon_{xy} = \varepsilon_{yz} = \varepsilon_{zx} = 0.$$

Now we can write the following constitutive relationships by inverting Equation 2.11) and using x, y, and z instead of 1, 2, and 3:

$$\begin{aligned}\sigma_x &= E/[(1+\nu)\,(1-2\nu)][(1-\nu)\varepsilon_x + \nu\,(\varepsilon_y + \varepsilon_z)] \\ &= E/[(1+\nu)\,(1-2\nu)] \cdot [0 + \nu\,(-\Delta/h)],\end{aligned}$$

or

$$\sigma_x = -[E\nu/(1+\nu)(1-2\nu)][\Delta/h].$$

Similarly,

$$\begin{aligned}\sigma_y &= E/[(1+\nu)(1-2\nu)][(1-\nu)\varepsilon_y + \nu(\varepsilon_x + \varepsilon_z)] \\ &= E/[(1+\nu)(1-2\nu)] \cdot [0 + \nu(-\Delta/h)],\end{aligned}$$

or

$$\sigma_y = -E\nu/[(1+\nu)(1-2\nu)][\Delta/h].$$

Finally,

$$\begin{aligned}\sigma_z &= E/[(1+\nu)(1-2\nu)][(1-\nu)\varepsilon_z + \nu(\varepsilon_y + \varepsilon_x)] \\ &= E/[(1+\nu)(1-2\nu)] \cdot [1 - \nu(-\Delta/h) + 0],\end{aligned}$$

or

$$\sigma_z = -E(1-\nu)/[(1+\nu)(1-2\nu)][\Delta/h].$$

The load–displacement relationship is obtained by writing

$$P = \sigma_z a^2,$$
$$\sigma_z = P/a^2 = -E(1-\nu)/[(1+\nu)(1-2\nu)][\Delta/h],$$

or

$$P = -E a^2(1-\nu)(\Delta/h)/[(1+\nu)(1-2\nu)].$$

Note the linear relationship between P and Δ, is as it should be because the material in the cavity is linear elastic.

2.7 Graphical Solution of a Biaxial State of Stress: the Mohr Circle

There are two common graphical methods to obtain the stresses in a general orientation from σ_{11}, σ_{12}, and σ_{22}. These methods are similar and are a graphical representation of the equations below, that can be found in any mechanics of materials text:

$$\sigma'_{11} = \frac{\sigma_{11}+\sigma_{22}}{2} + \frac{\sigma_{11}-\sigma_{22}}{2}\cos 2\theta + \sigma_{12}\sin 2\theta,$$
$$\sigma'_{12} = -\frac{\sigma_{11}-\sigma_{22}}{2}\sin 2\theta + \sigma_{12}\cos 2\theta$$

The angle θ can be eliminated from the two equations above, leading to a quadratic equation that represents a circle. We present below two graphical methods to obtain the values of normal and shear stresses in any orientation, as well as the maximum normal and shear stresses.

Figure 2.6(a) shows a biaxial (or bidimensional) state of stress. The graphical scheme developed by O. Mohr allows the determination of the normal and shear stresses in any orientation in the plane. The reader should be warned, right at the onset, that a *change in sign convention* for the shear stresses has to be introduced here. The former sign convention – positive shear stresses pointing toward the positive direction of axes in faces shown in Figure 2.5(a) – has to be *temporarily* abandoned and the following convention adopted: Positive shear stresses produce counterclockwise rotation of a cube (or square), and negative shear stresses produce clockwise rotation. The sign convention for normal stresses remains the same. Figure 2.6(b) shows Mohr's construction. The normal stresses are plotted on the abcissa, while the shear stresses are plotted on the ordinate axis. Point A in the diagram corresponds to a state of stress on the face of the cube perpendicular to Ox_1; point B represents the state of stress on the face perpendicular to Ox_2. From A and B, we construct a circle with center in the axis of the abcissa and passing through A and B. The center is the point where the segment AB intersects the abcissa. Note that the center occurs at $(\sigma_{11}+\sigma_{22})/2$. The stress states for all orientations of the cube (in the same plane) correspond to points diametrically

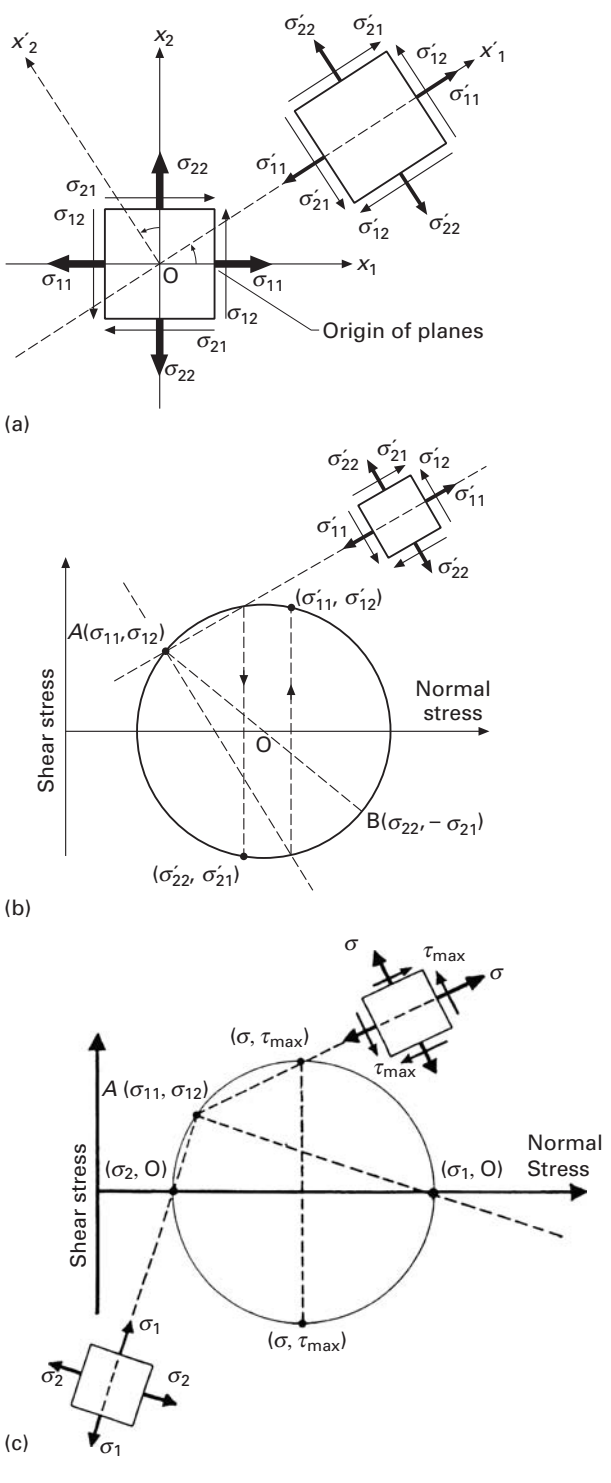

Fig. 2.6 (a) Biaxial (or bidimensional) state of stress. (b) Mohr circle and construction of general orientation $0_{x'_1 x'_2}$. (c) Mohr circle and construction of principal stresses and maximum shear stresses (Method I).

opposed in Mohr's circle. Hence, we can determine the state of stress for any orientation.

Method I is as follows: Point A (the stress system on the right-hand of the cube face) is called the "origin of planes." We will always start from it on the Mohr circle. We solve two problems.

First, we determine the stresses on a general coordinate direction Ox_1', Ox_2'. This is shown in Figure 2.6(b). Lines are drawn through A (the origin of planes) parallel to Ox_1' and Ox_2'. We seek the intersection of the axes with the circle. We draw lines perpendicular to the normal stress axis and find the new intersection. Thus, $(\sigma_{11}', \tau_{12}')$ represents stresses on the face perpendicular to Ox_1', and $(\sigma_{22}', \tau_{12}')$ represents stresses on face perpendicular to Ox_2'. These stresses are drawn in Figure 2.6(b). Remember that the clockwise–counterclockwise convention has to be used and that shear stresses are such that the summation of moments is zero.

Now we determine the maximum normal stresses (principal stresses) and maximum shear stresses. From point A (the origin of planes), we draw lines to the points corresponding to the maximum and minimum principal stresses (Figure 2.6(c)). Notice that these planes make an angle of 90°. Since we are on a normal stress axis, the intersection of the perpendicular to this axis corresponds to the initial point. We draw a square and place the stresses (σ_1, σ_2) on the square. This represents the orientation and values of the principal stresses. For the maximum shear stresses, we repeat the procedure $(\tau_{\max} = (\sigma_1 - \sigma_2)/2)$. At points of intersection, (Figure 2.6(c)), we go to the opposite intersection with respect to the normal stress axis) and obtain the values. We draw these on the square, with the convention that clockwise is positive. This represents the maximum shear stress value and orientation. Note that the normal stresses for this orientation (and the one 90° from it) are nonzero. Note also that $\tau_{\max}$ occurs in orientations that make 45° with the principal stress orientations.

In Method II the sign convention for the shear stresses is the same: clockwise positive, counterclockwise negative. Again, the normal stresses are plotted in the abscissa and the shear stresses in the ordinate. Point A in the diagram corresponds to a state of stress on the face of the cube perpendicular to Ox_1: point B represents the state of stress on the face perpendicular to Ox_2. From A and B we construct a circle with center in the axis of the abscissa and passing through A and B. The center is the point where the segment AB intersects the abscissa. The stress states for all orientations of the square (in the same plane) correspond to points diametrically opposed in Mohr's circle. Hence we can determine the state of stress for any orientation. The rotations in the square (real rotations) and in Mohr's circle have the same sense: however a rotation of θ in the square corresponds to 2θ in Mohr's circle. For instance, a rotation of 2θ in the counterclockwise direction leads to a state of stress defined by C and D in Mohr's circle. The shear stresses are zero for this orientation and the

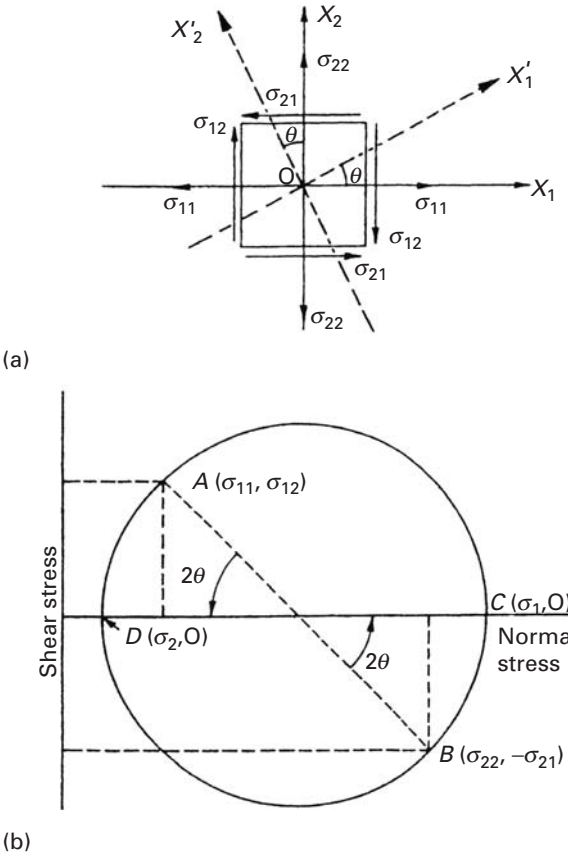

Fig. 2.7 (a) Biaxial (or bidimensional) state of stress: (b) Mohr circle construction (Method II).

normal stresses are called *principal* stresses. One subscript is sufficient to designate the stresses in these special orientations: σ_1, σ_2, σ_3. We use the convention $\sigma_1 > \sigma_2 > \sigma_3$. In Figure 2.7(a) a rotation of only θ was done in the same counterclockwise sense, leading to the same principal stresses. The orientations Ox_1 and Ox_2 are called *principal axes* (or directions). The curious reader should consult a mechanics of materials text, such as E. P. Popov, *Engineering of Solids* (Upper Saddle River, NJ: Prentice Hall, 1999).

Example 2.7

Elisabeth S., a bright, but somewhat nerdy, graduate student, went skiing in her brand-new boots. She had an unfortunate mishap on the slopes, and her right ski twisted beyond the strength of her femur, resulting in a fracture. The doctor took some X-rays and informed Elisabeth that she had a "spiral fracture." This triggered a spirited dialogue between Elisabeth and the doctor. Elisabeth claims that her fracture ("peeking" through the ruptured skin) is helical. With whom do you agree? Why? Show, using your knowledge of engineering, what is the

maximum torque? The tensile strength of bone is 80 MPa and the diameter of the femur is 25 mm.

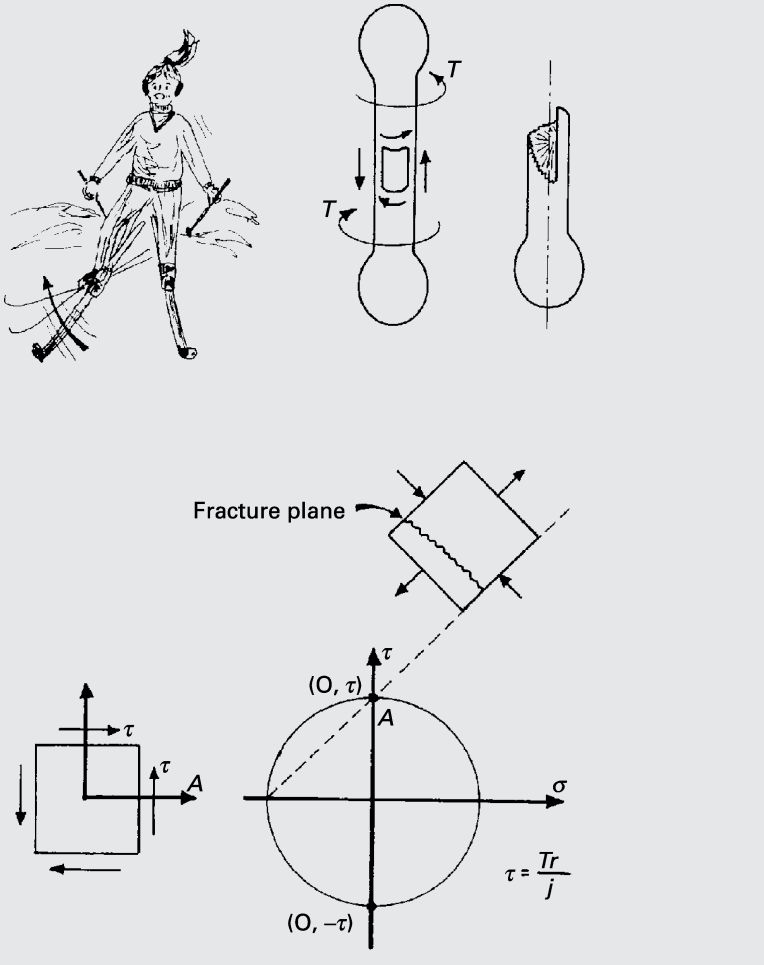

Fig. E2.7

The Mohr circle construction (see Figure E2.7) shows that the torsion T applied to the bone leads to a state of simple shear in the cross section. If the material were ductile, the failure plane would be the plane of maximum shear. Since bone is brittle, however, failure will occur along the surface where the tensile stresses are maximum. This surface is at angle of 45° with the cross-sectional plane. Thus, the fracture is helical, and not spiral. (Students should repeat this analysis by using a piece of chalk and subjecting it to torsion.) The maximum torque that the bone will withstand is

$$T = \frac{\tau J}{r},$$

where J is the polar moment on inertia. (The student should consult a text on the mechanics of materials). Now, since $\tau_{\max} = \sigma_{1\max}$, it follows

that $\tau_{\max} = 80$ MPa. Also,

$$J = \frac{\pi d^4}{32}.$$

Thus,

$$T = \frac{\tau_{\max} \pi d^3}{16} = 245\,\text{N}\cdot\text{m}.$$

The weight of a normal person is 750 N. Here is a ski tip, then: A distance of 1 meter from the axis of the leg can easily generate a torque of sufficient magnitude for a helical bone fracture to occur. Skiers, beware!

Example 2.8

A state of stress is given by

$$\sigma_{11} = 350 \text{ MPa},$$
$$\sigma_{12} = 70 \text{ MPa},$$
$$\sigma_{22} = 210 \text{ MPa}.$$

Determine the principal stresses, the maximum shear stress, and their angle with the given direction by the Mohr circle.

Solution: Figure E2.8 shows the desired quantities.

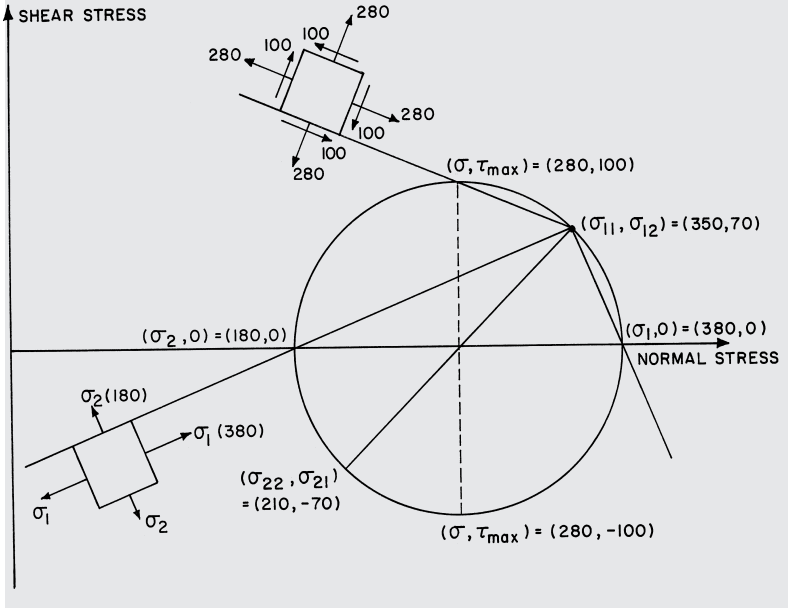

Fig. E2.8

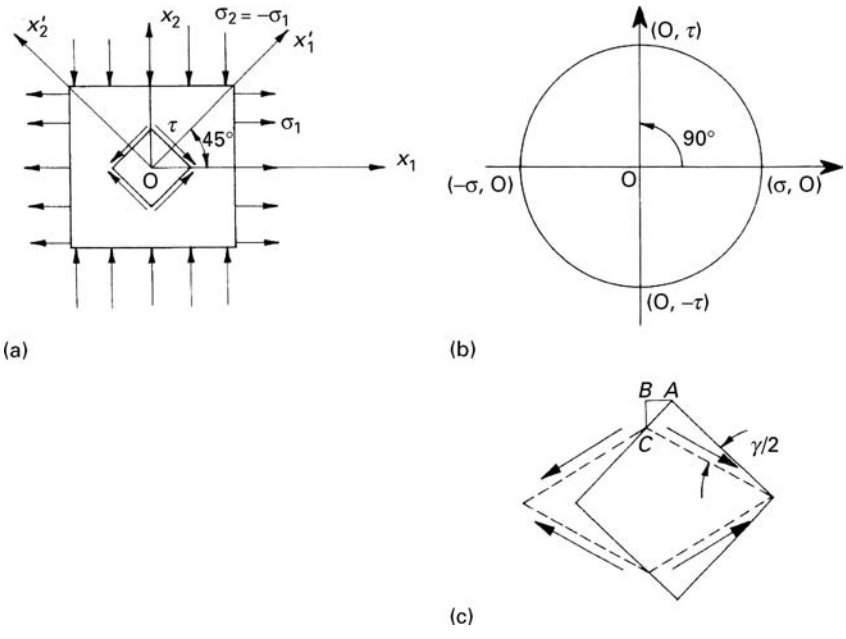

Fig. 2.8 Pure shear.

2.8 Pure Shear: Relationship between *G* and *E*

There is a special case of bidimensional stress in which $\sigma_{22} = -\sigma_{11}$. This state of stress is represented in Figure 2.8(a). It can be seen that $\sigma_{12} = 0$, implying that σ_{11} and σ_{22} are principal stresses. Hence, we can use the special subscripts for principal stresses and write $\sigma_2 = -\sigma_1$. In Mohr's circle of Figure 2.8(b), the center coincides with the origin of the axes. We can see that a rotation of 90° (on the circle) leads to a state of stress in which the normal stresses are zero. This rotation is equivalent to a 45° rotation in the body (real space). The magnitude of the shear stress at this orientation is equal to the radius of the circle. Hence, the square shown in Figure 2.8(c) is deformed to a lozenge under the combined effect of the shear stresses. Such a state of stress is called *pure shear*.

It is possible, from this particular case, to obtain a relationship between *G* and *E*; furthermore, the relationship has a general nature. The strain ε_{11} is, for this case,

$$\varepsilon_{11} = \frac{1}{E}(\sigma_1 - \nu\sigma_2) = \frac{\sigma_1}{E}(1 + \nu). \tag{2.12}$$

We have, for the shear stresses (using the normal, and not the Mohr, sign convention),

$$\tau = -\sigma_1. \tag{2.13}$$

But we also have,

$$\tau = G\gamma. \tag{2.14}$$

Substituting Equations 2.13 and 2.14 into Equation 2.12 yields

$$\varepsilon_{11} = -\frac{G\gamma}{E}(1+\nu).$$

It is possible, by means of geometrical considerations on the triangle *ABC* in Fig. 2.8(c), to show that

$$2\varepsilon_{11} = -\gamma.$$

The reader should do this, as an exercise. Hence,

$$G = \frac{E}{2(1+\nu)}.$$

Consequently, G is related to E by means of Poisson's ratio. This theoretical relationship between E and G is in good agreement with experimental results. For a typical metal having $\nu = 0.3$, we have $G = E/2.6$. The maximum value of G is $E/2$.

The state of *simple shear* should not be confused with *pure shear*; simple shear involves an additional rotation, so that two faces remain parallel after deformation.

2.9 Anisotropic Effects

Figure 2.5 shows that a general stress system acting on a unit cube has nine components and is a symmetrical tensor. (The off-diagonal components are equal, i.e., $\sigma_{13} = \sigma_{31}$, $\sigma_{12} = \sigma_{21}$, and $\sigma_{23} = \sigma_{32}$.) We can therefore write

$$\begin{pmatrix} \sigma_{11} & \sigma_{12} & \sigma_{13} \\ \sigma_{21} & \sigma_{22} & \sigma_{23} \\ \sigma_{31} & \sigma_{32} & \sigma_{33} \end{pmatrix} = \begin{pmatrix} \sigma_{11} & \sigma_{12} & \sigma_{13} \\ \sigma_{12} & \sigma_{22} & \sigma_{23} \\ \sigma_{13} & \sigma_{23} & \sigma_{33} \end{pmatrix}.$$

When the unit cube in Figure 2.5 is rotated, the stress state at that point does not change; however, the components of the stress change. The same applies to strains. A general state of strain is described by

$$\begin{pmatrix} \varepsilon_{11} & \varepsilon_{12} & \varepsilon_{13} \\ \varepsilon_{21} & \varepsilon_{22} & \varepsilon_{23} \\ \varepsilon_{31} & \varepsilon_{32} & \varepsilon_{33} \end{pmatrix} = \begin{pmatrix} \varepsilon_{11} & \varepsilon_{12} & \varepsilon_{13} \\ \varepsilon_{12} & \varepsilon_{22} & \varepsilon_{23} \\ \varepsilon_{13} & \varepsilon_{23} & \varepsilon_{33} \end{pmatrix}.$$

We can also use a matrix notation for stresses and strains, replacing the indices by the following:

$$\begin{array}{ll} 11 \to 1 & 12 \to 5 \\ 22 \to 2 & 13 \to 5 \\ 33 \to 3 & 12 \to 6 \end{array}$$

$$\begin{pmatrix} 11 & & 12 & \to & 13 \\ & \searrow & & & \uparrow \\ & & 22 & & 23 \\ & & & \searrow & \uparrow \\ & & & & 33 \end{pmatrix} = \begin{pmatrix} 1 & & 6 & \leftarrow & 5 \\ & \searrow & & & \uparrow \\ & & 2 & & 4 \\ & & & \searrow & \uparrow \\ & & & & 3 \end{pmatrix}$$

We now have the stress and strain, in general form, as

$$\begin{pmatrix} \sigma_1 & \sigma_6 & \sigma_5 \\ \sigma_6 & \sigma_2 & \sigma_4 \\ \sigma_5 & \sigma_4 & \sigma_3 \end{pmatrix} \quad \text{and} \quad \begin{pmatrix} \varepsilon_1 & \varepsilon_6/2 & \varepsilon_5/2 \\ \varepsilon_6/2 & \varepsilon_2 & \varepsilon_4/2 \\ \varepsilon_5/2 & \varepsilon_4/2 & \varepsilon_3 \end{pmatrix}.$$

It should be noted that $\varepsilon_1 = \varepsilon_{11}$, $\varepsilon_2 = \varepsilon_{22}$, and $\varepsilon_3 = \varepsilon_{33}$, but

$$\varepsilon_4 = 2\varepsilon_{23} = \gamma_{23},$$
$$\varepsilon_5 = 2\varepsilon_{13} = \gamma_{13},$$
$$\varepsilon_6 = 2\varepsilon_{12} = \gamma_{12}.$$

These differences in notation are important to preserve the equations (see shortly) that relate stresses to strains.

The foregoing transformation is easy to remember: One proceeds first along the diagonal (1→2→3) and then back (4→5→6). It is now possible to correlate the stresses and strains for a general case, in which the elastic properties of a material are dependent on its orientation. We use two elastic constants: C (stiffness) and S (compliance), or

$C \rightarrow$ Stiffness

$S \rightarrow$ Compliance.

Symbols are inverted to render treatment more confusing!
We have

$$\begin{pmatrix} \sigma_1 \\ \sigma_2 \\ \sigma_3 \\ \sigma_4 \\ \sigma_5 \\ \sigma_6 \end{pmatrix} = \begin{pmatrix} C_{11} & C_{12} & C_{13} & C_{14} & C_{15} & C_{16} \\ C_{21} & C_{22} & C_{23} & C_{24} & C_{25} & C_{26} \\ C_{31} & C_{32} & C_{33} & C_{34} & C_{35} & C_{36} \\ C_{41} & C_{42} & C_{43} & C_{44} & C_{45} & C_{46} \\ C_{51} & C_{52} & C_{53} & C_{54} & C_{55} & C_{56} \\ C_{61} & C_{62} & C_{63} & C_{64} & C_{65} & C_{66} \end{pmatrix} \begin{pmatrix} \varepsilon_1 \\ \varepsilon_2 \\ \varepsilon_3 \\ \varepsilon_4 \\ \varepsilon_5 \\ \varepsilon_6 \end{pmatrix}$$

In short notation, noting that repeated indices in one term imply summation, we have:

$$\sigma_i = C_{ij}\varepsilon_j,$$
$$\varepsilon_i = S_{ij}\sigma_j.$$

The elastic stiffness and compliance matrices are symmetric, and the 36 components (6×6) are reduced to 21. We now apply this general expression to crystals having different structures and, therefore, different symmetries to obtain successive simplifications. In the isotropic case, the elastic constants are reduced from 21 to 2.

The different crystal systems can be characterized exclusively by their symmetries. The proof of this is beyond the scope of the book; however, it is sufficient to say that the cubic system can be perfectly described by four threefold rotations. The seven crystalline systems can be perfectly described by their axes of rotation.

Table 2.1 presents the different symmetry operations defining the seven crystal systems. For example, a threefold rotation is a rotation of 120° ($3 \times 120° = 360°$); after 120°, the crystal system comes to a position identical to the initial one. The hexagonal system

Table 2.1 | Minimum Number of Symmetry Operations in Various Systems

System	Rotation
Triclinic	None (or center of symmetry)
Monoclinic	1 twofold rotation
Orthorhombic	2 perpendicular twofold rotations
Tetragonal	1 fourfold rotation around [001]
Rhombohedral	1 threefold rotation around [111]
Hexagonal	1 sixfold rotation around [0001]
Cubic	4 threefold rotations around <111>

exhibits a sixfold rotation around the c axis; after each 60°, the structure superimposes upon itself. In terms of a matrix, we have the following:

Orthorhombic

$$\begin{bmatrix} 11 & 12 & 13 & 0 & 0 & 0 \\ . & 22 & 23 & 0 & 0 & 0 \\ . & . & 33 & 0 & 0 & 0 \\ . & . & . & 44 & 0 & 0 \\ . & . & . & . & 55 & 0 \\ . & . & . & . & . & 66 \end{bmatrix},$$

Tetragonal

$$\begin{bmatrix} 11 & 12 & 13 & 0 & 0 & 16 \\ . & 11 & 13 & 0 & 0 & -16 \\ . & . & 33 & 0 & 0 & 0 \\ . & . & . & 44 & 0 & 0 \\ . & . & . & . & 44 & 0 \\ . & . & . & . & . & 66 \end{bmatrix},$$

Hexagonal

$$\begin{bmatrix} 11 & 12 & 13 & 0 & 0 & 0 \\ & 11 & 13 & 0 & 0 & 0 \\ & & 33 & 0 & 0 & 0 \\ & & & 44 & 0 & 0 \\ & & & & 44 & 0 \\ & & & & & x \end{bmatrix}$$

where

$$x \to 2(S_{11} - S_{12}), \quad \text{or}$$
$$x \to \frac{1}{2}(C_{11} - C_{12}).$$

Laminated composites made by the consolidation of prepregged sheets, with individual plies having different fiber orientations, have orthotropic symmetry with nine independent elastic constants. Orthotropic symmetry is analogous to orthorhombic symmetry: there are three mutually perpendicular axes of symmetry, and the elastic constants along these three axes are different. For the Cubic system, the elastic matrix is the following configuration:

$$\begin{bmatrix} 11 & 12 & 12 & 0 & 0 & 0 \\ . & 11 & 12 & 0 & 0 & 0 \\ . & . & 11 & 0 & 0 & 0 \\ . & . & . & 44 & 0 & 0 \\ . & . & . & . & 44 & 0 \\ . & . & . & . & . & 44 \end{bmatrix}.$$

The number of independent elastic constants in a cubic system is three.

For isotropic materials (most polycrystalline aggregates can be treated as such):

$$C_{44} = \frac{C_{11} - C_{12}}{2}. \tag{2.15}$$

The stiffness matrix is

$$\begin{bmatrix} C_{11} & C_{12} & C_{12} & 0 & 0 & 0 \\ . & C_{11} & C_{12} & 0 & 0 & 0 \\ . & . & C_{11} & 0 & 0 & 0 \\ . & . & . & \frac{C_{11} - C_{12}}{2} & 0 & 0 \\ . & . & . & . & \frac{C_{11} - C_{12}}{2} & 0 \\ . & . & . & . & . & \frac{C_{11} - C_{12}}{2} \end{bmatrix} \tag{2.16}$$

For anisotropic systems, Equation 2.15 does not apply, and we define an anisotropy ratio (also called the Zener anisotropy ratio, in honor of the scientist who introduced it):

$$A = \frac{2C_{44}}{C_{11} - C_{12}} \neq 1. \tag{2.17}$$

Some metals have high anisotropy ratios, whereas others, such as aluminum and tungsten, have values of A very close to 1. For the latter, even single crystals are almost isotropic.

For the elastic compliances, we have, for the isotropic case:

$$\begin{bmatrix} S_{11} & S_{12} & S_{12} & 0 & 0 & 0 \\ . & S_{11} & S_{12} & 0 & 0 & 0 \\ . & . & S_{11} & 0 & 0 & 0 \\ . & . & . & 2(S_{11} - S_{12}) & 0 & 0 \\ . & . & . & . & 2(S_{11} - S_{12}) & 0 \\ . & . & . & . & . & 2(S_{11} - S_{12}) \end{bmatrix}. \tag{2.18}$$

Hence, for the cubic system, the 81 components of the elastic constants have been reduced to three independent ones while for the isotropic case, only two independent elastic constants are needed. However, it is not under this form that the elastic constants are usually known.

Table 2.2 gives the various equations interrelating the foregoing parameters.

The relationships between stresses and strains for isotropic materials become

$$\varepsilon_1 = S_{11}\sigma_1 + S_{12}\sigma_2 + S_{12}\sigma_3 = \frac{1}{E}\left[\sigma_1 - \nu(\sigma_2 + \sigma_3)\right],$$

$$\varepsilon_2 = S_{12}\sigma_1 + S_{11}\sigma_2 + S_{12}\sigma_3 = \frac{1}{E}\left[\sigma_2 - \nu(\sigma_1 + \sigma_3)\right],$$

$$\varepsilon_3 = S_{12}\sigma_1 + S_{12}\sigma_2 + S_{11}\sigma_3 = \frac{1}{E}\left[\sigma_3 - \nu(\sigma_1 + \sigma_2)\right],$$

Table 2.2 | Relations among the Elastic Constants for Isotropic Materials

Elastic Constants	In Terms of: E, ν	E, G	$K. \nu$	K, G	λ, μ
E	$=E$	$=E$	$= 3(1–2\nu)K$	$=\frac{9K}{1+3K/G}$	$=\frac{\mu(3+2\mu/\lambda)}{1+\mu/\lambda}$
ν	$=\nu$	$=-1+\frac{E}{2G}$	$=\nu$	$=\frac{1-2G/3K}{2+2G/3K}$	$=\frac{1}{2(1+\mu/\lambda)}$
G	$=\frac{E}{2(1+\nu)}$	$=G$	$=\frac{3(1-2\nu)K}{2(1+\nu)}$	$=G$	$=\mu$
K	$=\frac{E}{3(1-2\nu)}$	$=\frac{E}{9-3E/G}$	$=K$	$=K$	$=\lambda+\frac{2\mu}{3}$
λ	$=\frac{E\nu}{(1+\nu)(1-2\nu)}$	$=\frac{E(1-2G/E)}{3-E/G}$	$=\frac{3K\nu}{1+\nu}$	$=K-\frac{2G}{3}$	$=\lambda$
μ	$=\frac{E}{2(1+\nu)}$	$=G$	$=\frac{3(1-2\nu)K}{2(1+\nu)}$	$=G$	$=\mu$

$$\varepsilon_4 = 2(S_{11} - S_{12})\sigma_4 = \frac{1}{G}\sigma_4,$$
$$\varepsilon_5 = 2(S_{11} - S_{12})\sigma_5 = \frac{1}{G}\sigma_5,$$
$$\varepsilon_6 = 2(S_{11} - S_{12})\sigma_6 = \frac{1}{G}\sigma_6.$$

Expressing the strains as function of the stresses, we have

$$\sigma_1 = C_{11}\varepsilon_1 + C_{12}\varepsilon_2 + C_{12}\varepsilon_3 = (2\mu + \lambda)\varepsilon_1 + \lambda\varepsilon_2 + \lambda\varepsilon_3,$$
$$\sigma_2 = C_{12}\varepsilon_1 + C_{11}\varepsilon_2 + C_{12}\varepsilon_3 = \lambda\varepsilon_1 + (2\mu + \lambda)\varepsilon_2 + \lambda\varepsilon_3,$$
$$\sigma_3 = C_{12}\varepsilon_1 + C_{12}\varepsilon_2 + C_{11}\varepsilon_3 = \lambda\varepsilon_1 + \lambda\varepsilon_2 + (2\mu + \lambda)\lambda\varepsilon_3,$$
$$\sigma_4 = \frac{1}{2}(C_{11} - C_{12})\varepsilon_4 = \mu\varepsilon_4,$$
$$\sigma_5 = \frac{1}{2}(C_{11} - C_{12})\varepsilon_5 = \mu\varepsilon_5,$$
$$\sigma_6 = \frac{1}{2}(C_{11} - C_{12})\varepsilon_6 = \mu\varepsilon_6.$$

Note that $\mu = G$.

The elastic compliance matrix for isotropic materials is directly obtained from the generalized Hooke law:

$$\begin{pmatrix} \varepsilon_1 \\ \varepsilon_2 \\ \varepsilon_3 \\ \varepsilon_4 \\ \varepsilon_5 \\ \varepsilon_6 \end{pmatrix} = \begin{pmatrix} 1/E & -\nu/E & -\nu/E & 0 & 0 & 0 \\ & 1/E & -\nu/E & 0 & 0 & 0 \\ & & 1/E & 0 & 0 & 0 \\ & & & 1/G & 0 & 0 \\ & & & & 1/G & 0 \\ & & & & & 1/G \end{pmatrix} \begin{pmatrix} \sigma_1 \\ \sigma_2 \\ \sigma_3 \\ \sigma_4 \\ \sigma_5 \\ \sigma_6 \end{pmatrix}.$$

The elastic stiffness matrix is obtained in a similar manner:

$$\begin{pmatrix} \sigma_1 \\ \sigma_2 \\ \sigma_3 \\ \sigma_4 \\ \sigma_5 \\ \sigma_6 \end{pmatrix} = \begin{pmatrix} 2\mu+\lambda & \lambda & \lambda & 0 & 0 & 0 \\ & 2\mu+\lambda & \lambda & 0 & 0 & 0 \\ & & 2\mu+\lambda & 0 & 0 & 0 \\ & & & \mu & 0 & 0 \\ & & & & \mu & 0 \\ & & & & & \mu \end{pmatrix} \begin{pmatrix} \varepsilon_1 \\ \varepsilon_2 \\ \varepsilon_3 \\ \varepsilon_4 \\ \varepsilon_5 \\ \varepsilon_6 \end{pmatrix}.$$

From the product of these two matrices ($= I$) we can obtain some of the relations in Table 2.2.

By comparing the terms of the elastic compliance and stiffness matrices for isotropic materials with the matrices in Equations 2.16 and 2.17, one can obtain the following relationships: Young's modulus:

$$E = \frac{1}{S_{11}}. \tag{2.19}$$

Rigidity or shear modulus:

$$G = \frac{1}{2(S_{11} - S_{12})}.$$

Compressibility (B) and bulk modulus (K):

$$B = \frac{1}{K} = \frac{\varepsilon_{11} + \varepsilon_{22} + \varepsilon_{33}}{-\frac{1}{3}(\sigma_{11} + \sigma_{22} + \sigma_{33})}.$$

Poisson's ratio:

$$\nu = -\frac{S_{12}}{S_{11}}.$$

Lamé's constants:

$$\mu = C_{44} = \frac{1}{2}\ (C_{11} - C_{12}) = \frac{1}{S_{44}} = G,$$

$$\lambda = C_{12}.$$

A great number of materials can be treated as isotropic, although they are not microscopically so. The individual grains exhibit the

crystalline anisotropy and symmetry, but when they form a polycrystalline aggregate and are randomly oriented, the material is macroscopically isotropic (i.e., the elastic constants are the same in all directions). Often, a material is not completely isotropic; if the elastic modulus E is different along three perpendicular directions, the material is orthotropic; composites are a typical case.

In a cubic material, the elastic moduli can be determined along any orientation, from the elastic constants, by application of the following equation:

$$\frac{1}{E_{ijk}} = S_{11} - 2\left(S_{11} - S_{12} - \frac{1}{2}S_{44}\right) \times \left(\ell_{i1}^2\ell_{j2}^2 + \ell_{j2}^2\ell_{k3}^2 + \ell_{i1}^2\ell_{k3}^2\right), \tag{2.20}$$

where E_{ijk} is the Young's modulus, respectively, in the [ijk] direction; l_{i1}, l_{j2}, and l_{k3} are the direction cosines of the direction [ijk].

The expression for the shear modulus is a little more complicated than that for Young's modulus, because it involves a direction of shear and a plane of shear. The Young's modulus, on the other hand, involves only a direction (the direction of extension or compression). The plane normal is the same as the direction. The shear modulus on the cube face planes $\{100\}$ is equal to:

$$G_0 = \frac{1}{S_{44}}.$$

This shear modulus is the same, for any direction in these planes. In the $\{111\}$ planes, on the other hand, the shear modulus varies with direction. For shear along [110], it is equal to:

$$G_1 = \frac{3}{S_{44} + 4(S_{11} - S_{12})}.$$

For isotropic materials,

$$S_{44} = 2(S_{11} - S_{12})$$

and

$$G = 1/S_{44}$$

for all orientations. For example, for copper $S_{11} = 1.498$, $S_{12} = -0.629$, $S_{44} = 1.329$ ($\times 10^{-2}$ GPa^{-1}); $G_0 = 75.4$ GPa, $G_1 = 30$ GPa.

Figure 2.9(a) illustrates the dependence on orientation of elastic Young's modulus for copper. The [100], [010], and [001] directions are "softer," whereas the [111], [$1\bar{1}1$], and [$11\bar{1}$] directions are stiffer. For cubic zirconia (Figure 2.9(b)), the opposite occurs: The coordinate axes correspond to the stiff directions. These diagrams illustrate very well the importance of anisotropy of elastic properties. For a cubic material that has the same Young's modulus along all directions (an isotropic material), we have the relationship

$$2(S_{11} - S_{12}) = S_{44}. \tag{2.21}$$

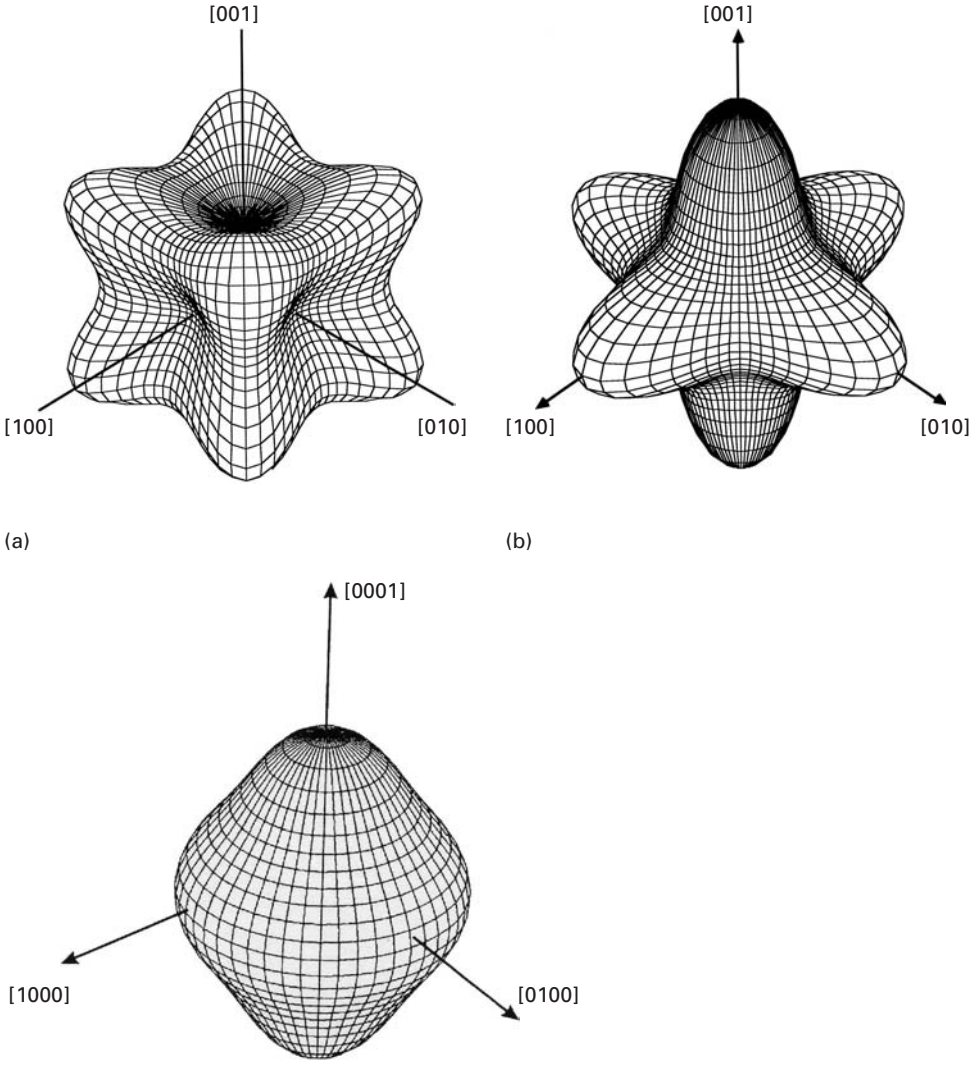

Fig. 2.9 Dependence on orientation of Young's modulus for monocrystalline (a) copper; (b) cubic zirconia. (Courtesy of R. Ingel.) (c) Tridimension polar plot for zirconium. (Courtesy of J. M. Gebert.)

The tridimensional picture in Figure 2.9(c) shows anisotropy of Young's modulus in the hexagonal structure in a clearer fashion. This corresponds to zirconium. The isotropy of E in the basal plane is responsible for the "flying saucer" aspect of the polar plot.

For hexagonal crystals, the Young's modulus is isotropic in the basal plane, but varies if one moves toward the c axis. The Young's modulus is given by:

$$\frac{1}{E} = \left(1 - l_3^2\right)S_{11} + l_3^4 S_{33} + l_3^2\left(1 - l_3^2\right)(2S_{13} + S_{44}),$$

where ℓ_3 is the cosine of the angle with the basal plane. Figure 2.10 shows the variation of E with orientation for SiC. It is constant and equal to 400 GPa in the basal plane. (Fig. 2.10(a)). In the c direction, it rises to 465 GPa (Figure 2.10(b)).

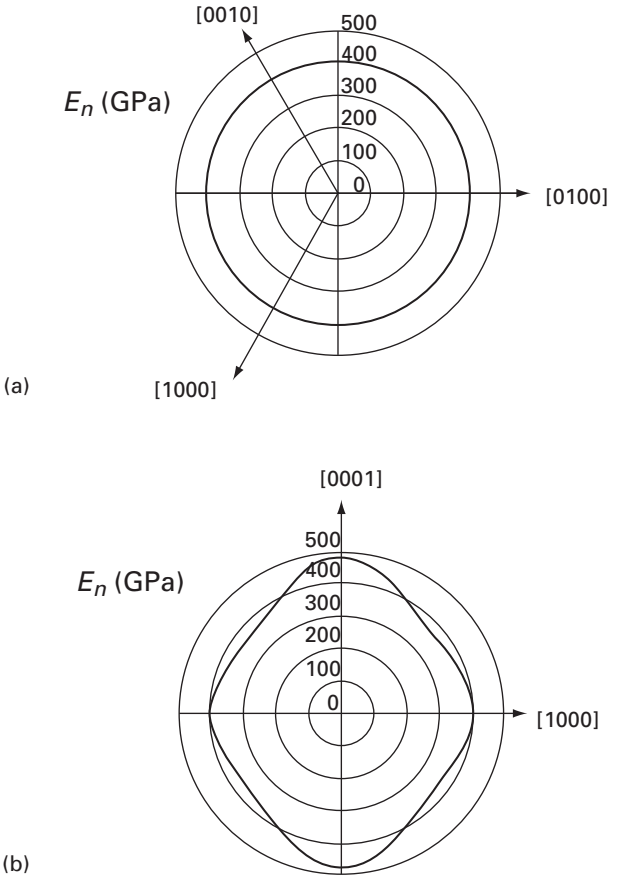

Fig. 2.10 Variation of effective E for silicon carbide as a function of orientation; (a) basal plane; (b) perpendicular to basal plane. (From C. J. Shih, M. A. Meyers, V. F. Nesterenko and S. J. Chen, *Acta Mater.*, 48 (2000) 2399.)

In Section 2.5 we defined the Poisson's ratio for isotropic materials. In anisotropic materials, we define Poisson's ratio in a similar manner. It is the magnitude of the ratio between the lateral and longitudinal strain (the direction along which the stress is applied). In the anisotropic case, the Poisson's ratio will depend on orientation and for each loading direction we have more than one Poisson's ratio. It is quite rare to find materials with negative Poisson's ratios. This did not deter Lubarda and Meyers[4] from finding one. Monocrystalline zinc, an HCP metal, has a negative Poisson's ratio in a certain orientation. In anisotropic materials, Poisson's ratio varies (as do all elastic constants) with orientation. We define θ as the angle with the basal plane. Figure 2.11 shows the variation of $\nu_{\ell n}$ (there is another Poisson's ratio in this case: ν_{mn}) with θ. For θ less than 18°, it is negative. It should be noted that for most HCP metals this negative regimen does not exist.

[4] V. A. Lubarda and M. A. Meyers, *Scripta Mater.*, 40 (1999) 975.

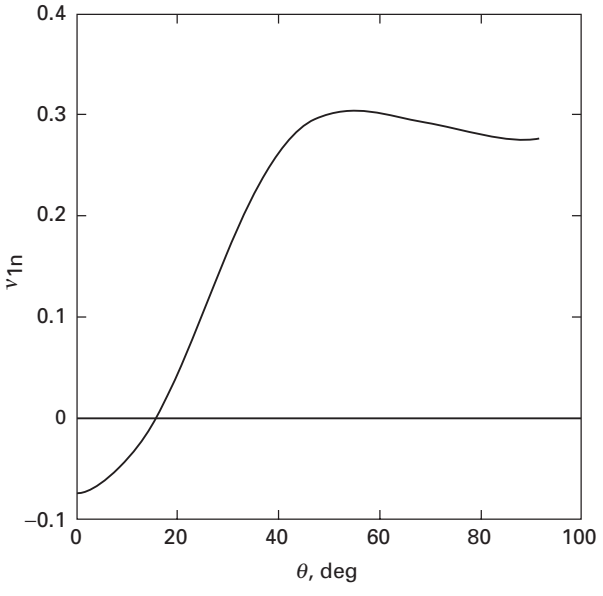

Fig. 2.11 Variation in Poisson's ratio ν_{1n} in direction 1 due to stress applied along direction n, making an angle θ with the basal plane of the zinc (HCP) crystal.

Example 2.9

A hydrostatic compressive stress applied to a material with cubic symmetry results in a dilation of -10^{-5}. The three independent elastic constants of the material are $C_{11} = 50$ GPa, $C_{12} = 40$ GPa, and $C_{44} = 32$ GPa. Write an expression for the generalized Hooke's law for this material, and compute the applied hydrostatic stress.

Solution: Dilation is the sum of the principal strain components:

$$\varepsilon = \varepsilon_1 + \varepsilon_2 + \varepsilon_3 = -10^{-5}.$$

Cubic symmetry implies that

$$\varepsilon_1 = \varepsilon_2 = \varepsilon_3 = -3.33 \times 10^{-6}$$

and

$$\varepsilon_4 = \varepsilon_5 = \varepsilon_6 = 0.$$

From Hooke's law,

$$\sigma_i = C_{ij}\varepsilon_j$$

and

$$\sigma_1 = C_{11}\varepsilon_1 + C_{12}\varepsilon_2 + C_{13}\varepsilon_3.$$

The applied hydrostatic stress is (see p. 98)

$$\begin{aligned}\sigma_p = \sigma_1 &= (50 + 40 + 40)(-3.33)\,10^3 \text{ Pa} \\ &= -130 \times 3.33 \times 10^3 \text{ Pa} \\ &= -433 \text{ kPa}.\end{aligned}$$

Example 2.10

From the elastic stiffnesses for a cubic material, Nb ($C_{11} = 242$ GPa; $C_{12} = 129$ GPa; $C_{44} = 286$ GPa), find the elastic compliances.

The relationship between stiffnesses and compliances is given by the product of their two matrices, which is an identity matrix:

$$\begin{pmatrix} S_{11} & S_{12} & \ldots\ldots & S_{16} \\ S_{21} & S_{22} & \ldots\ldots & S_{26} \\ \vdots & & & \\ \vdots & & & \\ S_{61} & S_{62} & \ldots\ldots & S_{66} \end{pmatrix} \begin{pmatrix} C_{11} & C_{12} & \ldots\ldots & C_{16} \\ C_{21} & C_{22} & \ldots\ldots & C_{26} \\ \vdots & & & \\ \vdots & & & \\ C_{61} & C_{62} & \ldots\ldots & C_{66} \end{pmatrix} = (I).$$

For materials with cubic symmetry,

$$\begin{pmatrix} S_{11} & S_{12} & S_{12} & 0 & 0 & 0 \\ S_{12} & S_{11} & S_{12} & 0 & 0 & 0 \\ S_{12} & S_{12} & S_{11} & 0 & 0 & 0 \\ 0 & 0 & 0 & S_{44} & 0 & 0 \\ 0 & 0 & 0 & 0 & S_{44} & 0 \\ 0 & 0 & 0 & 0 & 0 & S_{44} \end{pmatrix} \begin{pmatrix} C_{11} & C_{12} & C_{12} & 0 & 0 & 0 \\ C_{12} & C_{11} & C_{12} & 0 & 0 & 0 \\ C_{12} & C_{12} & C_{11} & 0 & 0 & 0 \\ 0 & 0 & 0 & C_{44} & 0 & 0 \\ 0 & 0 & 0 & 0 & C_{44} & 0 \\ 0 & 0 & 0 & 0 & 0 & C_{44} \end{pmatrix} = (I).$$

All the off-diagonal terms of the identity matrix are zero. The diagonal terms are equal to 1.

Row 1 and column 1 give

$$S_{11}C_{11} + S_{12}C_{12} + S_{12}C_{12} = 1. \tag{1}$$

From row 6 and column 6, we have

$$S_{44}C_{44} = 1.$$

Therefore,

$$S_{44} = \frac{1}{C_{44}}.$$

Row 1 and column 2 yield

$$S_{11}C_{12} + S_{12}C_{11} + S_{12}C_{12} = 0. \tag{2}$$

From equations 1 and 2, we get, for row 1 and column 1,

$$S_{12} = \frac{-C_{12}}{C_{11}^2 + C_{11}C_{12} - 2C_{12}^2} = \frac{-C_{12}}{(C_{11} + 2C_{12})(C_{11} - C_{12})}. \tag{3}$$

Substituting Equation 3 into Equation 1 yields

$$S_{11} = \frac{1}{C_{11}} + \frac{2C_{12}^2}{C_{11}(C_{11} + 2C_{12})(C_{11} - C_{12})} = \frac{C_{11} + C_{12}}{(C_{11} + 2C_{12})(C_{11} - C_{12})}$$

Thus,

$$S_{44} = 3.5 \times 10^{-3}\ \text{GPa}^{-1},$$
$$S_{12} = -0.22 \times 10^{-2}\ \text{GPa}^{-1},$$
$$S_{11} = 0.66 \times 10^{-2}\ \text{GPa}^{-1}.$$

These values are fairly close to the values given in Table 2.4 (p. 112).

2.10 Elastic Properties of Polycrystals

The elastic constants of materials are determined by the bonding between the individual atoms. While monocrystals have the elastic properties dictated by the crystalline symmetry, most metals and ceramics are polycrystalline. In polycrystals, the properties are determined from the individual grains by an averaging process.

In a polycrystalline aggregate, the deformation of one grain is not independent of the deformation of its neighbor. The compatibility requirements are such that we have to apply either one of two simplifying assumptions:

1. The local strain is equal to the mean strain (all grains undergo the same strain); this is called the *Voigt average*. The Young's modulus and shear moduli can then be obtained from:

$$E = \sum E_i V_i \quad \text{and} \quad G = \sum G_i V_i,$$

where E_i, G_i and V_i represent the Young's modulus, shear modulus, and volume fraction, respectively, of grains of different orientations. One possible form attributed to Hill[5] is:

$$E = \frac{1}{5}\,(3F + 2G^* + H)$$
$$G = \frac{1}{5}\,(F + 4G^* - 2H)$$

where

$$F = \frac{1}{2}\,(C_{11} + C_{22} + C_{33}),$$
$$G^* = \frac{1}{3}\,(C_{12} + C_{23} + C_{13}),$$
$$H = \frac{1}{3}\,(C_{44} + C_{55} + C_{66}).$$

We use G^* instead of G to avoid confusion with shear modulus, G.

2. The local stress is equal to the mean stress (all grains are under the same stress); this is called the *Reuss average*: $\frac{1}{E} = \sum \frac{V_i}{E_i}$. This provides

[5] R. Hill, *Proc. Phys. Soc.*, A65 (1952) 349.

a lower bound. The inverse of the Young's modulus is then

$$\frac{1}{E} = \frac{1}{5}\left(3F' + 2G' + H'\right)$$

where: $F' = \frac{1}{3}\left(S_{11} + S_{22} + S_{33}\right),$

$$G' = \frac{1}{3}\left(S_{12} + S_{23} + S_{13}\right),$$

$$H' = \frac{1}{3}\left(S_{44} + S_{55} + S_{66}\right).$$

The actual stress and strain configuration is probably between the two assumptions. There are more advanced methods, such as the Hashin–Shtrikman upper and lower bound method; however, this will not be treated here. The above equation assumes a distribution of orientation of grains within the polycrystalline aggregate.

Example 2.11

Determine the Young's moduli along [100], [110], and [111] for copper, tungsten, and ZrO_2. We use Equation 2.20:

$$\frac{1}{E_{ijk}} = S_{11} - 2\left(S_{11} - S_{12} - \frac{1}{2}S_{44}\right) \times \left(l_{i1}^2 l_{j2}^2 + l_{j2}^2 l_{k3}^2 + l_{il}^2 l_{k3}^2\right).$$

The direction cosines are as follows:

	l_{i1}	l_{j2}	l_{k3}	$\left(l_{i1}^2 l_{j2}^2 + l_{j2}^2 l_{k3}^2 + l_{i1}^2 l_{k3}^2\right)$.
[100]	1	0	0	0
[110]	$\sqrt{2}/2$	$\sqrt{2}/2$	0	1/4
[111]	$1/\sqrt{3}$	$1/\sqrt{3}$	$1/\sqrt{3}$	1/3

The compliances for Cu and W are given in later in this chapter Table 2.4; Table 2.6 provides the stiffnesses for cubic ZrO_2. We have:

W	Cu
$S_{11} = 0.257 \times 10^{-2}$ GPa^{-1}	$S_{11} = 1.498 \times 10^{-2}$ GPa^{-1}
$S_{44} = 0.66 \times 10^{-2}$ GPa^{-1}	$S_{44} = 1.326 \times 10^{-2}$ GPa^{-1}
$S_{12} = -0.073 \times 10^{-2}$ GPa^{-1}	$S_{12} = -0.629 \times 10^{-2}$ GPa^{-1}

This yields

$$\text{Cu}: E_{100} = 66 \text{ GPa}, \quad E_{110} = 130 \text{ GPa}, \quad E_{111} = 191 \text{ GPa},$$

$$\text{W}: E_{100} = E_{110} = E_{111} = 389 \text{ GPa}.$$

For ZrO_2, we have to use the equations derived in Example 2.10 to obtain the elastic compliances:

$$C_{11} = 410 \text{ GPa}, \quad C_{12} = 110 \text{ GPa}, \quad C_{44} = 60 \text{ GPa},$$

$$S_{44} = \frac{1}{C_{44}} = 1.6 \times 10^{-2} \text{ GPa}^{-1},$$

$$S_{12} = \frac{-C_{12}}{(C_{11} + 2C_{12})(C_{11} - C_{12})} = -0.058 \times 10^{-2} \text{ GPa}^{-1},$$

$$S_{11} = \frac{1}{C_{11}} + \frac{C_{12}^2}{C_{11}(C_{11} + 2C_{12})(C_{11} - C_{12})} = 0.275 \times 10^{-2}\ \text{GPa}^{-1}.$$

These yield

$$E_{100} = 363.5\ \text{GPa}$$
$$E_{110} = 196.7\ \text{GPa},$$
$$E_{111} = 171\ \text{GPa}.$$

Example 2.12

Determine the elastic anisotropy ratios of Ag, Al, Cu, Ni, Fe, Ta, and W. Which one of these metals has the greatest dependence on orientation for Young's modulus? Which one has the smallest?

Solution: First, we have

$$A = \frac{2C_{44}}{C_{11} - C_{12}}.$$

From Table 2.3 (later on), we obtain the following results:

$$\text{Ag}: \quad A = \frac{46.1 \times 2}{124 - 93.4} = 3.01.$$
$$\text{Al}: \quad A = \frac{28.5 \times 2}{108.2 - 61.3} = 1.22.$$
$$\text{Cu}: \quad A = \frac{75.4 \times 2}{168.4 - 121.4} = 3.21.$$
$$\text{Ni}: \quad A = \frac{124.7 \times 2}{246.5 - 147.3} = 2.51.$$
$$\text{Fe}: \quad A = \frac{116.5 \times 2}{228 - 132} = 2.43.$$
$$\text{Ta}: \quad A = \frac{82.5 \times 2}{267 - 161} = 1.56.$$
$$\text{W}: \quad A = \frac{151.4 \times 2}{501.0 - 198} = 1.00.$$

Copper has the highest and W the lowest anisotropy ratio. Elastic properties should therefore be most orientation-dependent for Cu and orientation-independent for W.

Example 2.13

Determine the Young's modulus for polycrystalline iron, using Reuss's and Voigt's averages. From Tables 2.3 and 2.4, we get the elastic stiffnesses and compliances:

$$C_{11} = 228\ \text{GPa}, \quad S_{11} = 0.762 \times 10^{-2}\ \text{GPa}^{-1},$$
$$C_{44} = 116.5\ \text{GPa}, \quad S_{44} = 0.858 \times 10^{-2}\ \text{GPa}^{-1},$$
$$C_{12} = 312\ \text{GPa}, \quad S_{12} = -0.279 \times 10^{-2}\ \text{GPa}^{-1}.$$

Voigt method:

We first calculate the parameters, taking into account cubic symmetry:

$$F = \frac{1}{3}(C_{11} + C_{22} + C_{33}) = C_{11},$$

$$G^* = \frac{1}{3}(C_{12} + C_{23} + C_{13}) = C_{12},$$

$$H = \frac{1}{3}(C_{44} + C_{55} + C_{66}) = C_{44}.$$

Then:

$$E = \frac{1}{5}(3F + 2G^* = H) = \frac{1}{5}(3C_{11} + 2C_{12} + C_{44})$$

$$E = 186.5 \text{ GPa}.$$

Reuss method:

$$F' = \frac{1}{3}(S_{11} + S_{22} + S_{33}) = S_{11},$$

$$G' = \frac{1}{3}(S_{12} + S_{23} + S_{13}) = S_{12},$$

$$H' = \frac{1}{3}(S_{44} + S_{55} + S_{66}) = S_{44},$$

$$\frac{1}{E} = \frac{1}{5}\left(3F' + 2G' + H'\right) = \frac{1}{5}(3S_{11} + 2S_{12} + S_{44}),$$

$$= 0.517 \times 10^{-2}.$$

So

$$E = 193 \text{ GPa}.$$

2.11 Elastic Properties of Materials

Figure 2.12 presents a comparison of the elastic constants of different classes of materials. At the top, we have diamond (with covalent bonding). For metals, there is a correlation between the melting point (indicative of the bonding energy between atoms) and the Young's modulus. Thus, the metals with the highest bonding energies have the highest melting points, interatomic forces, and Young's modulus. The ranking of the metals in the second column of the figure shows this relationship; at the top are osmium and tungsten, and at the bottom is lead. The third column of the figure shows the polymers, which have elastic constants that are much lower than those of the metals. The composites in the last column show a wide variation in elastic constants. The carbon-fiber reinforced polymers (CFRPs) can have a very high modulus.

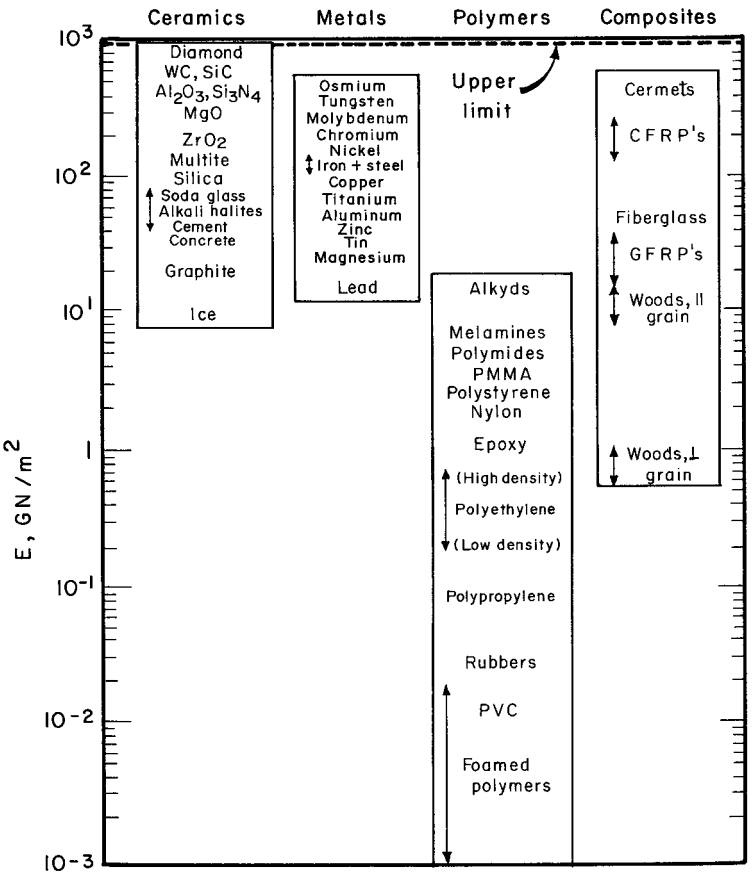

Fig. 2.12 Bar chart of data for Young's moduli. (Adapted from M. F. Ashby and D. R. H. Jones, *Engineering Materials* (Oxford: Pergamon Press, 1980), p. 32.)

2.11.1 Elastic Properties of Metals

Tables 2.3 and 2.4 give the elastic stiffnesses and compliances, respectively, of metallic monocrystals. One of the most complete compilations of elastic constants for crystals is that by Simmons and Wang. (See suggested reading.) The elastic constants for a number of polycrystalline metals are given in Table 2.5. We can also determine the polycrystalline (isotropic) elastic constants from the monocrystalline ones, using equations given earlier.

2.11.2 Elastic Properties of Ceramics

The elastic properties of ceramic monocrystals possess the symmetry of the crystal (see Table 2.6). As an example, consider the stiffnesses and compliances for MgO at room temperature. Magnesia is a cubic crystal, and alumina has the rhombohedral structure. The corresponding Young and shear moduli, computed along the three crystallographic axes of the monocrystal from Equation 2.20 are given in Table 2.7. Table 2.8 presents the elastic moduli for a number of ceramics and glasses. The largest elastic constant is that for diamond and is equal to 1,000 GPa. This is due to the C–C bonds, as is explained in Chapter 4.

Table 2.3 Elastic Stiffnesses of Monocrystals at Ambient Temperature (GPa)

Element	Structure	C_{11}	C_{44}	C_{12}	C_{33}	C_{66}	C_{13}	C_{14}
Ag	FCC	124.0	46.1	93.4				
Al	FCC	108.2	28.5	61.3				
Au	FCC	186.0	42.0	157.0				
Cu	FCC	168.4	75.4	121.4				
Ni	FCC	246.5	124.7	147.3				
Pb	FCC	49.5	14.9	42.3				
Fe	BCC	228.0	116.5	132.0				
Mo	BCC	460.0	110.0	176.0				
Ta	BCC	267.0	82.5	161.0				
W	BCC	501.0	151.4	198.0				
Co	HCP	307.0	75.3	165.0	358.1		103.0	
Zn	HCP	161.0	38.3	34.2	61.0		50.1	
Ti	HCP	162.4	46.7	92.0	180.7	69.0		
Be	HCP	292.3	162.5	26.7	336.4	14.0		
Zr	HCP	143.4	32.0	72.8	164.8	65.3		
Mg	HCP	59.7	16.7	26.2	61.7	21.7		
Sn	Tetragonal	73.5	22.0	23.4	87.0	22.6	28.0	
In	Tetragonal	44.5	06.6	39.5	44.4	12.2	40.5	
Hg	Rhombohedral	36.0	12.9	28.9	50.5		30.3	05.0

Table 2.4 Elastic Compliances for Monocrystalline Metals at Ambient Temperature (10^{-2} GPa^{-1})

Element	Structure	S_{11}	S_{44}	S_{12}	S_{23}	S_{13}
Ag	FCC	2.29	2.17	–0.983		
Al	FCC	1.57	3.51	–0.568		
Au	FCC	2.33	2.38	–1.065		
Cu	FCC	1.498	1.326	–0.629		
Ni	FCC	0.734	0.802	–0.274		
Pb	FCC	9.51	6.72	–4.38		
Fe	BCC	0.762	0.858	–0.279		
Mo	BCC	0.28	0.91	–0.078		
Nb	BCC	0.69	3.42	–0.249		
Ta	BCC	0.685	1.21	–0.258		
W	BCC	0.257	0.66	–0.073		
Be	HCP	0.348	0.616	–0.030	0.298	–0.031
Mg	HCP	2.20	6.1	–0.785	1.97	–0.50
Ti	HCP	0.958	2.14	–0.462	0.698	–0.189
Zr	HCP	1.013	3.13	–0.404	0.799	–0.241

The elastic moduli of ceramics are strongly dependent on porosity. Ceramics are porous owing to their fabrication, and one should be aware of the effect of porosity. Figure 2.13 shows the variations in the Young modulus of alumina with volume fraction of pores. For 10% porosity (a common value for commercial alumina), the Young's modulus is decreased by 20%.

The change in Young's modulus with porosity has been empirically expressed by Wachtman and MacKenzie,[6]

$$\boxed{E = E_0(1 - f_1 p + f_2 p^2)} \tag{2.22}$$

where p is the porosity and f_1 and f_2 are constants. For spherical voids, MacKenzie found that f_1 and f_2 are equal to 1.9 and 0.9, respectively, for a Poisson's ratio of 0.3. The data of Coble and Kingery[7] may be compared with the prediction of Equation 2.22. If one assumes the law of mixtures for the porosity, then, as a first approximation, one has

$$E = E_A(1 - f_B) + E_B f_B, \tag{2.23}$$

where f is the volume fraction of a phase and the subscripts A and B denote the two phases.

However, if phase B is the pore and denoting the pore fraction by p, one has

$$E = E_0(1 - p). \tag{2.24}$$

For relatively low porosity, the quadratic term in Equation 2.22 can be neglected, leaving

$$E = E_0(1 - 1.9p). \tag{2.25}$$

If E varied linearly with p, the form would be $E = E_0(1 - p)$. Thus, the physical significance of MacKenzie's equation is that porosity has an effect of E equal to approximately double the volume of pores.

Another effect of considerable importance on Young's modulus for ceramics is the presence of microcracks, which decrease the stored elastic energy and reduce the effective Young's modulus. Figure 2.14 shows schematically how the presence of microcracks would affect the slope of the stress–strain curve. The initial slope, E_0, is decreased by microcracking. Microcracks can also form during the cooling of the ceramic due to thermal expansion (or contraction) anisotropy. Different grains contract by different amounts along different orientations, resulting in a buildup of elastic stress in the boundary area. Elastic stress can generate microcracks. Similarly, the anisotropy of elastic constants can generate elastic stress concentrations at the grain boundaries, where the neighboring grains undergo different strains (due to differences in crystallographic orientation). The change in the Young's modulus with microcracking has been computed by a

[6] See J. B. Wachtman, in *Mechanical and Thermal Properties of Ceramics*, ed. J. B. Wachtman, NBS Special Publication 303, NBS Washington, 1963, p. 139; and J. K. MacKenzie, *Proc. Phys. Soc.*, B63 (1950) 2.

[7] R. L. Coble and W. D. Kingery, *J. Am. Cer. Soc.* 39 (1956) 377.

Table 2.5 | Elastic and Shear Moduli and Poisson Ratios for Polycrystalline Metals[a]

Metal (20°C)	E (GPa)	G (GPa)	ν
Aluminum	70.3	26.1	0.345
Cadmium	49.9	19.2	0.300
Chromium	279.1	115.4	0.210
Copper	129.8	48.3	0.343
Gold	78.0	27.0	0.440
Iron	211.4	81.6	0.293
Lead	16.0	5.5	0.450
Magnesium	44.7	17.3	0.291
Nickel	199.5	76.0	0.312
Niobium	104.9	37.5	0.397
Silver	82.7	30.3	0.367
Tantalum	185.7	69.2	0.342
Titanium	115.7	43.8	0.321
Tungsten	411.0	160.6	0.280
Vanadium	127.6	46.7	0.365

[a] Adapted with permission from R. W. Hertzberg, *Deformation and Fracture Mechanics of Engineering Material*, New York: John Wiley, 1976, p. 8.

Table 2.6 | Elastic Constants for Ceramics (S_{ij} in 10^{-10} Pa^{-1}; C_{ij} in GPa)

Material	C_{11}	C_{12}	C_{44}	C_{13}	C_{33}	S_{11}	S_{12}	S_{44}
MgO	289.2	88.0	154.6			4.03	−0.94	6.47
Al_2O_3	497.1	162.3	147.7	117	502			
ZrO_2	410	110	60					
$MgAl_2O_4$	279	153	153			5.83	−2.08	6.54
TiC	513	106	178	0.2	2.1	−0.36	5.61	
Diamond	1076	125	576					
LiF	112	46	63					
NaCl	49	13	13					
ThO_2	367	106	797			3.13	−0.70	12.5
LlO_2	395	121	64.1			2.96	−0.70	15.6
SiC (hexagonal)	500	186	168	176	521			
SiC (cubic)	352	140	233					

number of investigators. The formulations give predictions that vary with the orientation of the cracks with respect to the tensile axis, among other parameters. An expression developed by Salganik[8] is

$$\boxed{\frac{E}{E_0} = \left[1 + \frac{16(10 - 3\nu_0)(1 - \upsilon_0^2)}{45(2 - \nu_0)} N a^3\right]^{-1} = \left(1 + AN a^3\right)^{-1}}, \qquad (2.26)$$

[8] R. L. Salganik, *Izv. Akad. Nauk SSR Mekh. Tverd. Tela*, 8 (1973) 149.

Table 2.7 Orientation Dependence of Young's Modulus and Shear Modulus for MgO and Al_2O_3 at 25 °C

Crystal Orientation	Young's Modulus, Al_2O_3 (GPa)	Young's Modulus, MgO (GPa)	Shear Modulus, MgO (GPa)
<100>	299	248.2	154.6
<110>	330	316.4	121.9
<111>	344	348.9	113.8

where E is the Young's modulus of the cracked ceramic, v_0 and E_0 are, respectively, Poisson's ratio and Young's modulus of the uncracked material, a is the radius of a mean crack, and N is the number of cracks per unit volume. The factor

$$A = \frac{16(10 - 3v_0)(1 - v_0^2)}{45(2 - v_0)} \tag{2.27}$$

varies between 1.77 and 1.5 when v_0 varies between 0 and 0.5. To a first approximation, one can say that

$$\frac{E}{E_0} = [1 + 1.63\ Na^3]^{-1}. \tag{2.28}$$

O'Connell and Budiansky arrived at a slightly different expression:[9]

$$\frac{E}{E_0} = 1 - \frac{16(10 - 3v)(1 - v^2)}{45(2 - v)} f_s. \tag{2.29}$$

Here, f_s is defined as the volume fraction of cracks. (i.e., the number of cracks per unit volume, N, multiplied by the cube of the mean crack radius, a^3) and v is Poisson's ratio of the porous material, which is related to Poisson's ratio of the fully dense material by

$$v = v_0\left(1 - \frac{16 f_s}{9}\right). \tag{2.30}$$

By applying the same approximation as in Salganik's equation, we arrive at

$$\boxed{\frac{E}{E_0} = 1 - 1.63\ Na^3.} \tag{2.31}$$

Note that Na^3 is a measure of the fraction of the material that is under the effect of the cracks. Figure 2.15 shows the effect of microcracks on the Young's modulus of alumina. This effect is substantial. For $f_s = 0.1$, the Young's modulus is reduced by 20%. Both Salganik's and O'Connell and Budiansky's predictions are plotted, and it can be seen that they are in fairly close agreement for values of f_s smaller than 0.1. For higher values, O'Connell and Budiansky's equation predicts a more rapid decrease in E.

[9] R. J. O'Connell and B. Budiansky, *J. Geol. Res.* 79 (1974) 5412.

Table 2.8 | Modulus of Elasticity of Some Ceramic Materials

Material	E (GPa)
Aluminum oxide crystals	378
Sintered alumina*	365
Alumina porcelain (90–95% Al_2O_3)	365
Sintered beryllia	310
Hot-pressed boron nitride*	82.7
Hot-pressed boron carbide*	289
Graphite*	9
Sintered magnesia*	210
Sintered molybdenum silicide*	406
Sintered spinel*	238
Dense silicon carbide (cubic or hexagonal)	280–510
Sintered titanium carbide*	310
Sintered stabilized zirconia*	152
Silica glass	72.3
Vycor glass	72.3
Pyrex glass	68.9
Superduty fire-clay brick	96.4
Magnesite brick	172.2
Bonded silicon carbide**	345
Silicon nitride	320–365
Aluminum nitride	
Mullite (aluminosilicate) porcelain	69
Steatite (magnesia aluminosilicate)	69
Diamond	450–650
Tungsten carbide	400–530
Cobalt/tungsten carbide cermets	379
Titanium dioxide	290
Titanium diboride	440

* (c. 5% porosity).
** (c. 20% porosity).
Adapted from W. D. Kingery, H. K. Bowen, and D. R. Uhlmann, Introduction to Ceramics, 2nd ed., (New York: John Wiley, 1976) p. 3.

2.11.3 Elastic Properties of Polymers

Polymers have elastic constants that range from the lower end of the metallic elastic constants to values even lower by several orders of magnitude. As an example, melamines have elastic constants of 6–7 GPa (E (lead) $=$ 14 GPa), while the elastic constant of polymeric foams is between 3 and 10 MPa. Table 2.9 lists the elastic constants of a number of polymers. The bar chart of Figure 2.12 provides a comparison of the elastic constants of the different classes of materials. The elastic behavior of polymeric materials is more difficult to describe than that of metals or ceramics, because it is strongly dependent on both temperature and time. This behavior, called *viscoelastic* or *anelastic*, is described separately in Section 2.12. Here we merely introduce the

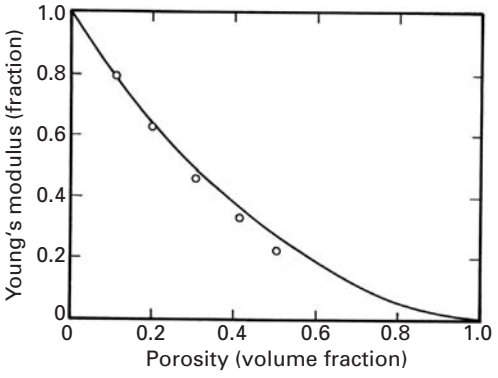

Fig. 2.13 Effect of porosity on elastic modulus of alumina. Circles represent experimental measurements. (After R. L. Coble and W. D. Kingery, *J. Am Ceram. Soc.*, 39 (1956) 377.)

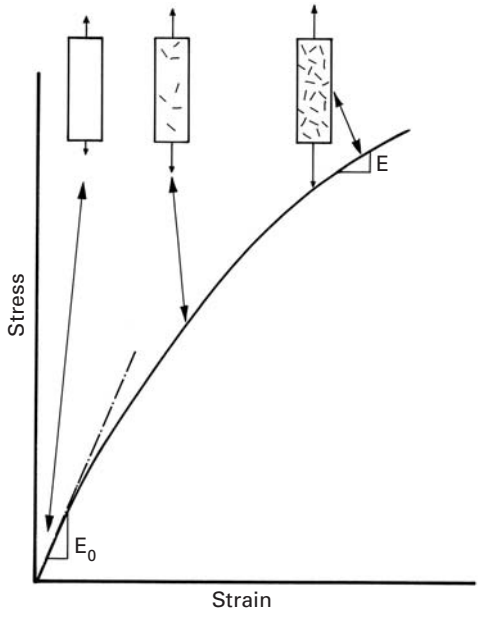

Fig. 2.14 Effect of microcracks on Young's modulus for ceramics.

subject briefly. In most polymers, there are dramatic changes in E between 20°C and 200°C; for most metals and ceramics, the changes in E in this range can be neglected. The glass transition temperature T_g plays an important role in polymers. Above T_g, E is considerably low, and the behavior of the polymer can be described as rubbery and viscous. Below T_g, the modulus of elasticity is considerably higher, and the behavior is closer to linear elastic. Figure 2.16 shows schematically the elastic behavior of a linear polymer as a function of temperature. The modulus of elasticity ranges from 10^3 to 10^{-1} MPa.

2.11.4 Elastic Constants of Unidirectional Fiber Reinforced Composite

An orthotropic material has three mutually perpendicular axes of symmetry, which reduces the number of independent elastic

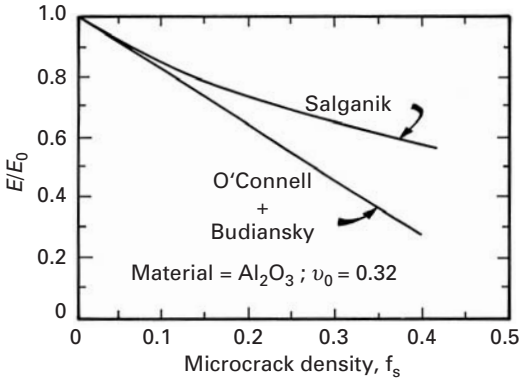

Fig. 2.15 Comparison of predictions of Young's modulus.

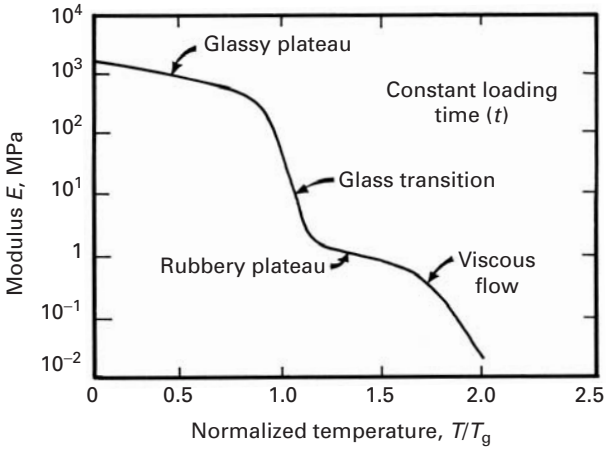

Fig. 2.16 Schematic variation in the modulus of elasticity of a linear polymer with temperature.

constants to nine. The S_{ij} matrix for an orthotropic material is:

$$S_{ij} = \begin{bmatrix} S_{11} & S_{12} & S_{13} & 0 & 0 & 0 \\ & S_{22} & S_{23} & 0 & 0 & 0 \\ & & S_{33} & 0 & 0 & 0 \\ & & & S_{44} & 0 & 0 \\ & & & & S_{55} & 0 \\ & & & & & S_{66} \end{bmatrix}$$

The compliance matrix for orthotropic materials in terms of E, G, and ν corresponds to:

$$S_{ij} = \begin{bmatrix} 1/E_1 & -\nu_{21}/E_2 & -\nu_{31}/E_3 & 0 & 0 & 0 \\ & 1/E_2 & -\nu_{32}/E_3 & 0 & 0 & 0 \\ & & 1/E_3 & 0 & 0 & 0 \\ & & & 1/G_{23} & 0 & 0 \\ & & & & 1/G_{13} & 0 \\ & & & & & 1/G_{12} \end{bmatrix}$$

Table 2.9 Elastic Constants of Some Polymers[a]

Material	E (GPa)
Phenolformaldehyde	8
Melamines	6–7
Polymides	3–5
Polyesters	1.3–4.5
Acrylics	1.6–3.4
Nylon	2–4.5
PMMA	3.4
Polystyrene	3–3.4
Polycarbonate	2.1
Epoxies	2.1–5.5
Polypropylene	1.2–1.7
Polyethylene, high-density	0.15–0.24
Foamed polyurethane	0.01–0.06
Polyethylene, low-density	0.15–0.24
Rubbers	0.01–0.1
PVC (unplasticized)	2.4–3.0
Foamed polymers	0.001–0.01

[a] Adapted from M. F. Ashby and D. R. H. Jones, *Engineering Materials* (Oxford: Pergamon Press, 1986), p. 31, Table 3.1.

Notice that there are three different Young's moduli on three perpendicular planes, three shear moduli, and three Poisson's ratios. Thus, we have nine elastic constants, as in the stiffness matrix.

Unidirectionally fiber reinforced composites represent a special case of orthotropy. The plane transverse to the fibers is isotropic, see Figure 2.17. Such a material is called transversely isotropic and has five independent elastic constants. The compliance matrix for such unidirectionally fiber reinforced composite is:

$$S_{ij} = \begin{bmatrix} S_{11} & S_{12} & S_{13} & 0 & 0 & 0 \\ & S_{11} & S_{13} & 0 & 0 & 0 \\ & & S_{33} & 0 & 0 & 0 \\ & & & S_{44} & 0 & 0 \\ & & & & S_{44} & 0 \\ & & & & & 2(S_{11} - S_{12}) \end{bmatrix}$$

In terms of the elastic constants E, G, and ν, the elastic compliance matrix for a transversely isotropic material is represented as:

$$S_{ij} = \begin{bmatrix} 1/E_1 & -\nu_{21}/E_1 & -\nu_{31}/E_3 & 0 & 0 & 0 \\ & 1/E_1 & -\nu_{31}/E_3 & 0 & 0 & 0 \\ & & 1/E_3 & 0 & 0 & 0 \\ & & & 1/G_{13} & 0 & 0 \\ & & & & 1/G_{13} & 0 \\ & & & & & \frac{2}{E_1}(1 - \nu_{21}) \end{bmatrix}.$$

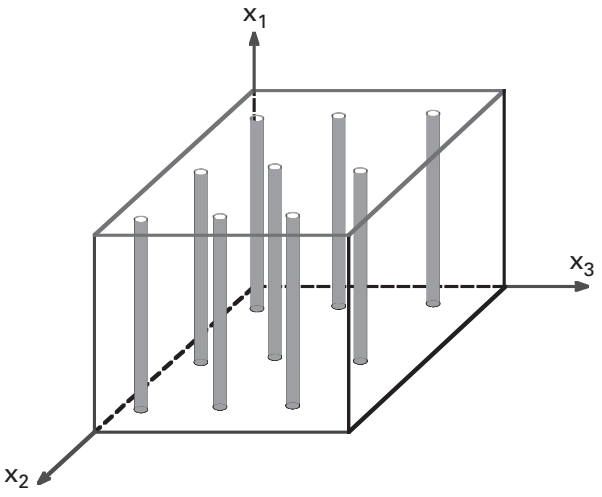

Fig. 2.17 A transversely isotropic fiber composite. The plane transverse to fibers (x_2–x_3 plane) is isotropic.

Notice that there are two Young's moduli, one for any direction in the transverse plane and one for the fiber direction. There are two Poisson's ratios and one shear modulus. Thus, we have five elastic constants.

Another example of a transversely isotropic material is a laminate composite. The elastic properties perpendicular to the plane of the layers are different than in the layer plane.

There are many examples of laminate composites used in everyday life, for example, plywood and cardboard. GLARE is a laminate composed of alternate layers of aluminum and glass fibers in an epoxy matrix. It is used in the aircraft industry, specifically in the Airbus A380 superjumbo jet. The laminate structure gives it excellent fatigue resistance because the cracks are arrested at the interface. Another laminate, ARALL, consists of alternate aluminum and aramid fibers in an epoxy matrix.

Figure 2.18 gives the elastic constants for the titanium (20%)–titanium aluminide (80%) laminate. The Young's moduli E_{11} $(=1/S'_{11})$ and E_{22} $(=1/S'_{22})$ were transformed according to orientation β. Their variation can be seen in Figure 2.18. Likewise, Poisson's ratios ν_{21} and ν_{31} vary with orientation.

2.12 Viscoelasticity

Glasses or amorphous materials show the phenomenon of time-dependent strain, called *viscoelasticity* or *anelasticity*. The deformation of an amorphous material does not involve atomic displacements on specific crystallographic planes, as is the case in crystalline metals. Rather, a continuous displacement of atoms or molecules takes place with time at a constant load. This flow mechanism of noncrystalline

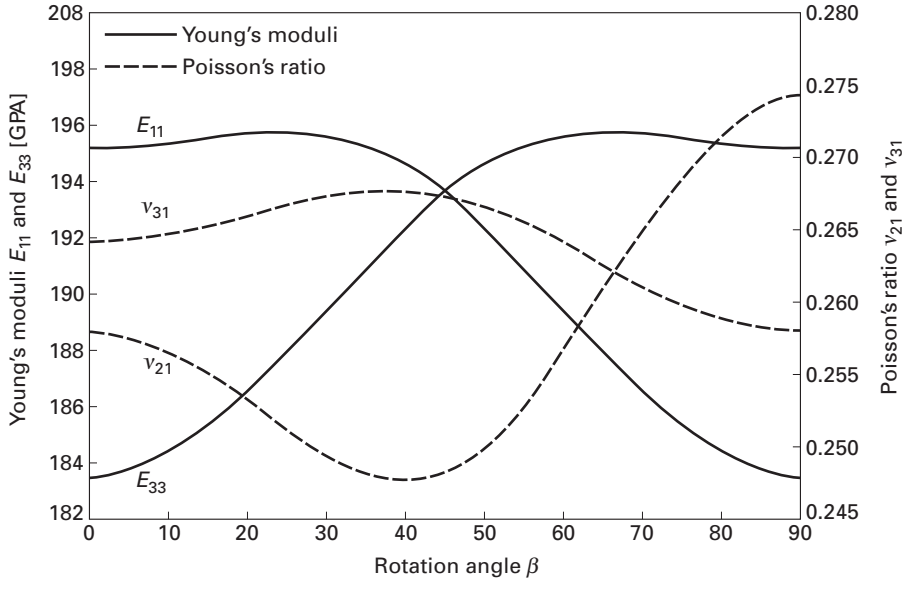

Fig. 2.18 Elastic constants of 20% Ti–80% Al_3Ti laminate composite as a function of angle β with laminate plane. (Adapted from T. Li, F. Grignon, D. Benson, K. S. Vecchio, E. Olevsky, C. F. Jiang, and M. A. Meyers, *Mater. Sci. Eng.*, A374 (2004) 10.)

materials is associated with the diffusion of atoms or molecules within the material; that is, it is a thermally activated process and is thus described by an Arrhenius-type equation. Of course, at sufficiently high temperatures, where diffusion becomes important, crystalline as well as amorphous materials show a large amount of thermally activated plastic flow. Liquids and even fluids in general show a characteristic resistance to flow called *viscosity*. The viscosity of a fluid results in a frictional energy loss, which appears as heat. The more viscous a fluid, the higher is the frictional energy loss.

Over a range of temperatures, the viscosity η can be described by the Arrhenius-type relationship

$$1/\eta = A\exp(-Q/RT), \tag{2.32}$$

or

$$\boxed{\eta = A\exp(Q/RT),}$$

where Q represents the activation energy for the atomic or molecular process responsible for the viscosity, R is the universal gas constant, and T is the temperature in kelvin. The S. I. units of the viscosity η are Nm^{-2} s or $Pa \cdot s$. Another common unit of viscosity is poise, P; 1 P = 0.1 $Pa \cdot s$.

A purely viscous material shows stress proportional to strain rate. Thus, if we apply a shear stress τ to a glassy solid above its glass

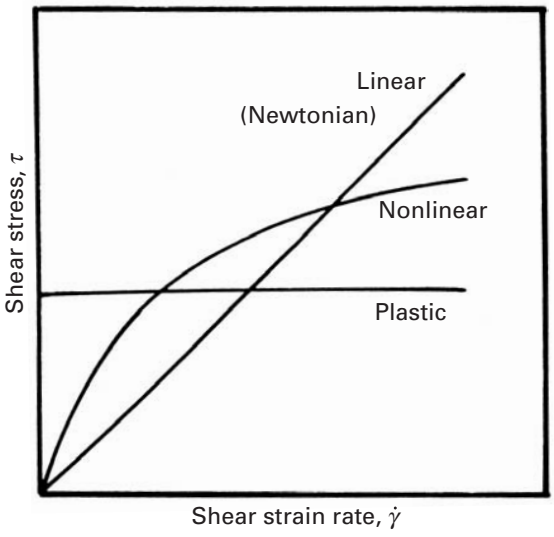

Fig. 2.19 Linear or Newtonian response (stress proportional to deformation rate), nonlinear response, and plastic response (stress independent of deformation rate).

transition temperature, then we can write, for the rate of shear deformation,

$$\dot{\gamma} = \frac{d\gamma}{dt} = \frac{\tau}{\eta} = \phi\tau, \tag{2.33}$$

where ϕ is the *fluidity* (the reciprocal of viscosity) of the material.

Equation 2.33 can be written as

$$\boxed{\tau = \eta\dot{\gamma}.} \tag{2.34}$$

If the viscosity of a material does not change with the strain rate (i.e., if the stress is linearly proportional to the strain rate), then we call the viscosity a *Newtonian viscosity* and such a material a *Newtonian material*. Figure 2.19 shows a Newtonian (or linear) response curve. If the stress is not directly proportional to the strain rate, we have a non-Newtonian response, which can be written as

$$\tau = \eta\dot{\gamma}^n. \tag{2.35}$$

This is shown by the curve marked "nonlinear" in the figure. If the stress is independent of the strain rate, we have a plastic material. A special case is that of a material whose viscosity decreases when subjected to high strain rates. Such a material is called a *thixotropic* material, a good example of which is a latex paint. When we apply the paint to a vertical wall, it does not sag, because its viscosity is very high on the wall. However, we can stir and brush the paint easily because its viscosity decreases when subjected to shear stress in the stirring action.

Polymers, polymer solutions and dispersions, metals at very high temperatures, and amorphous materials (organic and inorganic) show viscoelastic behavior – that is, characteristics intermediate between perfectly elastic and perfectly viscous behavior. Commercial

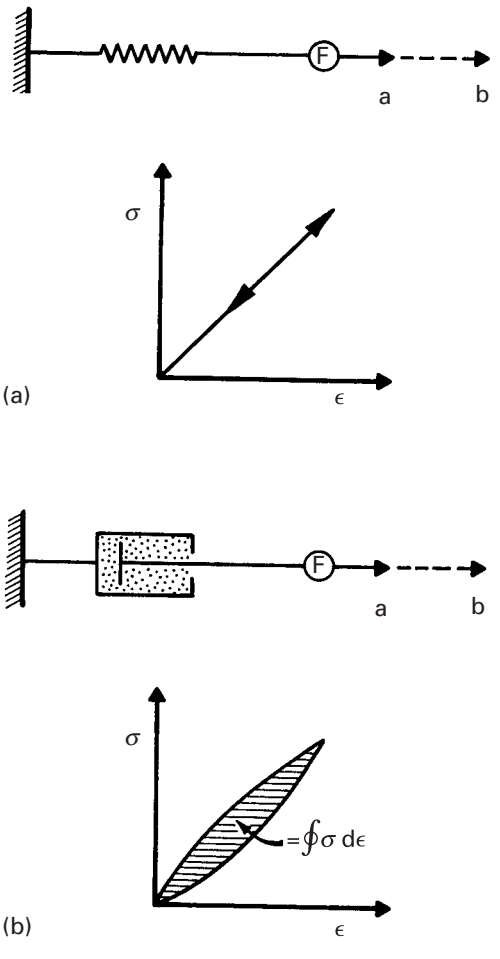

Fig. 2.20 Stress–strain plots for (a) elastic behavior (no energy is lost during a load–unload cycle) and (b) viscoelastic behavior (energy equal to the shaded area is lost in a load–unload cycle).

silica-based glasses have a high proportion of additives: about 30% in soda–lime glass and 20% in high-temperature glasses such as Pyrex. The main purpose of the additives is to lower the viscosity by breaking up the silica network, thus making the processing of glass easy.

Conventionally, glasses are formed by melting an appropriate composition and then casting or drawing the melt into a desired form. It is interesting to compare the viscosity values of liquid metals with glasses. Molten metals have about the same viscosity as that of water ($\sim 10^{-3}$ Pa·s) and transform to a crystalline solid state in a discontinuous manner when cooled. The viscosity of glasses, however, falls slowly and continuously with temperature. The shaping of glass is carried out in the viscosity range of 10^3–10^6 Pa·s. Polymers are formed in the range 10^3–10^5 Pa·s. Perhaps the most important characteristic of a viscoelastic material is that its rheological properties are dependent on time. This characteristic is manifested very markedly by amorphous or noncrystalline materials such as polymers.

A viscoelastic substance has a viscous and an elastic component. Figure 2.20(a) shows the stress–strain curve of an ideal elastic material. The load and unload curves are the same, and the energy lost as

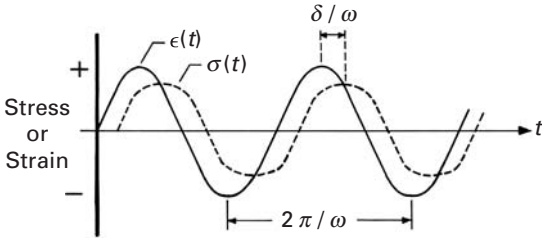

Fig. 2.21 Viscoelastic response of material with time lag between stress and strain.

heat per cycle is zero in this case. In practice, there is always present an anelastic (i.e., a time-dependent) component, with the result that the unload curve does not in fact follow the load curve. Energy equal to the shaded area in Figure 2.20(b) is dissipated in each cycle. This phenomenon is exploited in damping out vibrations. Some polymers and soft metals (e.g., lead) have a high damping capacity. In springs and bells, a high damping capacity is undesirable. For such applications, one uses materials such as bronze, spring steel, etc., which have a low damping capacity.

2.12.1 Storage and Loss Moduli

In order to characterize the viscoelastic behavior of a material, the material is sinusoidally deformed, and the resulting stress is recorded. For an ideal elastic material, the stress and strain are *in phase*, and the phase shift $\delta = 0$. For an ideal viscous material, the stress and strain are 90° *out of phase* (i.e., $\delta = 90^\circ$). As pointed out before, a viscoelastic behavior – a combination of an ideal elastic response and an ideal viscous response – is more common. Figure 2.21 shows a viscoelastic response with a phase lag between the stress and the strain. Dynamic (commonly sinusoidal) perturbations are used to study the viscoelastic behavior of a material. The material is subjected to an oscillatory strain with frequency ω. From the figure, we can write the following expressions for strain and stress:

$$\epsilon = \epsilon_0 \sin \omega t,$$
$$\sigma = \sigma_0 \sin (\omega t + \delta).$$

In the equation for stress, δ is the phase angle or phase lag between the stress and strain. From these expressions, we can define two moduli,

$$E' = \left(\frac{\sigma_0}{\epsilon_0}\right) \cos \delta$$

and

$$E'' = \left(\frac{\sigma_0}{\epsilon_0}\right) \sin \delta,$$

where E' is the tensile storage modulus and E'' is the tensile loss modulus.

Alternatively, we can use complex variables and write

$$\epsilon = \epsilon_0 \exp i (\omega t),$$

$$\sigma = \sigma_0 \exp i(\omega t + \delta),$$
$$E = \frac{\sigma}{e} = \frac{\sigma_0}{\epsilon_0} \exp i\delta = \frac{\sigma_0}{\epsilon_0}(\cos\delta + i\sin\delta)$$
$$= E' + iE'',$$

where i is the imaginary number $\sqrt{-1}$.

Figure 2.22 shows graphically the relationship among these quantities. Proceeding in a manner similar to that for deriving the tensile modulus, we can obtain the shear modulus. (Experimentally, this is generally obtained by means of a torsion pendulum.) The complex modulus

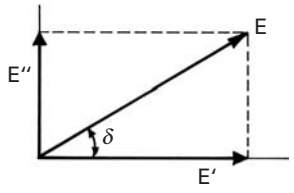

Fig. 2.22 Relationship between tensile storage and tensile loss modulus.

$$G = G' + iG'',$$

where G' is the shear storage modulus and G'' is the shear loss modulus. The storage modulus is a measure of the stored energy, i.e., the elastic part. The loss modulus is a measure of the energy lost as heat, i.e., the viscous part. These two modulus components can be written in terms of the phase shift as

$$G'' = G\sin\delta, \quad E'' = E\sin\delta,$$
$$G' = G\cos\delta, \quad E' = E\cos\delta.$$

We can now define a term called the *loss tangent* as follows:

$$\text{Loss tangent} = \tan\delta = \frac{\text{energy loss}}{\text{energy stored}} = \frac{G''}{G'} = \frac{E''}{E'}.$$

Sometimes, a related term called the *logarithmic decrement* Δ is used, which is defined as

$$\text{Logarithmic decrement } \Delta = \pi\tan\delta = \frac{\pi E''}{E'}.$$

The logarithmic decrement is the natural logarithm of the amplitude ratio between successive vibrations; that is,

$$\Delta = \frac{\theta_n}{\theta_{n+1}},$$

where θ_n and θ_{n+1} are the amplitudes of two successive vibrations.

Both the loss tangent and the logarithmic decrement are proportional to the ratio of the maximum energy dissipated per cycle to the maximum energy stored in the cycle.

Example 2.14

In a free-vibration test, a polymer showed a drop of 50% in two successive amplitudes. Compute the logarithmic decrement for this polymer.

Solution: If θ_n and θ_{n+1} are the successive amplitudes, then the logarithmic decrement, $\Delta = \ln(\theta_n/\theta_{n+1}) = \ln 2 = 0.69$.

Example 2.15

Recall that the stress–strain relationship involving real and imaginary moduli is given by

$$\sigma = \left(E' + iE''\right)\varepsilon = E\varepsilon.$$

Derive an expression for the complex modulus E in terms of E' and tan δ. Show that for small values of tan δ, $E \approx E'$.

Solution: The magnitude of the complex modulus is given by

$$E = \frac{\sigma}{\varepsilon} = \left(E'^2 + E''^2\right)^{1/2} = E'\left[1 + \tan^2\delta\right]^{1/2}.$$

For tan $\delta < 0.2$, E will be within 2% of E'.

2.13 Rubber Elasticity

A polymeric molecule is generally not rigid like a straight rod, although there are some special liquid crystal polymers that do have a rigid, rodlike molecule (e.g., the aramid fibers). Barring these special cases, the polymeric molecule is a very long and flexible chain that can change form easily because many independent vibrations and rotations of the individual atoms that compose the molecular chain are possible. Long, flexible polymeric chains can change their configuration and lengths rather easily when a stress is applied. When the number of configurations available is very large and the chains are cross-linked to form a network, we get a special polymer called an *elastomer*. Elastomers characteristically show very high reversible, nonlinear extensions (5–700%) in response to an applied stress. The requirement of cross-linking (i.e., the existence of a network) is established to avoid chains slipping past one another in a *permanent* manner. This process is called 'vulcanization' of rubber and is accomplished by adding sulfur. High chain mobility is also required. Glassy and crystalline polymers will not have enough chain mobility, and therefore, the reversible strains are not very large. In crystalline materials such as metals and ceramics, the deformation involves a change in equilibrium interatomic distance, which requires the application of rather large forces. This is why the elastic modulus values of metals and ceramics are very high.

The first law of thermodynamics says that the internal energy of a system is given by

$$dU = dQ + dW, \tag{2.36}$$

where dQ is the heat absorbed and dW is the work done on the system by the surroundings. Also, for a reversible process, we can write, from the second law of thermodynamics,

$$dQ = T\,dS \tag{2.37}$$

and

$$dW = F\,dl - P\,dV, \tag{2.38}$$

where T is the temperature, V is the volume, P is the external pressure, S is the entropy, and F is the tensile force causing a change in the length ℓ.

From Equations 2.36 and 2.38, we get the following for the internal energy:

$$dU = T\,dS + F\,d\ell - P\,dV.$$

For conditions of constant temperature and volume, we can write

$$\begin{aligned} F &= \left(\frac{\delta U}{\delta \ell}\right)_{T,V} - T\left(\frac{\delta S}{\delta \ell}\right)_{T,V} \\ &= F_e + F_s, \end{aligned} \tag{2.39}$$

where F_e is the energy contribution and F_s is the entropy contribution to the tensile force.

In the case of crystalline metals, the first term in Equation 2.39 is predominant, while the second term is negligible. This is because the crystalline structure of a metal remains essentially unchanged with deformation. Such is not the case with amorphous polymers, especially the polymers that are rubberlike and which show rather large elastic deformations. On deforming these kinds of polymers, the form of the molecular chains can change considerably, and the entropy contribution $F_s = -T(\delta S/\delta \ell)_{T,V}$ becomes considerably large (see Figure 2.23). In fact, the first term (i.e., the energy term) in Equation 2.39 is equal to zero for an ideal rubbery material. The rubber elasticity thus has its origins in the entropy effects. For such polymers, one can write an expression for the entropy of the form

$$S = k \ln p$$

where k is Boltzmann's constant and p is the probability of finding a particular chain configuration for which the entropy effects will be very important.

When an elastomer is stretched, the distance between cross-linked points increases and the number of possible chain configurations decreases. Consider a piece of rubber in the form of a cube. Let the side of the cube be ℓ_o, as shown in Fig. 2.24(a). Then, the volume of rubber before deformation or undeformed volume is equal to $\ell_o{}^3$. Let us now deform the rubber cube in direction 1. The rubber gets elongated in direction to ℓ_1 and the two transverse directions get shortened to ℓ_2 and ℓ_3. The volume of the cube after deformation is equal to $\ell_1\,\ell_2\,\ell_3$. In order to describe the large deformations involved in stretching rubbery materials, we define strain in terms of a parameter called draw ratio, λ = final length/original length. Thus, we can write for the draw ratio along direction 1,

$$\lambda_1 = \ell_1/\ell_o,$$

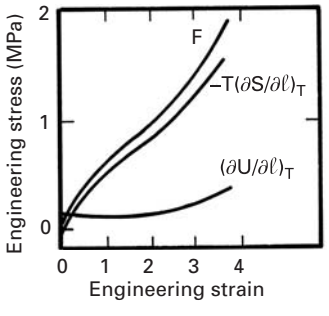

Fig. 2.23 Changes in internal energy, U, and entropy, S, accompanying the extension of rubber. F is the sum of the two contributions.

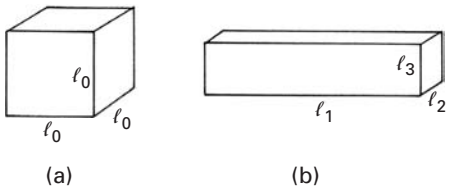

Fig. 2.24 Deformation at constant volume. (a) Unstrained state. (b) Strained state.

or,

$$\ell_1 = \lambda_1 \ell_o.$$

We remind the reader that $\lambda = 1 + \varepsilon$.

Elastomeric materials are treated as incompressible materials, i.e., constancy of volume condition holds. Also, taking the strains in the transverse directions to be equal, i.e., $\ell_2 = \ell_3$, we can write

$$\ell_1 \ell_2 \ell_3 = (\lambda_1 \ell_o)\ell_2^2 = \ell_o^3, \tag{2.40}$$

or,

$$\ell_2 = \ell_3 = \ell_o / \sqrt{\lambda_1} \tag{2.41}$$

Thus, the tensile force applied to the rubber cube in direction 1 leads to draw ratios λ_1, λ_2, and λ_3 along directions 1, 2, and 3, respectively. Rearranging Equation 2.41

$$\lambda_2 = \lambda_3 = 1/\sqrt{\lambda_1}. \tag{2.42}$$

Flexible polymeric chains are joined by bonds at cross-link points, forming a network. When we stretch a rubber or elastomer, these chains get stretched. The number of configurations available to a stretched polymer is less than the number of configuratons available to an unstretched polymer, i.e. *the entropy is reduced on stretching*. We need to use statistics to to treat the properties of a single polymeric chain and those of a network of chains. We assume the polymeric chain is freely jointed and has no volume (it is called *volumeless*). One end of the chain is at the origin while the other end is at a distance, r, from the origin; r is called the end-to-end distance of the chain. The chain is assumed to be freely jointed and volumeless. The network is treated as a Gaussian network, i.e. a Gaussian distribution function is used to evaluate the probability of finding the other end of the chain in some volume element, dV $(= dx \cdot dy \cdot dz)$.

Let the end-to-end distance of a chain be r_1. We consider a polymer chain with an end fixed at the origin and the other end at the extremity of the vector r_1, whose magnitude is:

$$r_1 = \left(x^2 + y^2 + z^2\right)^{1/2}.$$

Assuming that the polymer chain follows "random walk" statistics, it can be shown that the distribution of lengths, r, follows a Gaussian distribution. This provides a bell-shaped curve for the distribution of

r. The probability that end-to-end distance is r_1 is given by:

$$P_1(r_1) = \frac{\beta^3}{\pi^{1/2}} \exp\left(-\beta^2 r_1^2\right) = \frac{\beta^3}{\pi^{1/2}} \exp\left(-\beta^2\left(x^2 + y^2 + z^2\right)\right).$$

The parameter β is related to the number of monomers (units), n, in the chain and to their length, a:

$$\beta = \frac{(1.5)^{1/2}}{n^{1/2}a}.$$

This comes from Gaussian statistics, and the intelligent student will readily consult his/her old class notes.

When a cube of rubber is deformed, it becomes a parallelepiped, as shown in Figure 2.24. Internally, the coordinates of the end-to-end vector of a typical flexible chain change from x, y, and z to $\lambda_1 x$, $\lambda_2 y$, $\lambda_3 z$, respectively. The new probability of finding the end of a chain is equal to:

$$P_2(r_2) = \frac{\beta}{\pi^{1/2}} \exp\left[-\beta^2\left(\lambda_1^2 x^2 + \lambda_2^2 y^2 + \lambda_3^2 z^2\right)\right].$$

The ratio of probabilities corresponding to the initial and deformed states can be expressed as:

$$\frac{P_2(r_2)}{P_1(r_1)} = \exp\left\{-\beta^2\left[\left(\lambda_1^2 - 1\right)x^2 + \left(\lambda_2^2 - 1\right)y^2 + \left(\lambda_3^2 - 1\right)z^2\right]\right\}.$$

We assume that $x = y = z$. This leads to a mean value r_0, equal to:

$$r_0(x^2 + y^2 + z^2)^{1/2} = 3^{1/2}x = 3^{1/2}y = 3^{1/2}z$$

Thus:

$$\frac{P_2(r_2)}{P_1(r_1)} = \exp -\beta^2\left(\lambda_1^2 + \lambda_2^2 + \lambda_3^2 - 3\right)\frac{r_0^2}{3}.$$

The entropy change for one molecular chain associated with the deformation is defined by:

$$\Delta S = k \ln \frac{P_2(r_2)}{P_1(r_1)}.$$

Inserting the expression for the ratio between the probabilities:

$$\Delta S = -k\beta^2\left(\lambda_1^2 + \lambda_2^2 + \lambda_3^2 - 3\right)\frac{r_0^2}{3}.$$

The value of $r_0\left(= n^{1/2}a\right)$ and that of β can be substituted, yielding:

$$\Delta S = -\frac{k}{2}\left(\lambda_1^2 + \lambda_2^2 + \lambda_3^2 - 3\right).$$

The entropy change for N chains is given by

$$\Delta S = -\frac{1}{2}Nk\left(\lambda_1^2 + \lambda_2^2 + \lambda_3^2 - 3\right) \tag{2.43}$$

where N is the number of chains and k is the Boltzmann's constant. Substituting Equation 2.42 into Equation 2.43, we can write for the change in entropy as

$$\Delta S = -\frac{1}{2}Nk\left(\lambda_1^2 + 2\lambda_1^{-1} - 3\right) \tag{2.44}$$

Recall that Equation 2.39 gives the expression for the tensile force causing a change in length of a rubber or elastomer. It has two components: an energy contribution and an entropic contribution. As explained above, the energy contribution, $(\delta U/\delta \ell)$ is negligible for rubber for isothermal deformation. So,

$$F = -T\left(\delta S/\delta \ell\right)_{T,V}. \tag{2.45}$$

Differentiating Equation 2.44 and substituting into Equation 2.45, we obtain

$$F = \frac{NkT}{\ell_o}\left(\lambda_1 - \lambda_1^{-2}\right) \tag{2.46}$$

If we divide the tensile force by the area of cross section, we get the tensile stress. Recall that the volume remains unchanged, i.e., $A_1\ell_1 = A_o\ell_o$. Thus,

$$\sigma = \frac{F}{A_1} = \frac{NkT}{\ell_o}\left(\frac{\ell_1}{A_o\ell_o}\right)\left(\lambda_1 - \lambda_1^{-2}\right) \tag{2.47}$$

Let us denote the number of chain segments per unit volume $(N/A_o\ell_o)$ by n and recall that $\ell_1/\ell_o = \lambda_1$; then we write

$$\boxed{\sigma = nkT\left(\lambda_1^2 - \lambda_1^{-1}\right)} \tag{2.48}$$

In Equation 2.48, the strength of the rubber is seen to increase with n, the number of chain segments per unit volume. The more cross-linked the polymer, the greater the number of segments and the smaller the length of molecule from one cross-link to the next. Thus, Equation 2.48 correctly predicts the strengthening of rubber with increasing cross-linking.

Equation 2.48 also shows a linear dependence of stress, at a given strain, on temperature. This follows from the dominance of the entropic elasticity. Any deviation from this linear relationship between stress and temperature of a rubbery or elastomeric materials can be taken as a measure of its deviation from thermodynamic ideal behavior. For an ideal rubbery behavior, the energetic component of force is zero. Also, the stress is not linearly dependent on strain, i.e., the Hooke's law is not obeyed in tension for an elastomer. Up to ~400% strain, the theoretical stress–strain curve is in quite good accord with experimental values as shown in Figure 2.25. At very large strains, i.e., at strains > 400% ($\lambda = 5$) secondary bonds form between the partially aligned chains, i.e., strain induced crystallization occurs. At such large strain values, the chains begin to align

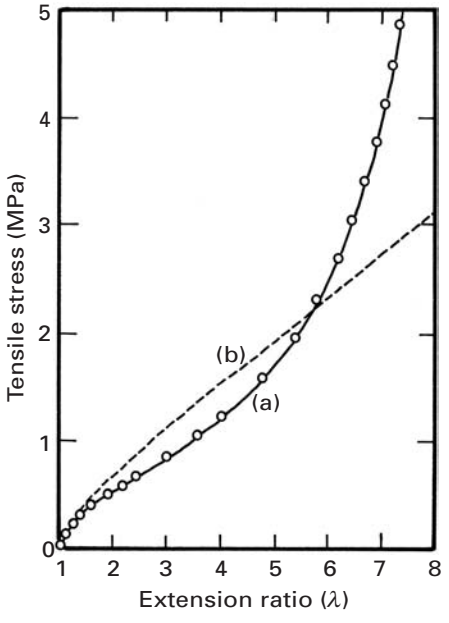

Fig. 2.25 Force–extension curve for cross-linked rubber. (a) Experimental. (b) Theoretical. (After L. R. G. Treloar, *The Physics of Rubber Elasticity*, 3d ed. (Oxford: Clarendon Press, 1975), p. 87.)

themselves and stretching of the primary bonds in the chain becomes important.

Because the tensile stress–strain curve of rubber is nonlinear, Young's modulus cannot be defined for rubber, as it can be for crystalline metals and ceramics. One can, however, define a secant modulus at a given strain. Another important thing that a perceptive reader may have noticed is that the number of network chains per unit volume and, correspondingly, the modulus of an elastomer increases as the degree of cross-linking increases. This is as expected if we just compare a lightly cross-linked rubber band with a highly cross-linked bowling ball.

For metals, the ordered crystalline structure is retained during elastic deformation. Thus, the entropy, which is a measure of disorder (or randomness) is constant. On the other hand, the internal energy is increased by the work of deformation, which is stored in the metal as elastic energy.

In rubbers, the chains become more aligned with stretching. This decreases the entropy of the stsyem. The internal energy, on the other hand, is constant.

2.14 Mooney–Rivlin Equation

The treatment given above is based on what is called Gaussian network theory. Well before that, in the 1940s, Mooney[10] derived the

[10] M. Mooney, *J. Appl. Phys.*, 11 (1940) 582.

following equation, based on a phenomenological continuum mechanics model of rubber elasticity:

$$\boxed{\sigma = 2\left(C_1 + \frac{C_2}{\lambda}\right)\left(\lambda - \frac{1}{\lambda^2}\right)'}$$

where C_1 and C_2 are constants (not to be confused with WLF constants discussed in Chapter 13) This equation is referred to as Mooney–Rivlin equation in the literature because of later contributions from Rivlin and Saunders.[11] They formulated the material law as a strain energy function in terms of the first and second principal invariants of the deformation. The formulation is called a strain energy function as the energy is conserved during deformation of these materials under constant temperature. It seems to describe well the deformation of highly elastic bodies which are incompressible (volume is conserved during deformation) and isotropic (the material has the same mechanical properties in all directions at a material point).

The above expression can be rearranged to the following form:

$$\frac{\sigma}{2\left(\lambda - \frac{1}{\lambda^2}\right)} = \left(C_1 + \frac{C_2}{\lambda}\right).$$

A plot of:

$$\frac{\sigma}{2\left(\lambda - \frac{1}{\lambda^2}\right)} \quad \text{against} \quad \left(C_1 + \frac{C_2}{\lambda}\right),$$

called Mooney plot, would give a straight line of slope C_2 and an ordinate of $(C_1 + C_2)$ at $1/\lambda$.

The Mooney–Rivlin equation or its modification by Ogden[12] are commonly used in Finite Element Method codes for elastomeric materials.

Example 2.16

Make a schematic plot of the internal energy and entropy as a function of strain for a crystalline solid (e.g., a metal) and for a rubbery solid (e.g., an elastomer). Make a drawing showing the structure before and after deformation in the two cases.

[11] R. S. Rivlin and D. W. Saunders, *Philosophical Transactions of the Royal Society of London, Series A*, 243 (1951) 251–288.

[12] R. W. Ogden, *Rubber Chemistry and Tech.*, 59 (1986) 386.

Solution: Figure E2.16 shows the requested plots.

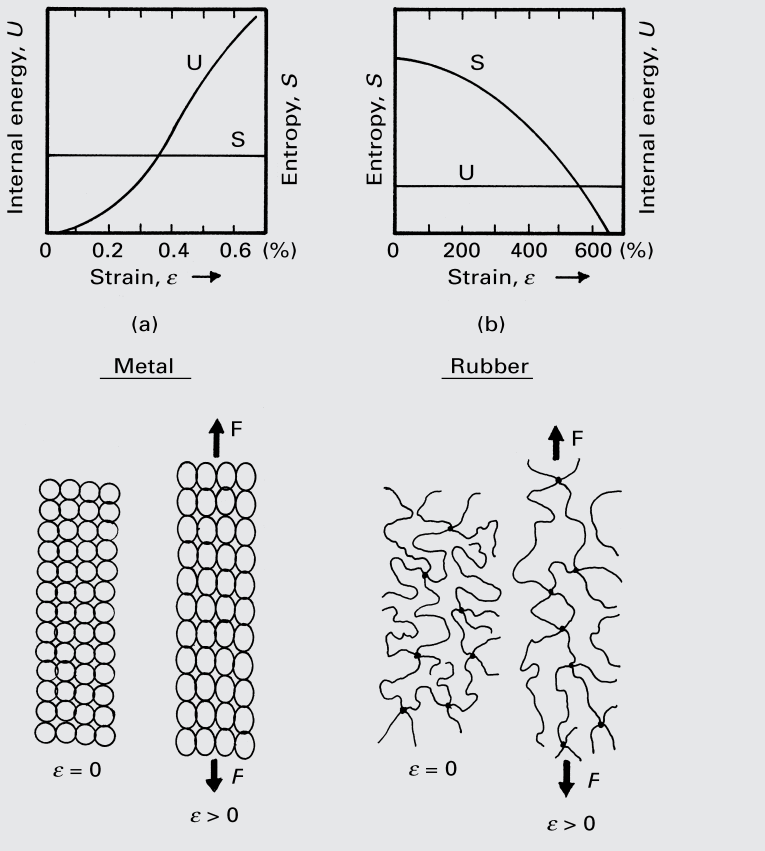

Fig. E2.16

Example 2.17

It is frequently said that elastic deformation on loading and the recovery of strain on unloading involves the stretching of atomic bonds. Would this statement be true of the large elastic deformation that is observed in rubbery, or elastomeric, materials?

Solution: No. The large elastic deformation observed in elastomeric materials involves the *uncoiling* of randomly coiled polymeric chains. When we deform an elastomeric material, the end-to-end distance of the chains increases. When the material is unloaded, the chains return to the original random configuration. This uncoiling of chains results in the entropy effects discussed in the text. Such entropy effects are insignificant in metals and other nonelastomeric materials.

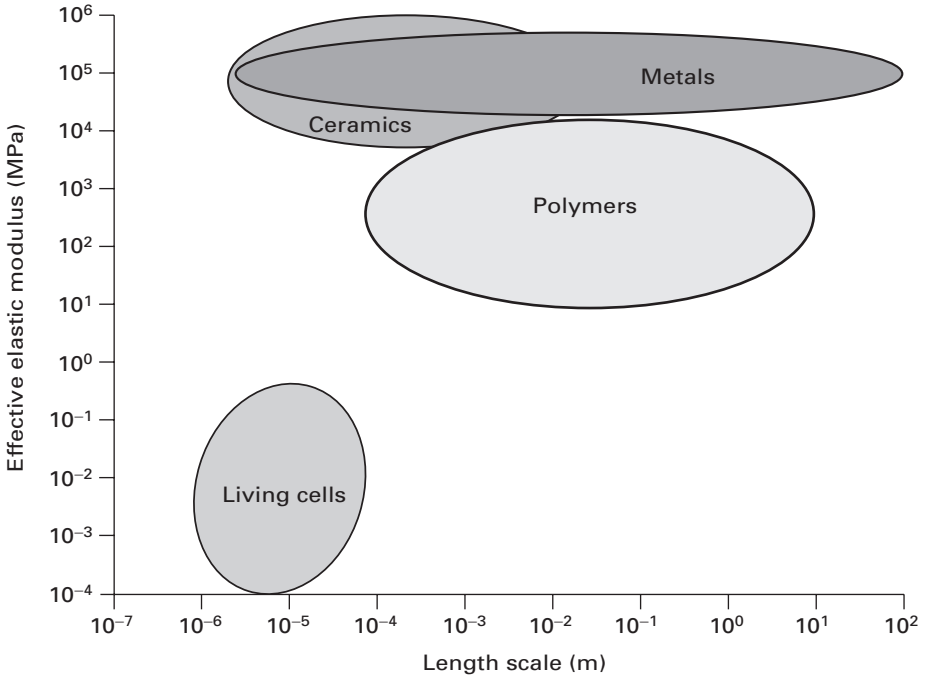

Fig. 2.26 Range of elastic moduli of biological cells and conventional materials. (After G. Bao and S. Suresh, *Nature Materials*, 2 (2003) 715.)

2.15 Elastic Properties of Biological Materials

Biological materials have complex elastic properties. Soft tissues exhibit nonlinear elasticity. Hard tissues, such as bone, have a linear elastic response conditioned by their density. Figure 2.26 gives an idea of the range of elastic properties of soft biological materials (in this case, living cells) compared to conventional materials. It is interesting to note the elastic moduli of cells are low compared to conventional structural materials by a factor of $\sim 10^4$. This is an extreme but illustrates the differences. We give in the following sections two examples of the elastic behavior of materials that occur in our body: blood vessels and cartilage.

2.15.1 Blood Vessels

The vascular system provides the transport of nutrients, oxygen, and other chemical signals to the various parts of the body. The vascular system is divided into two subsystems: the pulmonary and the circulatory system. We will not go into any details of the pathology of these two subsystems. We will concentrate on their mechanical properties. Arteries (which carry blood from the heart to the various parts of the body) and veins (that collect blood back to the heart) exhibit some significant differences in structure. Arteries are exposed to higher pressures and fluctuations associated with the diastolic and systolic portions of the cardiac cycle. Figure 2.27 shows the longitudinal and

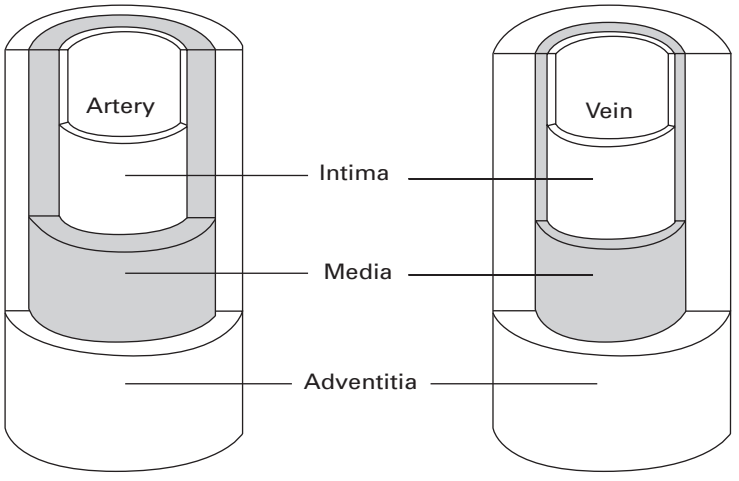

Fig. 2.27 Cross section of an artery and vein, composed of the endothelium, tunica intima, tunica media, and tunica adventitia.

normal sections of an artery. The structure is layered with three distinct regions: tunica intima (innermost), tunica media (middle), and tunica adventitia (outermost).

Bursting (longitudinal splitting) of blood vessels or aneurysm (tensile instability forming a local bulge) are highly undesirable but all too frequent events in humans. There are two unique aspects of the mechanical response of arteries and veins that are instrumental in minimizing the chance of the aforementioned problems: nonlinear elasticity and residual stresses.

Nonlinear Elasticity

The three layers comprising blood vessels have different functions and composition. Table 2.10 summarizes the similarities and differences between arteries and veins, including main vessels such as the aorta. The composition of arteries is made up primarily of elastic fibers (elastin), collagen, and smooth muscle. Compared to veins, arteries contain much more elastic material. Thicker arteries, such as the aorta, contain less smooth muscle than both smaller arteries and also veins. These differences account for the ability of arteries to resist large pressure fluctuations during the cardiac cycle.

The mechanical response of blood vessels is shown in Figure 2.28(a). This is the longitudinal stress–strain response of human vena cava. The response is nonlinear elastic. We know that it is elastic because on unloading the artery returns to its original dimension. However, there is a slight hysteresis on loading and unloading, due to viscoelastic processes. We know that it is nonlinear because the slope of the curve increases with strain. This slope approaches infinity as the strain approaches 0.3. This increase in slope is due to the extension of the collagen and elastin fibers. If they are stretched beyond this point, failure takes place. Instead of the strain, ε, the stretch ratio ($\lambda = \varepsilon + 1$) is often used.

It is instructive to plot the slope, $d\sigma/d\varepsilon = E$, as a function of stress. This is done in Figure 2.28(b) for the aorta of a dog (circumferential strip). The slope first increases by a relationship that can be described

Table 2.10 | Dimensions and composition of blood vessels

Vessel	Dimensions	Composition
Artery	*Aorta* Vessel diameter, 25 mm Thickness, 2 mm	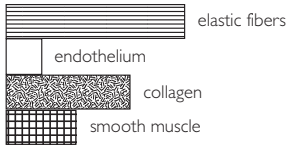
	Medium-sized artery Vessel diameter, 4 mm Thickness, 1 mm	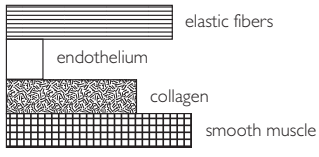
Vein	Vessel diameter, 20 mm Thickness, 1 mm	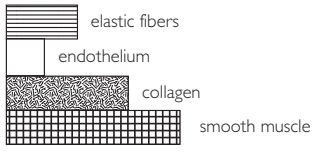

by a power function. Then, it reaches a linear range, in which the increase is more gradual. This nonlinear elastic behavior is a characteristic feature of many soft tissues in the human body. It serves as an important function: as the pressure in the blood vessels is increased, the vessels become stiffer.

This response, typical of arteries, has been successfully represented by the Fung equation:

$$\sigma = (\sigma^* + \beta)e^{\alpha(\varepsilon - \varepsilon^*)} - \beta,$$

where α andβ are parameters defined in Figure 2.28(b). α is the slope of the linear portion and β is related to the intercept. σ^* and ε^* correspond to the onset of the linear portion. This equation can also be expressed in terms of λ, the stretch ratio.

Residual Stresses

Biological materials such as arteries contain residual stress. In the case of a segment of artery that is not under internal blood pressure, the walls of the artery are under strain and therefore have residual stress. Fung[13] has shown that if one makes an axial cut in the wall of an artery, the artery will spontaneously open. This geometry is known as the zero-stress state. The angle by which the artery springs open is defined as the opening angle. As this opening angle increases the stress distribution in the wall becomes more uniform. This makes sense since under normal blood pressure arteries inflate, causing higher strain on the inner wall of the artery (compared to the

[13] Y. C. Fung, *Biomechanics* (New York: Springer, 1993).

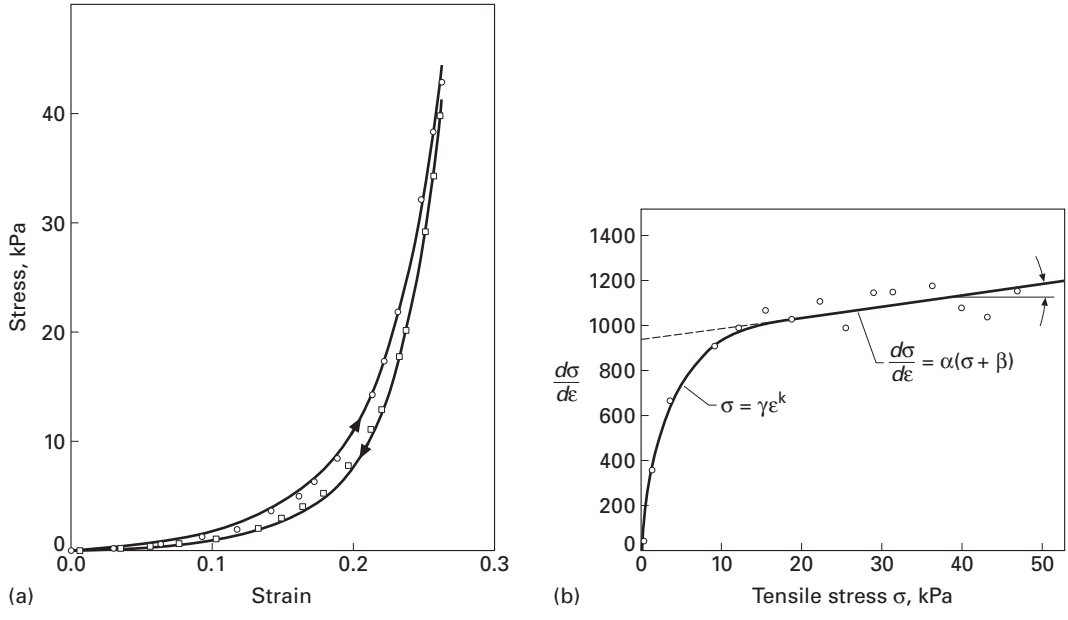

Fig. 2.28 (a) Stress–strain response of human vena cava: circles – loading; squares – unloading. (Adapted from Y. C. Fung, *Biomechanics* (New York: Springer, 1993), p. 366.) (b) Representation of mechanical response in terms of tangent modulus (slope of stress–strain curve) vs. stress. (Adapted from Y. C. Fung. *Biomechanics*, New York: Springer, 1993), p. 329.)

outer wall). In arteries, stress is an exponential function of strain, so the observed increase in strain at the inner wall will be accompanied by an increase in stress at the inner wall. This is shown in Figure 2.29. Four different arteries, with different zero-stress angles, are shown: $\alpha = 0$, 10, 70, and 155°. For the same arteries, the wall stresses at two values of the applied internal pressure are shown. For zero pressure, there is a detrimental effect on the stress distribution. However, this is not the critical condition. For 100 mm Hg internal pressure (in the range of pressure of blood inside our body), the artery with the highest value of α has the lowest stress in the wall. Thus, the residual stress reduces the maximum stress in the artery walls.

2.15.2 Articular Cartilage

Articular cartilage, which covers the ends of long bones and bones within synovial joints, is a highly hydrated connective tissue. It consists of two distinct phases: a solid phase made up of collagen, proteoglycans (aggrecan), proteins, and chondrocytes and a liquid phase composed of water and electrolytes. Aggrecan and collagen are primary components of the solid phase, or extracellular matrix, and are responsible for the biomechanical properties (compressive and tensile, respectively) of articular cartilage. Figure 2.30 shows a schematic

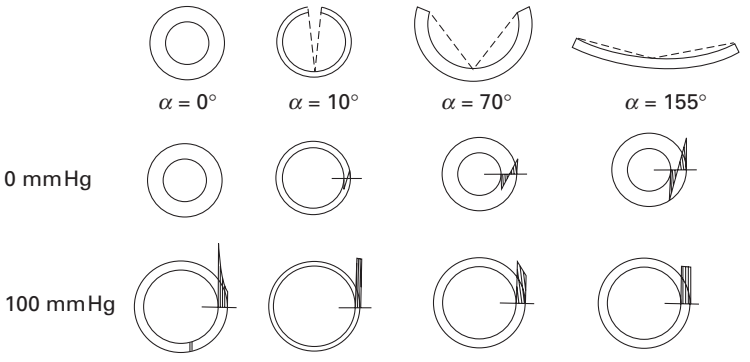

Fig. 2.29 Residual stresses in arteries; the artery is sliced longitudinally and the angle α is measured. (From Y. C. Fung, *Biomechanics* (New York: Springer, 1993), p. 389.)

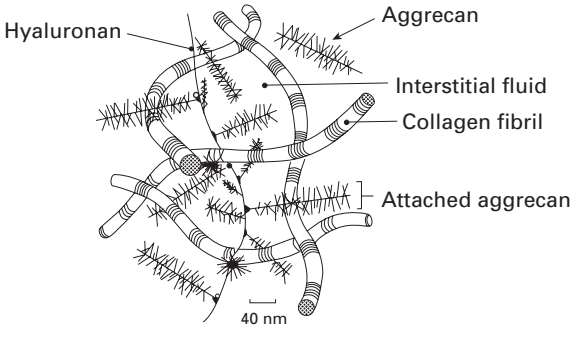

Fig. 2.30 Schematic of aggrecan–collagen meshwork in cartilage tissue. (After V. C. Mow and A. R. Ratcliffe, Structure and Function of Articular Cartilage and Meniscus, In *Basic Orthopedic Biomechanics*, ed. V. C. Mow and W. C. Hayes (New York: Raven Press, 1997), pp. 113–178.)

of the aggrecan–collagen meshwork in cartilage tissue. The characteristic banded structure of collagen is shown (coral snake-like).

Cartilage is a low friction, weight-bearing, viscoelastic material which distributes stresses generated by translational and rotational motion to the underlying bone. It possesses a stratified architecture made of distinct zones – superficial, middle, and deep. Figure 2.31(a) shows these regions. At the surface, the collagen is arranged parallel to the surface. The chondrocites are elongated along the surface. In the middle zone, which comprises between 40 and 60% of the cartilage, the chondrocites are dispersed in a matrix of collagen. The deep zone is composed of spheroidal chondrocites in columnar arrays. The collagen fibers are of large diameter and are arranged perpendicular to the bone. The last zone and interface with the bone consists of calcified cartilage. The chondrocites are round and less organized. The cartilage can be considered, from a materials viewpoint, as a gradient material, since the properties and structure vary in a continuous fashion. Figure 2.31(b) shows the mesostructure of human cartilage. The four regions drawn schematically in Figure 2.31(a) are seen in Figure 2.31(b).

The mechanical properties of articular cartilage depend very much on the orientation of the collagen fibrils. At the surface of cartilage, collagen fibrils are oriented parallel to the surface. Therefore, it is not surprising to find that under tension samples from the superficial zone are very strong. This is directly due to collagen content and orientation. Figure 2.32 shows that the cartilage is much stronger

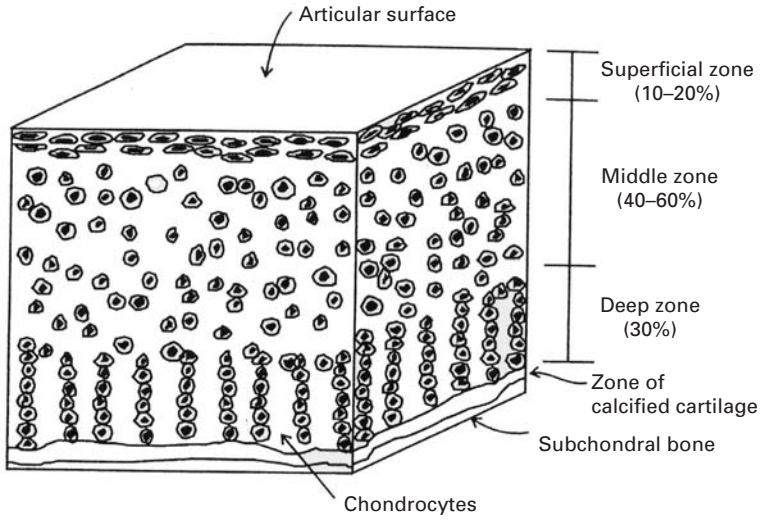

Fig. 2.31 (a) Mesostructure of cartilage (consisting of four zones) showing differences in structure as a function of distance from surface; the bone attachment is at bottom. (From G. L. Lucas, F. W. Cooke, and E. A. Friis, *A Primer on Biomechanics* (New York: Springer, 1999), p. 273.) (b) Cross-section of human cartilage showing regions drawn schematically in (a). (Courtesy of K. D. Jadin and R. I. Sah.)

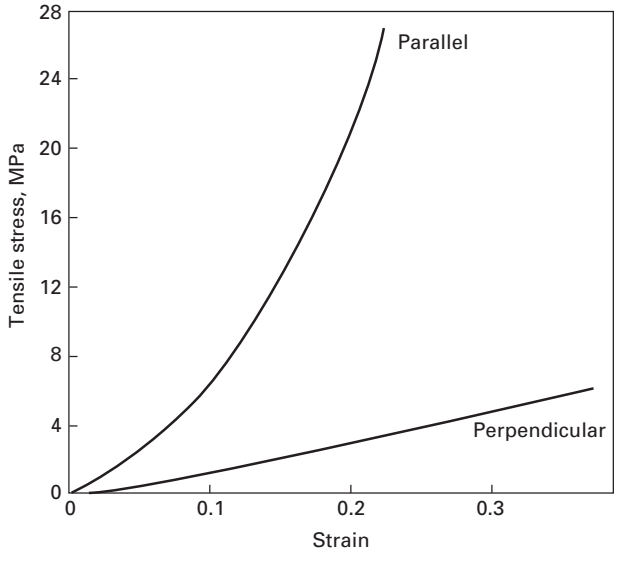

Fig. 2.32 Stress–strain curve for samples from the superficial zone of articular cartilage. Samples were cut parallel and perpendicular to collagen fiber orientation. (From G. E. Kempson, Mechanical Properties of Articular Cartilage. In *Adult Articular Cartilage*, ed. M. A. R. Freeman (London: Sir Isaac Pitman and Sons Ltd., 1973), pp. 171–228.)

parallel to the surface than perpendicular to it. When cartilage begins to degenerate, due to age and/or excessive exercise (load), defects may form. The stiffness of cartilage is approximately 1/20 of that of subchondral cancellous bone and 1/60 of that of cortical bone. Unfortunately, cartilage does not have capacity to repair itself. For this

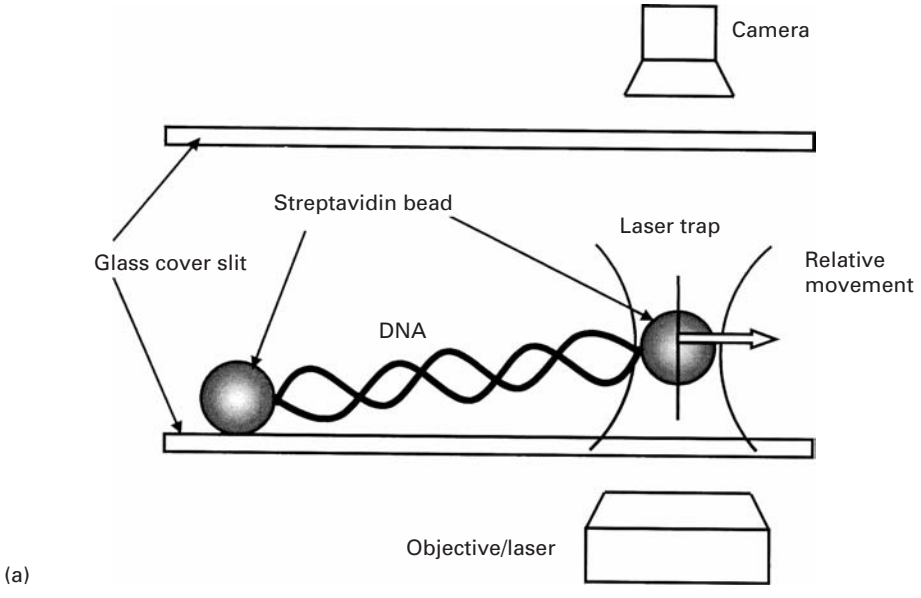

(a)

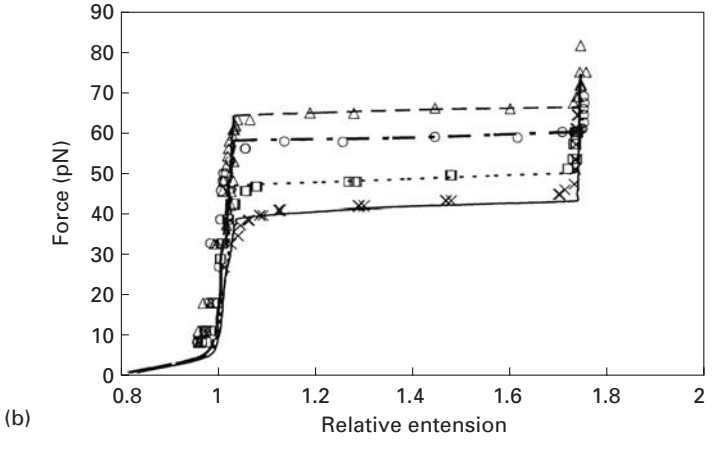

(b)

Fig. 2.33 (a) Schematic of the optical trap setup for the stretching of a double-stranded DNA molecule. (b) Plots of stretching force against relative extension of the single DNA molecule at increasing (from bottom to top curves) concentrations of salt. (Courtesy of C. T. Lim, National Singapore University.)

reason, along with the large numbers of people affected by joint- and arthritis-related ailments, tissue engineering alternatives are explored as an option for repairing cartilage defects.

2.15.3 Mechanical Properties at the Nanometer Level

Figure 2.33 shows the degree of miniaturization that can be attained with modern methods to establish the mechanical properties of biomaterials. It is possible to stretch single strands of DNA. This is accomplished by using a contraption called optical (laser) tweezer, shown in Fig. 2.33(a). Microsized beads are attached to the DNA strand, one end

is fixed and the other, trapped in the optical tweezer, is pulled. The mechanical response of the DNA is definitely nonlinear, Figure 2.33(b). There is a plateau at a force varying from 40 to 65 pN (depending on the concentration of NaCl). At this plateau, the strand can receive a stretch of up to 1.8. Beyond this value, the DNA stiffness increases considerably. These results show that salinity has a definite effect on DNA mechanical properties.

Example 2.18

Calculate the stress on the femur (a) with and (b) without a total hip replacement prosthesis (see Figure E2.18(a)). Assume that the cross-sectional diameter of the femur is equal to 3 cm and that of the implant is 1.5 cm. (c) What would you do to improve the situation?

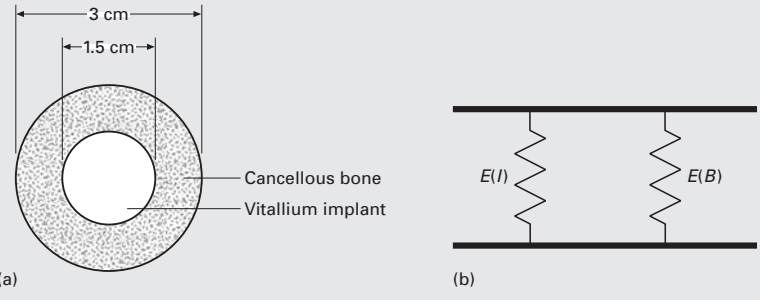

Fig. E2.18

Given:

Weight = 1000 N (100 kg),
E_I = 210 GPa,
E_B = 20 GPa,

where E_I and E_B are the moduli of the implant and bone, respectively.

Solution:

(a) In the presence of the implant, we can consider the situation analogous to two springs in parallel, as shown in Figure E2.18(b). For two springs in parallel (the analog for a bone joined to the implant stem), the strains are equal:

$$\varepsilon_I = \varepsilon_B,$$

where ε_I and ε_B are the strains in the implant and bone, respectively. The elastic deformation of bone and implant can be expressed as:

$$\frac{\sigma_B}{E_B} = \varepsilon_B$$

and

$$\frac{\sigma_I}{E_I} = \varepsilon_I.$$

The areas are:

$$A_B = \pi \times \left[\left(\frac{3}{2}\right)^2 - \left(\frac{1.5}{2}\right)^2 \right] \times 10^{-4} = 5.3 \times 10^{-4}\ m^2$$

and

$$A_I = 1.76 \times 10^{-4}\ m^2.$$

The total load is

$$P_T = P_I + P_B = \sigma_I A_I + \sigma_B A_B.$$

But:

$$\frac{\sigma_B}{E_B} = \frac{\sigma_I}{E_I};$$

Thus:

$$\sigma_B = \left(\frac{A_I}{E_B} E_I + A_B \right) = P_T$$

$$\sigma_B = \frac{P_T}{\left(\frac{A_I}{E_B} E_I + A_B \right)} = 0.42 \times 10^6\ N/m^2.$$

(b) In the absence of implant,

$$\sigma_B = \frac{1000}{\pi \left[\left(\frac{3}{2}\right)^2 - \left(\frac{1.5}{2}\right)^2 \right] 10^{-4}} = \frac{1000}{5.301 \times 10^{-4}} = 1.89 \times 10^6\ N/m^2.$$

It can be seen that the stresses in the bone are significantly reduced by the introduction of the implant: they are one-fourth of the original stresses. This has a deleterious effect on the bone growth and leads to weakening of the implant.

(c) One solution would be to develop a metallic foam with a Young's modulus of 20 GPa. This would have the added advantage of enabling bone growth into the implant. However, the strength of this stem would be severely reduced.

Example 2.19

From the curves (Figure E2.19) reporting the force–strain response of human skin along the direction of loading (extension) and perpendicular to it (lateral contraction) determine the in-plane Poisson's ratio at 20, 40, and 60 N.

What can you conclude from the results?

Solution: We can see that the behavior of the skin is nonlinear elastic, with the slope increasing with load.

Poisson's ratio is defined as:

$$\upsilon = -\frac{\varepsilon_{lat}}{\varepsilon_{lon}},$$

where ε_{lat} is the lateral strain and ε_{lon} is the longitudinal strain The following values are obtained from Figure E2.19:

$$(P = 20\ N)\nu = 0.81,$$
$$(P = 40\ N)\nu = 0.91,$$
$$(P = 70\ N)\nu = 0.95.$$

The values are close to 1. If we assume that the skin volume remains constant during deformation, then we can write for the volume change

$$\varepsilon_{lat} + \varepsilon_{lon} + \varepsilon_{th} = 0,$$

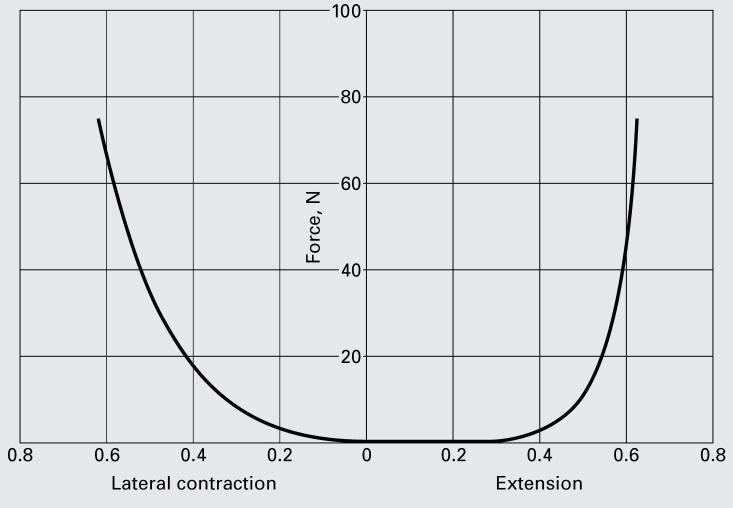

Fig. E2.19 Force–extension and force–lateral contraction curves for human skin in uniaxial tension. (Adapted from R. M. Kenedi, T. Gibson, J. H. Evans, and J. C. Barbanel, *Phys. Med. Biol.*, 20 (1975) 619.)

where the subscripts lat, long, and th indicate lateral, longitudinal, and thickness directions. Dividing the equation by ε_{lon}:

$$\nu - 1 + \nu_{th} = 0.$$

Since $\upsilon \sim 0.9$, we have:

$$\nu_{th} \sim 0.1.$$

The results indicate that the strain in the thickness direction is small in comparison with the in-plane strains. Thus, the thickness of human skin remains approximately constant when it is uniaxially stretched.

2.16 Elastic Properties of Electronic Materials

Microelectronic integrated circuit materials are characteristically composed of a silicon (monocrystalline) substrate and thin film layers (Section 1.3.10). The thickness of the substrate is of the order of

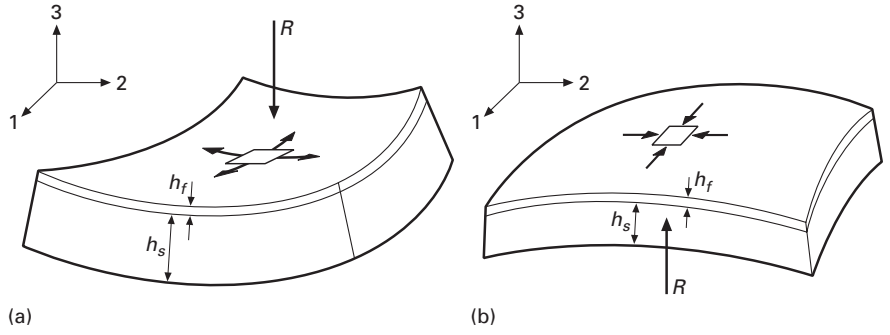

Fig. 2.34 Effect of stresses acting on thin film on bending of substrate; (a) tensile stresses in thin film; (b) compressive stresses in thin film.

0.5–1 mm, and the thin films are characteristically 1 μm thick. The thin film and substrate have often different coefficients of thermal expansion. Additionally, the substrate density might change as it grows. There are also epitaxial strains, caused by a lattice parameter mismatch between the substrate and film. As a result, the thin film is either under compression or tension. Figure 2.34 shows both situations. If the film is under tension, it will bend the substrate up (Figure 2.34(a)); on the other hand, if the film is under compression, it will bend the substrate down (Figure 2.34(b)). It is possible to estimate the radius of curvature and the stresses. We start with the generalized Hooke's law and set σ_{33} equal to zero in the thin film. We do this because we have a state of plane stress. For isotropic materials, from Equation 2.11:

$$\varepsilon_{11} = \frac{1}{E}\left[\sigma_{11} - \nu\sigma_{22}\right],$$
$$\varepsilon_{22} = \frac{1}{E}\left[\sigma_{22} - \nu\sigma_{11}\right],$$
$$\varepsilon_{33} = \frac{1}{E}\left[-\nu(\sigma_{11} + \sigma_{22})\right].$$

Therefore:

$$\varepsilon_{11} = \frac{1-\nu}{E}\sigma_{11}.$$

The term $E/(1-\nu)$ can be defined as a biaxial modulus. For the substrate:

$$M_s = \frac{E_s}{1-\nu_s}$$

E_s and ν_s are the Young's modulus and Poisson's ratio of the substrate, respectively. This is the so-called Stoney equation.

The radius of curvature of the system can be estimated from an equation for plates:

$$R = \frac{E_s h_s^2}{6(1-\nu_s)\sigma_f h_f},$$

where h_s and h_f, defined in Figure 2.34, are the thickness of substrate and film, respectively. σ_f is the maximum stress in the film.

For a monocrystalline substrate, one has to compute the biaxial modulus using the elastic stiffness components C_{mn}.

For instance, the values for Si are:

$C_{11} = 166$ GPa,
$C_{12} = 64$ GPa,
$C_{44} = 80$ GPa.

For the anisotropic case, when the cube plane is parallel to the interface, the following expression can be derived (see Section 2.9):

$$\frac{1}{E_{100}} = S_{11}.$$

For Poisson's ratio, we use the expression:

$$\nu = -\frac{S_{12}}{S_{11}}.$$

Thus:

$$M_{100} = \frac{1/S_{11}}{1 + \frac{S_{12}}{S_{11}}}.$$

We obtain the stiffnesses from the compliances by inverting the matrix (Section 2.9, Example 2.10). The result is:

$$M_s = C_{11} + C_{12} - \frac{2C_{12}^2}{C_{11}} = 180.7 \text{ GPa}.$$

For the (111), we repeat the procedure and obtain:

$$M_{111} = \frac{6C_{44}(C_{11} + 2C_{12})}{C_{11} + 2C_{12} + 4C_{44}}.$$

For the (110) plane, the stiffness depends on direction. For more details, the reader is referred to Nix[14] and Freund and Suresh.[15]

We can also use the isotropic Young's modulus of Si (= 163 GPa) and a Poisson's ratio of 0.2. This would give us close enough results. For $h_f = 1$ μm and $h_s = 500$ μm, we have, assuming a maximum stress in the film of 500 MPa:

$$R = M_s \frac{h_s^2}{6\sigma_f h_f} = 15m.$$

2.17 Elastic Constants and Bonding

There are four types of bonds between atoms:

- Metallic: metals,
- Ionic: ceramics,
- Covalent: ceramics, backbone of polymers and biological materials,
- van der Waals: polymers and biological materials.

[14] W. D. Nix, *Met. Trans.*, 20A (1989) 2217.
[15] L. B. Freund and S. Suresh, *Thin Film Materials* (Cambridge, U.K.: Cambridge University Press, 2003), Ch. 3.

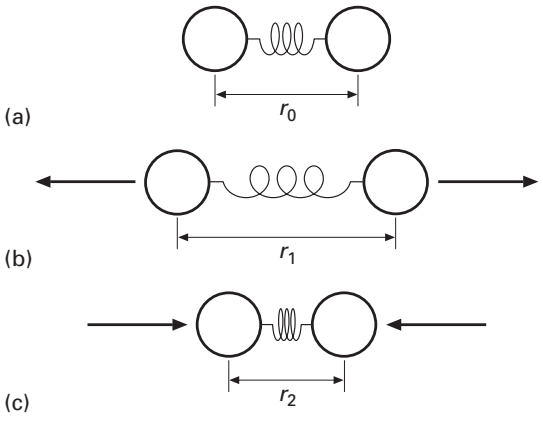

Fig. 2.35 Two atoms with an imaginary spring between them; (a) equilibrium position; (b) stretched configuration under tensile force; (c) compressed configuration under compressive force.

The first three are called primary bonds. van der Waals bonds (which include the hydrogen bond) are called secondary bonds. The primary bonds are in general much stronger than secondary bonds. Secondary bonds "melt" between 100 and 500 K.

Many materials have mixed bonds. Intermetallic compounds may be bonded by as mixture of metallic and ionic bonds. Many ceramic and semiconducting compounds have a mix of covalent and ionic bonding. Polymers and biological materials have covalent bonds along the primary chains (C–C, Si–Si, etc.) and van der Waals (often, hydrogen) bonds between segments inside a chain.

The interaction energy between two adjacent atoms is often considered as the sum of an attractive and a repulsive term. The resultant curve gives the potential well. There are many calculations of interatomic potentials, the Condon–Morse and Lennard–Jones being examples.

The linear theory of elasticity makes the assumption that the material is a continuum. The assumption is good when we are dealing with large bodies; the micromechanics of deformation, on the other hand, describes a scale where the continuum breaks down into a periodic array of atoms: the crystalline structure. It is theoretically possible to calculate the elastic constants from the consideration of the interatomic forces. These calculations can be conducted for ionic structures, such as NaCl, considering only electrostatic forces using measured values of the ion sizes. In metals the situation is more complex. Even approximate quantitative determinations require the use of wave mechanics. The effect of temperature on atomic vibrations and/or the lattice parameter is discussed, as well as the attendant changes in elastic properties.

Figure 2.35 shows two atoms, which are at their equilibrium separation r_0. Tensile forces increase the separation to r_1; compressive forces decrease it to r_2. The variation of the interaction energy with atomic separation is shown in Figure 2.36. At equilibrium, the interaction energy is minimum; the equilibrium separation r_0

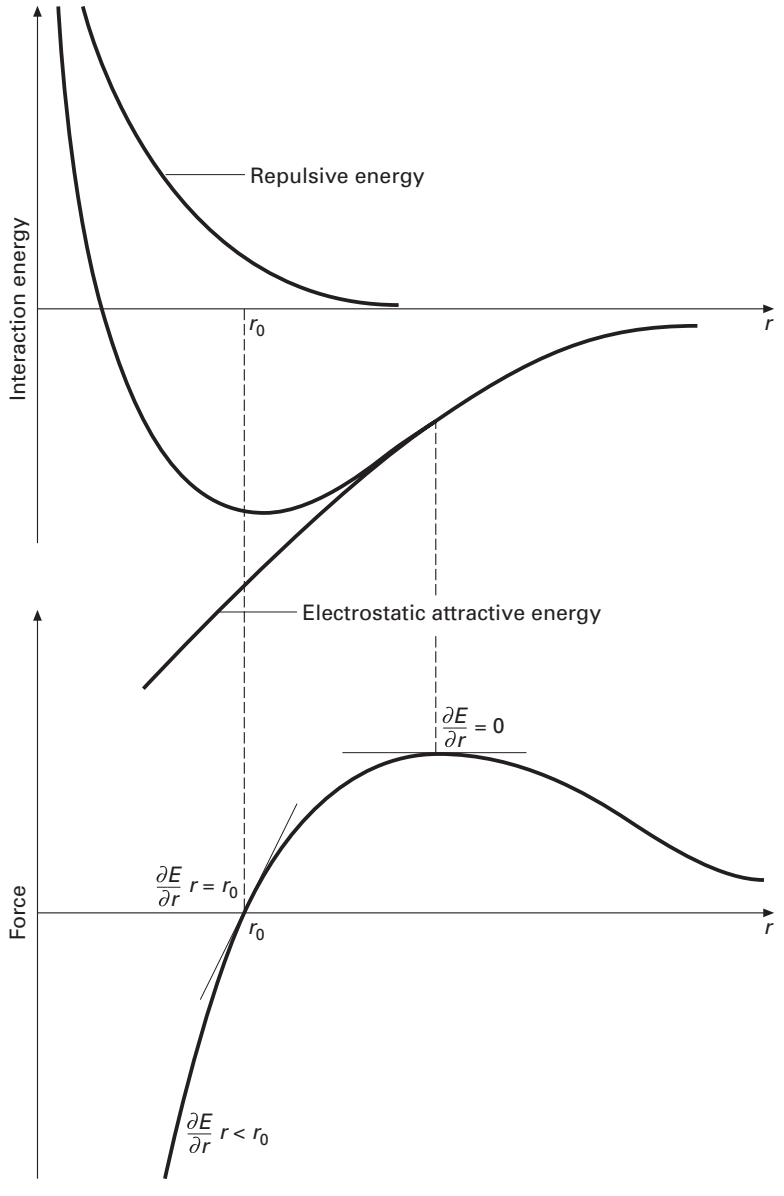

Fig. 2.36 (a) Interaction energies (attractive and repulsive terms) as a function of separation; (b) Force between two atoms as a function of separation; notice decrease in slope as separation increases.

corresponds to the bottom of the well. One can represent the energy by:

$$U_i = -\frac{A}{r^m} + \frac{B}{r^n}, \tag{2.49}$$

where the first term represents the attraction and the second term the repulsion. The exponent of the repulsive term, n, is usually much larger than m because, as the two atoms are brought together, their electronic orbitals superimpose and strong repulsion (due to Pauli's exclusion principle) ensues. This is reflected in Figure 2.36(a), where the repulsive term increases sharply as as the separation is decreased

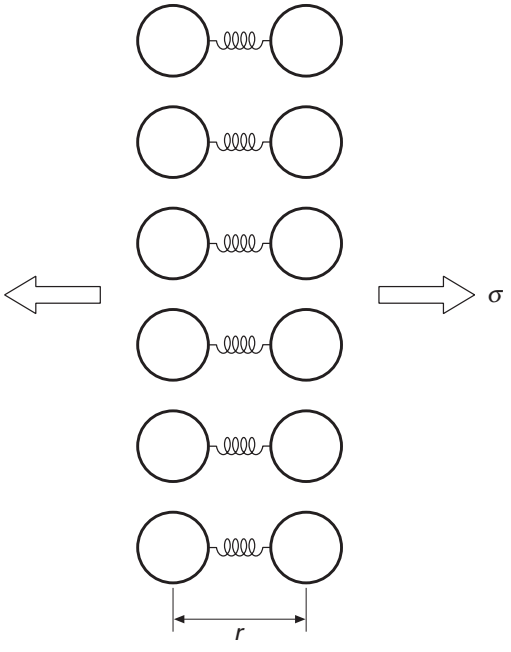

Fig. 2.37 Array of atoms representing tensile stress applied to crystal.

below r_0. The repulsive force operates at a close range. The interatomic force is obtained from:

$$F = \frac{\partial U_i}{\partial r}.$$

This force is equal to zero at the bottom (trough) of the interaction energy curve, which corresponds to the equilibrium separation, r_0. It is possible to estimate the elastic modulus from $\partial F/\partial r$. This can be accomplished by expressing stress and strain in terms of atomic positions. Figure 2.37 shows, in a schematic fashion, an array of atoms. We consider only the nearest neighbors aligned with the stress direction. In a more accurate calculation next-nearest and next to next-nearest neighbors have to be included, since they play an important role.

The engineering strain can be expressed as:

$$d\varepsilon = \frac{dr}{r_0},$$

where r_0 is the equilibrium atomic separation and dr is the change in atomic separation. The stress is equal to:

$$d\sigma = N\,dF,$$

where N is the number of atoms per unit area of cross section and dF is the interatomic force producing a displacement dr. If we ascribe an area $r_0 \times r_0$ per atom, we have:

$$d\sigma = \frac{dF}{r_0^2}.$$

The Young's modulus is expressed as:

$$E = \left|\frac{d\sigma}{d\varepsilon}\right|_{\varepsilon=0} = r_0^{-1}\left|\frac{dF}{dr}\right|_{r=r_0} = r_0^{-1}\left|\frac{d^2U_i}{dr^2}\right|_{r=r_0}. \tag{2.50}$$

From Equation 2.49:

$$\frac{dU_i}{dr} = \frac{Am}{r^{m+1}} - \frac{Bn}{r^{n+1}}.$$

At $r = r_0$:

$$\frac{Am}{r_0^{m+1}} - \frac{Bn}{r_0^{m+1}} = 0$$
$$Bn = Amr_0^{n-m}.$$

Thus:

$$\frac{dU_i}{dr} = \frac{Am}{r^{m+1}} - \frac{Amr_0^{n-m}}{r^{m+2}}$$
$$\frac{d^2U_i}{dr^2} = \frac{dF}{dr} = -\frac{Am(m+1)}{r^{m+2}} + \frac{Am(n+1)r_0^{n-m}}{r^{n+2}}.$$

At the equilibrium separation, r_0:

$$\left|\frac{dF}{dr}\right|_{r=r_0} = -\frac{Am(m+1)}{r_0^{m+2}} + \frac{Am(n+1)r_0^{n-m}}{r_0^{n+2}}$$
$$\left|\frac{dF}{dr}\right|_{r=r_0} = \frac{Am(n-m)}{r_0^{m+2}} \tag{2.51}$$

Substituting Equation 2.51 into Equation 2.50:

$$E = \frac{Am(n-m)}{r_0^{m+3}}. \tag{2.52}$$

The attraction forces in ionic solids are of a coulombic nature and the exponent in Equation 2.52 is $m = 1$.

Thus:

$$E = \frac{A(n-1)}{r_0^4}.$$

The parameter A is related to the electrical charges of the ions. For monovalent ions:

$$A = \frac{e^2}{4\pi\varepsilon_0},$$

where e is the electric charge of an electron and ε_0 is the permittivity of vacuum. One can thus estimate the elastic modulus of ionic solids. Thus:

$$\boxed{E = \frac{ke^2}{r_0^4},}$$

where k comes from the grouping of constants. The r_0^{-4} dependence of elastic constants is actually much more general.

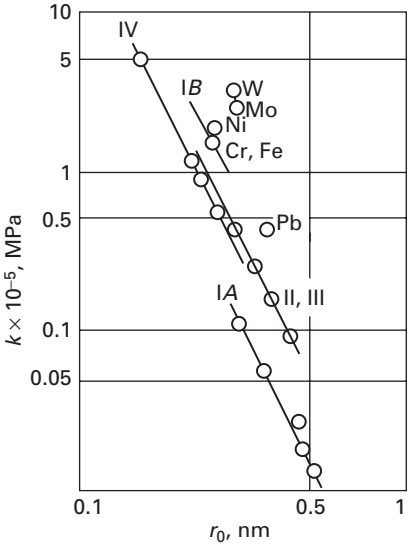

Fig. 2.38 Effect of radius of closest approach on bulk modulus for groups I, II, III, IV, and transition elements.

The electrostatic nature of the forces between ionic crystals renders the determination of elastic constants less arduous. The NaCl structure is a simple cubic structure, with Na and Cl occupying alternate positions in the lattice. Each Na^+ ion is surrounded by six Cl^- ions. If we consider one isolated ion (either Na^+ or Cl^-) and compute all attractive and repulsive forces by neighbors, next-neighbors, and so on, it is possible to determine the resultant electrostatic force.

The force between individual ions is coulombic (i.e. it varies with the square of the distance). Computing all the forces and transforming the resultant force into a stress and the displacement into strain, we showed above that one obtains an equation of the form:

$$E = \frac{ke^2}{r_0^4}, \tag{2.53}$$

where r_0 is the interatomic distance, k a constant, and e the charge of an electron. This very simplified calculation shows that Young's modulus should vary with r_0^{-4}. The same dependence should exist for the bulk modulus k. Figure 2.38 shows that this type of dependence is actually observed. In the log–log plot, the slope of -4 corresponds to the dependence shown in Equation 2.53. Elements from groups I, II, III, and IV obey that relationship. Elements of the same group were taken together because they have the same valence. Group I elements are monovalent and have the weakest bonding. Hence their line is the lowest in Figure 2.38.

In spite of the fact that bonding is more complex in metals than in ionic crystals, Gilman[16] has shown that an r_0^{-4} type of relationship can be found for metals. This is shown in Figure 2.39. The alkali

[16] J. J. Gilman, *Electronic Basis of the Strength of Materials* (Cambridge, U.K.: Cambridge University Press, 2003).

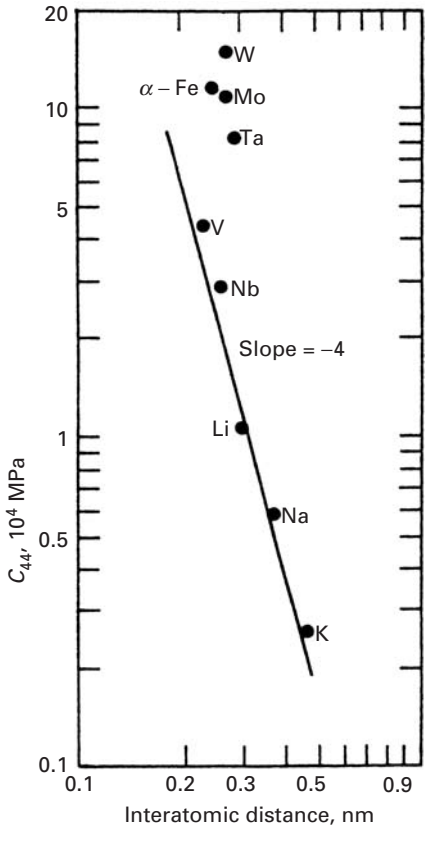

Fig. 2.39 Variation of elastic constant C_{44} with r_0 for BCC metals. (Adapted from J. J. Gilman, Mechanical Behavior of Crystalline Solids, *NBS Monograph*, 59 (1963) 79.)

metals seem to obey the r_0^{-4} (where r_0 is the interatomic distance) quite well; the transition metals are situated above them. The elastic properties are strongly dependent, obviously, on bonding. Figure 2.40 shows a plot of the bulk modulus versus melting point for a number of transition metals. The melting point is the temperature at which thermal energy is sufficient to disrupt the metallic bonding. Hence, the stronger the bonding, the higher the melting point. This correlation is clearly evident in Figure 2.40. The lines join elements from the same column in the periodic table. Some of the series of three elements fall remarkably well in a straight line: Cr–Mo–W, V–Nb–Ta, Ag–Cu–Au.

A plot that emphasizes the importance of the electronic structure on elastic constants is shown in Figure 2.41. The periodicity in the variation of the Young's moduli (lines represent rows in the periodic table) is indicative of the importance of the electronic structure. Transition metals, which are characterized by strong bonding by electrons from the *d* shell, have particularly high Young's moduli. Os, Ru, and Fe have six *d* electrons each and are the elements that have the highest melting point for each of the three rows of transition elements in the periodic table. In Figure 2.40, it can be seen that the transition elements have C_{44} higher than would have been predicted from the r_0^{-4} relationship. This confirms the indication that the strong *d*

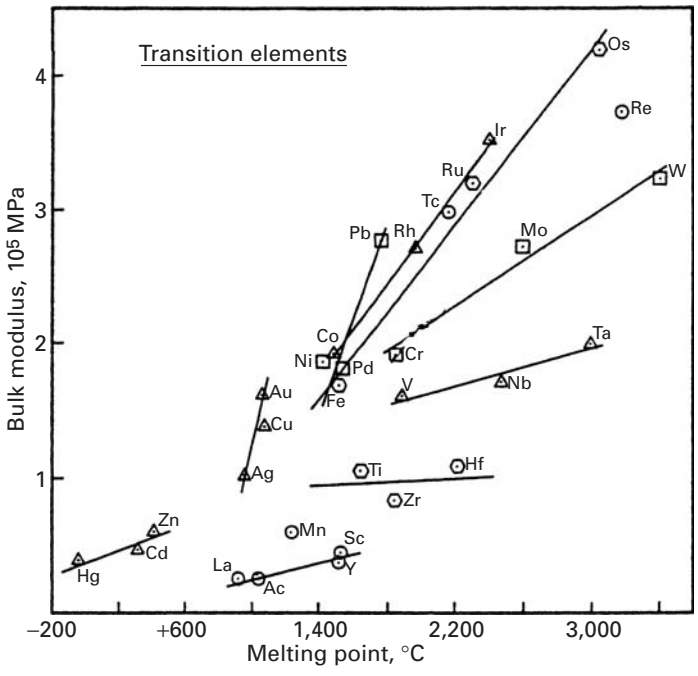

Fig. 2.40 Relationship between melting point and bulk modulus for transition elements.

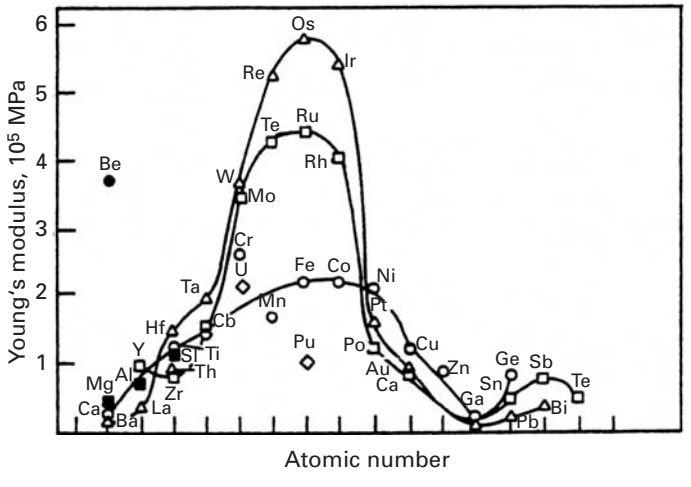

Fig. 2.41 Periodic variation of Young's modulus of elements. The three lines represent the rows in the periodic table. (Adapted with permission from O. D. Sherby, in *Nature and Properties of Materials*, ed. J. Park (New York: Wiley, 1967), p. 373.)

bonding is responsible for additional stiffness. One element stands out in Figure 2.41: *beryllium*. Having a relatively small atomic number, it has an extremely high stiffness, comparable with that of tungsten and molybdenum. The ratio between Young's modulus and density is extremely high (six to seven times as high as for titanium and aluminium). It has unique applications in the aerospace industry. Its first use was in spacers for the Minuteman missile, and it is used in space vehicles. A high stiffness is required in large satellites because the lowest natural frequency of vibration must exceed a specified value to avoid resonant coupling with the booster control system during powered flight. The higher the stiffness, the higher the natural

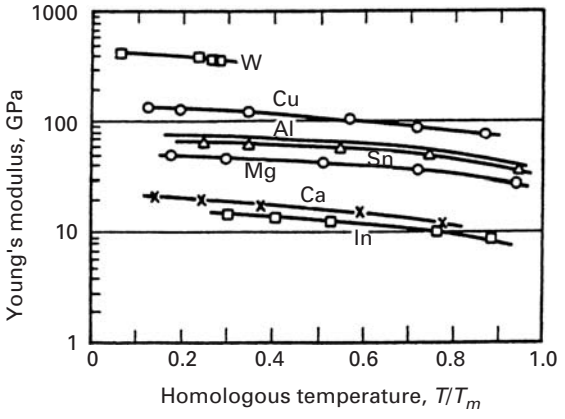

Fig. 2.42 Effect of temperature on dynamic Young's modulus. (Adapted with permission from O. D. Sherby, in *Nature and Properties of Materials*, ed. J. Park (New York: Wiley, 1967), p. 376.)

frequency of vibration. However, the metallurgical problems posed in beryllium production are many, because of its structure (HCP), high chemical reactivity, and high toxicity.

The dependence of elastic properties of a metal on interatomic separation (which can, as a first approximation, be expressed as r_0^{-4}) may be applied to rationalize two different phenomena: the temperature dependence of elastic properties and the effect of magnetic fields on elastic properties. They will be discussed below. As the temperature increases, the metals expand; this lattice expansion is treated in detail by Mott and Jones,[17] but is beyond the scope of this book. Suffice to say that as the temperature increases, the amplitude of vibration of the atoms increases. This amplitude increase will accommodate the thermal energy term (kT) and the expanded lattice will have a larger r_0. This, in turn, will produce a decrease in the elastic constants. The change in elastic constants with temperature is much less pronounced than the change of yield stress, tensile strength, and strain to failure. The Young's modulus at the melting point is usually between one-half to two-thirds of the low-temperature value. The temperature dependence of the yield point is much more pronounced because plastic deformation is a thermally activated process. Figure 2.42 illustrates the changes in E with temperature for some metals.

The effect of magnetic fields can be explained by the same rationale. A magnetic field, due to the magnetostrictive effect, changes the lattice parameter slightly; this, in turn, affects the elastic properties. When the Young's modulus of nickel in the presence and absence of a magnetic field is measured, appreciable differences are found. Actually, between 200 and 360 °C (Curie temperature, where ferromagnetic–paramagnetic transformation takes place) the Young's modulus of nickel increases with temperature.[18] By appropriate alloying it is possible to obtain alloys that have essentially a constant

[17] N. F. Mott and H. Jones, *The Theory of the Properties of Metals and Alloys* (New York: Dover, 1958).

[18] O. D. Sherby, in *Nature and Properties of Materials*, ed. J. Park (New York: Wiley, 1967), pp. 373, 375, 376.

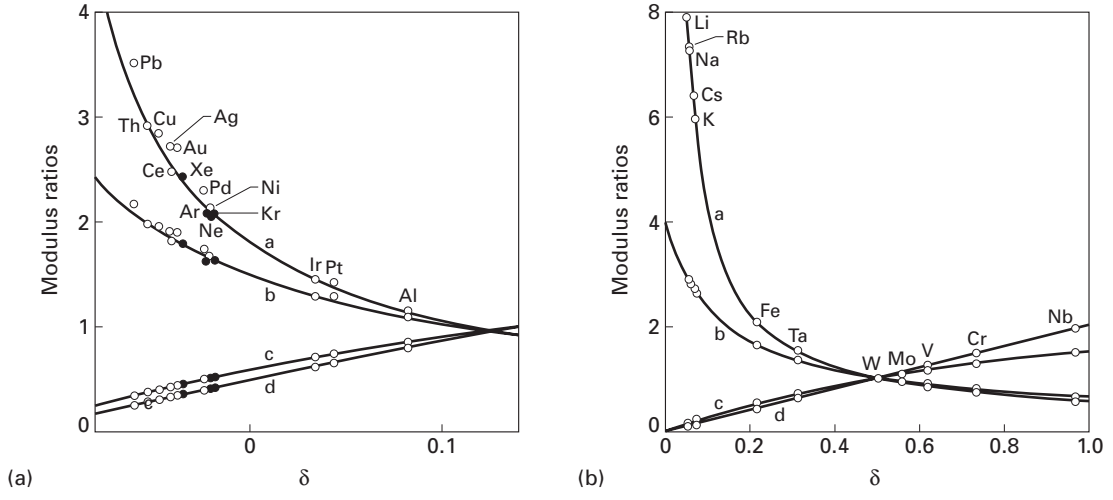

Fig. 2.43 Young's and shear moduli ratios as a function of δ, a parameter that is a measure of the strength of the second neighbour interaction compared to that of the first neighbor interaction. (a) FCC and (b) BCC crystals (data points – experimental; lines – calculated). In each of these figures a, b, c, and d refer to E_{111}/E_{100}, E_{110}/E_{100}, $G_{(111)}/G_{(100)}$, and $G_{(100)[110]}/G_{(100)}$, respectively. (From T. Milstein and T. Marchall, *Acta Mater.*, 40 (1992) 1229.)

Young's modulus over a certain temperature range. Such an alloy is Elinvar (36% Ni, 12% Cr, 1 to 2% Si, 0.8% C, balance Fe), and it has an essentially constant E between 15 and 40 °C; it is ideal for springs in watches and other precision instruments.

The crystal structure has a very marked effect on the elastic anisotropy of crystals. The standard ordering of Young's moduli in FCC and BCC crystals is:

$$E_{111} > E_{110} > E_{100},$$

where the subscripts indicate the cubic axes.

This was clearly seen earlier in Figure 2.9(a), for copper. For simple cubic crystals, the ordering is:

$$E_{100} > E_{110} > E_{111}.$$

This corresponds to the elastic moduli of cubic zirconia, as was seen in Figure 2.9(b). The bonding of atoms along different crystallographic orientations has been correlated with the relative values of Young's moduli.

Milstein and Marschall[19] defined a parameter, δ, which is a measure of the strength of the second-neighbor interaction compared with that of the nearest-neighbor interaction. The moduli ratios for FCC and BCC materials as a function of this parameter are shown on Figure 2.43(a) and (b), respectively. We plot ratios E_{111}/E_{100}, E_{110}/E_{100}, $G_{(111)}/G_{(100)}$, and $G_{(100)[110]}/G_{(100)}$. Note that among FCC, aluminium has

[19] T. Milstein and T. Marschall, *Acta Mater.*, 40 (1992) 1229.

the least anisotropy; for BCC, W is at the interaction of all curves, corresponding to a ratio of 1, i.e., perfect isotropy. The ratios for Young's moduli values range from 3.2 to 1 for FCC structures and from 8 to 0 for BCC structures. The important conclusion is that second-neighbor interactions are very important in determining these ratios.

The Poisson's ratios (ν) for monocrystals has values that range widely, and can be quite different from the polycrystalline values ($\sim$0.3). These values vary much more than the bounds calculated earlier for isotropic materials ($0 < \nu < 0.5$).

Suggested Reading

Y. C. Fung. *A First Course in Solid Mechanics*, 2nd. ed. Upper Saddle River, NJ: Prentice Hall, 1997.

H. B. Huntington. *The Elastic Constants of Crystals*. New York, NY: Academic Press, 1958.

A. Kelly and G. W. Groves. *Crystallography and Crystal Defects*. Reading, MA: Addison-Wesley, 1970.

J. Lemaitre, and J.-L. Chaboche. *Mechanics of Solid Materials*. Cambridge, U.K.: Cambridge University Press, 1990.

A. E. H. Love. *The Mathematical Theory of Elasticity*. New York, NY: Dover, 1952.

F. A. McClintock and A. S. Argon, eds. *Mechanical Behavior of Materials*. Reading, MA: Addison-Wesley, 1966.

J. F. Nye. *Physical Properties of Crystals*. London: Oxford University Press, 1957.

G. Simmons and H. Wang. *Single Crystal Elastic Constants*. Cambridge, MA: MIT Press, 1971.

I. S. Sokolnikoff. *Mathematical Theory of Elasticity*, 2nd ed. New York, NY: McGraw-Hill, 1956.

S. Timoshenko and J. N. Goodier. *Theory of Elasticity*. New York, NY: McGraw-Hill, 1951.

L. R. G. Treloar. *The Physics of Rubber Elasticity*, 3d ed. Oxford, U.K.: Clarendon Press, 1975.

Exercises

2.1 Rubber specimens, having an initial length of 5 cm, are tested, one in compression and one in tension. If the engineering strains are -1.5 and $+1.5$, respectively, what will be the final lengths of the specimens? What are the true strains, and why are they numerically different?

2.2 An aluminum polycrystalline specimen is elastically compressed in plane strain. If the true strain along the compression direction is -2×10^{-4}, what are the other two longitudinal strains?

2.3 Determine K, λ, and G for polycrystalline niobium, titanium, and iron, from E and γ.

2.4 A state of stress is given by
$\sigma_{11} = 250$ MPa,
$\sigma_{12} = 70$ MPa,
$\sigma_{22} = 310$ MPa.

Determine the principal stresses and the maximum shear stress, as well as their angle with the system of reference.

2.5 Calculate the anisotropy ratio for the cubic metals in Table 2.3.

2.6 Show that a uniaxial compressive stress can be decomposed into a hydrostatic pressure and two states of pure shear. Use sketches if necessary.

2.7 Determine the principal stresses and the maximum shear stress, as well as their angles with the system of reference given by the following stress state:

$$[\sigma_{ij}] = \begin{pmatrix} 3 & 2 \\ 2 & 0 \end{pmatrix} \text{MPa}.$$

2.8 Extensometers attached to the external surface of a steel pressure vessel indicate that $\varepsilon_t = 0.002$ and $\varepsilon_t = 0.005$ along the longitudinal and transverse directions, respectively. Determine the corresponding stresses. What would be the error if Poisson's ratio were not considered?

2.9 Calculate Young's and shear moduli for monocrystalline iron along [100], [110], and [111].

2.10 From the values obtained in Exercise 2.9, obtain a rough estimate of the Young's modulus of a polycrystalline aggregate, assuming that there are only three orientations for the grains ([100], [110], and [111]) and that they occur proportionally to their multiplicity factors. Compare your result with the predictions of Voigt averages (isostrain) and Reuss averages (isostress).

2.11 A silver monocrystal is extended along [100]. Obtain the values for the Young's and shear moduli, as well as Poisson's ratio.

2.12 (a) For Figure 2.25, plot the curve of true stress vs. true strain. (b) Taking the slopes of the curve at various strains, plot the elastic modulus of rubber as a function of strain. (c) Schematically draw polymer chains at different positions in the curve.

2.13 A steel specimen is subjected to elastic stresses represented by the matrix

$$\sigma_{ij} = \begin{pmatrix} 2 & -3 & 1 \\ -3 & 4 & 5 \\ 1 & 5 & -1 \end{pmatrix} \text{MPa}.$$

Given that $E = 200$ GPa, $\nu = 0.3$, calculate the corresponding strains.

2.14 Ultrasonic equipment was used to determine the longitudinal and shear sound velocities of a metallic specimen having a density of 7.8 g/cm^3. The values obtained are
$V_e = 5{,}300$ m/s,
$V_s = 3{,}300$ m/s.
Determine the Young's and shear moduli and Poisson's ratio for this material. What is the material?

2.15 A tubular specimen is being subjected to a torsional moment $T = 600$ Nm. If the shear modulus of the material (Al) is equal to 26.1 GPa, what

is the total angular deflection if the length is 1 m? The tube has a diameter of 5 cm and a wall thickness of 0.5 cm. Assume the process to be elastic.

2.16 Using the Mohr circle construction, calculate the principal stresses and the maximum shear stresses, as well as their orientation, for the sheet subjected to the stresses shown in Figure Ex2.16.

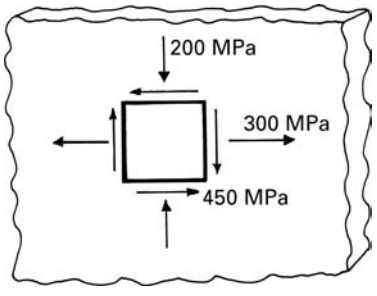

Fig. Ex2.16

2.17 A state of stress is given by
$\sigma_{11} = -500$ MPa,
$\sigma_{22} = 300$ MPa,
$\sigma_{12} = 150$ MPa.

Determine the principal stresses and the maximum shear stress, as well as their orientation, using the Mohr circle construction.

2.18 From the elastic stiffnesses for copper (see Table 2.3), determine the elastic compliances.

2.19 From the elastic compliances S_{11}, S_{12}, and S_{14} for iron and tungsten, determine the Young's moduli along [111], [110], and [100].

2.20 Determine the elastic Young's moduli for tungsten and ZrO_2 along [112], [122], and [123].

2.21 Determine the polycrystalline Young's modulus for molybdenum using Reuss's and Voigt's averages. Use elastic stiffnesses and compliances from Tables 2.3 and 2.4.

2.22 Consider a bar made of steel with a cross-sectional area of 25 cm^2 and length of 20 cm. If we apply a load of 500 N along its length, what is the strain energy density. Take $E = 210$ GPa.

2.23 Derive an expression for the strain energy stored in a circular bar of length L subjected to a torque, T, along its axis. Recall that the shear stress resulting from the torque T is given by $\tau = Tr/J$, where r is the distance from the centroid of the cross section and J is the polar moment of inertia. Use G as the shear modulus of the material.

2.24 Plot Young's modulus as a function of porosity for alumina, and show what the value should be for a specimen having 5% porosity ($E_{Al_2O_3} = 378$ GPa).

2.25 A specimen of Al_2O_3 contains microcracks that are approximately equal to its grain size (20 μm). One grain in each 10 grains contains cracks. If the uncracked materials has $E_0 = 378$ GPa, determine Young's modulus for the

cracked material by use of Budiansky and O'Connell's and Salganik's equations.

2.26 Young's modulus (E) of a cubic single crystal as a function of orientation is given by

$$\frac{1}{E_{hkl}} = \frac{1}{E_{100}} - 3\left(\frac{1}{E_{100}} - \frac{1}{E_{111}}\right)\left(\ell_1^2\ell_2^2 + \ell_2^2\ell_3^2 + \ell_3^2\ell_1^2\right),$$

where ℓ_1, ℓ_2, and ℓ_3 are the direction cosines between the direction hkl and [100], [010], and [001], respectively. This is another version of the expression given in Example 2.10. For copper, $E_{111} = 19$ GPa and $E_{100} = 66$ GPa. Calculate Young's modulus for a copper single crystal in the [110] direction, and check your answer against the one in Example 2.10.

2.27 A polymer has a viscosity of 10^{12} Pa, at 150 °C. If this polymer is subjected to a tensile stress of 100 MPa at that temperature, compute the deformation after 10 h. Assume the polymer to behave as a Maxwell solid. Take $E = 5$ GPa, and use the equation

$$\varepsilon_1 = \frac{\sigma}{E} + \frac{1}{3\eta}\sigma t.$$

2.28 For a given polymer, the activation energy for stress relaxation was measured to be 10 kJ/mol. If the stress relaxation time for this polymer at room temperature is 3,600 s, what would be the relaxation time at 100 °C?

2.29 For an elastomeric material, we have the constitutive equation

$$\sigma = G\left(\lambda - \frac{1}{\lambda^2}\right) = \frac{E}{3}\left[\lambda - \frac{1}{\lambda^2}\right],$$

where E is the elastic modulus at zero elongation. Show that, for very small strains, this equation reduces to $\sigma = E\varepsilon$.

2.30 A cylindrical aluminum specimen (length = 100 mm, diameter = 10 mm) is subjected to a torque equal to 40 Nm. If one end of the specimen is fixed what is the deflection of the other end? Take $E = 70$ GPa and $\nu = 0.3$.

2.31 A steel bolt has 12 threads per mm. If the nut is tightened by one turn, what stress will be generated in the steel bolt and aluminium sleeve? The bolt diameter is 10 mm and the sleeve thickness is 2 mm.

2.32 Calculate Young's modulus for rubber with a density of 1000 g/mol and having intercross-link segments with a molecular weight of 2000 g/mol.

2.33 Describe dilation that occurs in the elastic deformation of a solid. Give a mathematical expression in terms of strain components.

2.34 Consider a solid subjected to hydrostatic pressure, p, that results in a dilation or volumetric strain given by

$$\Delta V/V = \varepsilon_p.$$

The bulk modulus, K, is defined by the ratio p/ε_p. By use of the generalized Hooke's law, show that

$$K = E/3(1 - 2\nu),$$

where E is the Young's modulus and ν is the Poisson's ratio.

2.35

(a) Compute the Poisson's ratio for a material that is undergoing a uniaxial tensile test with zero dilation.

(b) A student was given three different unidentified materials to determine their Posson's ratio. She determined the Poisson's ratios to be 0.5, 0.3, and 0. She needs your help in identifying the class of material for each of these ν values.

2.36 Discuss the advantages and disadvantages of Al, Ti, and Vitalium for use in total hip replacement prostheses.

2.37 From Table 2.5, estimate the theoretical shear and cleavage strength for nickel and titanium.

2.38 From Table 2.5, estimate the theoretical shear and cleavage strength for magnesium and niobium.

2.39 From Table 2.3 find the elastic compliances for nickel.

2.40 From Table 2.3 find the elastic compliances for aluminum.

2.41 Plot the stress–strain curve for alumina in tension, knowing that the density of microcracks increases linearly with stress ($N = k\sigma$). The grain size is 30 μm and the failure stress is 1 GPa; $k = 5.45 \times 10^4$ m^3/Pa, $E_0 = 380$ GPa.

2.42 The following are given for tantalum:

$C_{11} = 267$ GPa,
$C_{44} = 82.5$ GPa,
$C_{12} = 161$ GPa. E

Determine the Young's moduli in the directions [100], [110], and [111] after calculating the elastic compliances.

2.43 The following values are given for niobium:

$E = 105$ GPa,
$\nu = 0.4$.

Calculate the values of G, B, K, and λ.

2.44 Plot the engineering stress–engineering strain curve for a rubber at ambient temperature and liquid nitrogen temperature, up to a strain of 10, using the Equation 2.48. The number of chain segments per unit volume (m^3) is 2×10^{25}.

2.45 From the elastic stiffness for a cubic material, Nb ($C_{11} = 242$ GPa, $C_{12} = 129$ GPa, $C_{44} = 286$ GPa), find the elastic compliances.

2.46 The potential energy of a Na^+ Cl^- ion pair at the distance r is given by:

$$U = U_i - \frac{q^2}{4\pi\varepsilon_0 r} + \frac{B}{r^9},$$

where $q = 1.6 \times 10^{-19}$ C is the electronic charge, $\varepsilon_0 = 8.85 \times 10^{-12}$ C^2/(Nm^2) is the permittivity of vacuum, and $U_i = 1.12$ eV is the reference energy of two infinitely separated ions. If the equilibrium distance between the ions is $r_0 = 0.276$ nm, calculate:

(a) the value of the constant B;

(b) the total force between ions, and its attractive and repulsive portions, when $r = 0.25$ nm;

(**c**) the total force between ions, and its attractive and repulsive portions, when $r = 0.3$ nm;
(**d**) the potential energy between two ions when they are at a distance $r = 1$ nm.

2.47 The potential energy of two atoms, a distance r apart, is

$$U = -\frac{A}{r^m} + \frac{B}{r^n}.$$

Given that the atoms form a stable molecule at a separation $r = r_0$, with a binding energy $U = U_0$, derive:

(**a**) the expressions for the constants A and B in terms of m, n, r_0, and U_0;
(**b**) the expressions for the stiffness S of the bond at arbitrary r and at r_0;
(**c**) the expression for the distance r^* of the maximum tensile force (needed to break the bond between atoms), and the expression for that force (F^*);
(**d**) Given that $m = 2$, $n = 10$, and that the atoms form a stable molecule at a separation $r_0 = 0.3$ nm, with a binding energy $U_0 = -4$ eV, evaluate A, B, r^*, F^*, and the stiffness S_0 of the bond at $r = r_0$.

2.48 Plot the stress–strain curve for SiC in tension, knowing that the density of microcracks increases linearly with stress ($N = k\sigma$). The grain size is 20 μm. The failure stress is 1 GPa; given: $k = 5.45 \times 10^4$ m^3/Pa, $E_0 = 420$ GPa.

2.49 Derive the expression:

$$G = \frac{E}{2(1+\nu)}.$$

The symbols have their usual significance.

2.50 Describe the microscopic changes that occur during the solidification and cooling process of a partly crystalline thermoplastic as it encounters the glass transition regimen.

2.51 From the data on elastic stiffness and compliances for HCP zirconium (Tables 2.3 and 2.4), determine the elastic stiffness, C_{13}, missing in Table 2.3.

2.52 Using the elastic stiffness of tin (exhibiting a tetragonal structure) given in Table 2.3, find the elastic compliances.

2.53
(**a**) Describe the internal structure of an artery, and state the importance of its components to the mechanical response.
(**b**) Explain how you would go about developing an artificial blood vessel, taking into account materials selection and properties, the harsh environment within the body, and biocompatibility.

Chapter 3

Plasticity

3.1 Introduction

Upon being mechanically stressed, a material will, in general, exhibit the following sequence of responses: elastic deformation, plastic deformation, and fracture. This chapter addresses the second response: plastic deformation. A sound knowledge of plasticity is of great importance for the following reasons.

- Many projects are executed in which small plastic deformations of the structure are accepted. The "theory of limit design" is used in applications where the weight factor is critical, such as space vehicles and rockets. The rationale for accepting a limited plastic deformation is that the material will work-harden at that region, and plastic deformation will cease once the flow stress (due to work-hardening) reaches the applied stress.
- It is very important to know the stresses and strains involved in deformation processing, such as rolling, forging, extrusion, drawing, and so on. All these processes involve substantial plastic deformation, and the response of the material will depend on its plastic behavior during the processes. The application of plasticity theory to such processes is presented later in this chapter.
- The mechanism of fracture can involve plastic deformation at the tip of a crack. The way in which the high stresses that develop at the crack can be accommodated by the surrounding material is of utmost importance in the propagation of the crack. A material in which plastic deformation can take place at the crack is "tough," while one in which there is no such deformation is "brittle."
- The stress at which plastic deformation starts is dependent upon the stress state. A material can have a much greater strength when it is confined – that is, when it is not allowed to flow laterally – than when it is not confined. This will be discussed in detail later. A number of criteria for plastic deformation and fracture will be examined in this chapter.

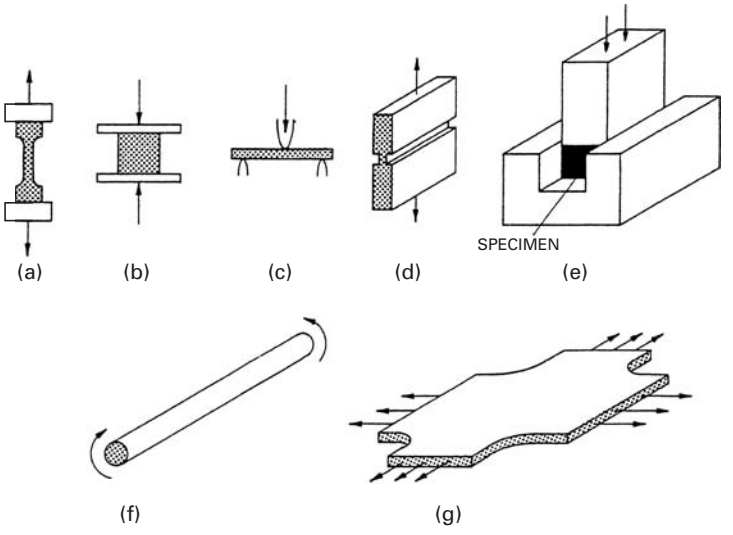

Fig. 3.1 Common tests used to determine the monotonic strength of materials. (a) Uniaxial tensile test. (b) Upsetting test. (c) Three-point bending test. (d) Plane-strain tensile test. (e) Plane-strain compression (Ford) test. (f) Torsion test. (g) Biaxial test.

The mechanical strength of a material under a steadily increasing load can be determined in uniaxial tensile tests, compression (upsetting) tests, bend tests, shear tests, plane-strain tensile tests, plane-strain compression (Ford) tests, torsion tests, and biaxial tests. The uniaxial tensile test consists of extending a specimen whose longitudinal dimension is substantially larger than the two lateral dimensions (Figure 3.1(a)). The upsetting test consists of compressing a cylinder between parallel platens; the height/diameter ratio has to be lower than a critical value in order to eliminate the possibility of instability (buckling) (Figure 3.1(b)). After a certain amount of strain, "barreling" takes place, destroying the state of uniaxial compression. The three-point bend test is one of the most common bending tests. A specimen is simply placed between two supports; a wedge advances and bends it through its middle point (Figure 3.1(c)). Plane-strain tests simulate the conditions encountered by a metal in, for instance, rolling. Loading is imparted in such a way as to result in zero strain along one direction. The two most common geometries are shown in Figure 3.1(d) and (e). In the tensile mode, two grooves are made parallel to each other, on opposite sides of a plate. The width of the plate is much greater than its thickness in the region of reduced thickness; hence, flow is restricted in the direction of the width. In the compressive mode (Ford test), a parallelepiped of metal is machined and inserted between the groove-and-punch setup of Figure 3.1(e). As the top punch is lowered, the specimen is plastically deformed. Strain is restricted in one direction. In the torsion test (Figure 3.1(f)), the cylindrical (or tubular) specimen is subjected to a torque and undergoes an attendant angular displacement. One of the problems in the analysis of the torsion test is that the stress varies as the distance from the central axis of the specimen. Accordingly, the biaxial test is usually applied to thin sheets, and one of the configurations is shown

Fig. 3.2 A servohydraulic universal testing machine linked to a computer. (Courtesy of MTS Systems Corp.)

in Figure 3.1(g). Other configurations involve testing a tubular specimen in tension with an internal pressure and testing a tubular specimen in tension with torsion. The results of the tests just described can be expressed graphically as stress-versus-strain curves. They can be compared directly by using effective stresses and effective strains. A machine commonly used to carry out the tests is the so-called universal testing machine. Both screw-driven (Figure 2.1) and servohydraulic machines are very useful for mechanical testing. Figure 3.2 shows a typical servohydraulic testing machine.

3.2 Plastic Deformation in Tension

Figure 3.3 shows a number of stress–strain curves for the same material: AISI 1040 steel. This might look surprising at first, but it merely reflects the complexity of the microstructural–mechanical behavior interactions. Both engineering and true stress–strain curves are shown. (The definitions of these are given in Chapter 2.) Engineering (or nominal) stress is defined as P/A_0, while true stress is P/A, where A_0 and A are the initial and current cross-sectional areas, respectively. Engineering (or nominal) strain is defined as $\Delta L/L_0$, while true strain is $\ln L/L_0$, where L and L_0 are the current and initial lengths,

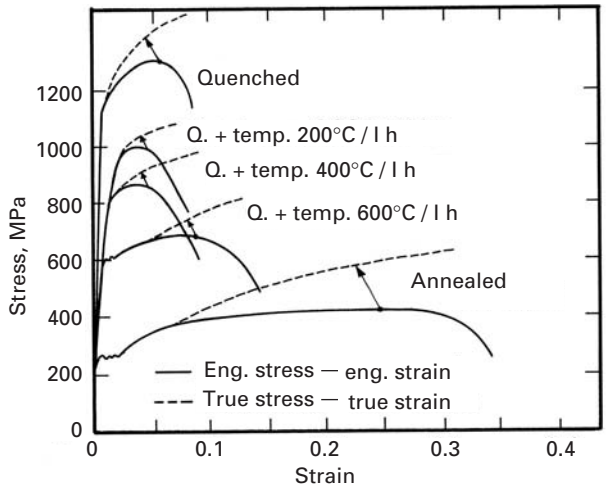

Fig. 3.3 Stress–strain curves for AISI 1040 steel subjected to different heat treatments; curves obtained from tensile tests.

respectively. The yield stress varies from 250 to 1,100 MPa, depending on the heat treatment. Conversely, the total strain varies from 0.38 to 0.1. The properties of steel are highly dependent upon heat treatment, and quenching produces a hard, martensitic structure, which is gradually softened by tempering treatments at higher temperatures (200, 400, and 600 °C). The annealed structure is ductile, but has a low yield stress. The ultimate tensile stresses (the maximum engineering stresses) are marked by arrows. After these points, plastic deformation becomes localized (called *necking*), and the engineering stresses drop because of the localized reduction in cross-sectional area. However, the true stress continues to rise because the cross-sectional area decreases and the material work-hardens in the neck region. The true-stress–true-strain curves are obtained by converting the tensile stress and its corresponding strain into true values and extending the curve.

We know that the volume V is constant in plastic deformation:

$$V = A_0 L_0 = AL\,.$$

Consequently,

$$A = \frac{A_0 L_0}{L}. \tag{3.1}$$

In what follows, we use the subscripts e and t for engineering (nominal) and true stresses and strains, respectively. We have

$$\varepsilon_e = \frac{L - L_0}{L_0} = \frac{A_0}{A} - 1, \tag{3.2}$$

$$\frac{\sigma_t}{\sigma_e} = \frac{P}{A} \times \frac{A_0}{P} = \frac{A_0}{A} = 1 + \varepsilon_e, \tag{3.3}$$

$$\boxed{\sigma_t = (1 + \varepsilon_e)\sigma_e.} \tag{3.4}$$

On the other hand, the incremental longitudinal true strain is defined as

$$d\varepsilon_t = \frac{dL}{L}. \tag{3.5}$$

For extended deformations, integration is required:

$$\varepsilon_t = \int_{L_0}^{L} \frac{dL}{L} = \ln \frac{L}{L_0}, \tag{3.6}$$

$$\exp(\varepsilon_t) = \frac{L}{L_0}. \tag{3.7}$$

Substituting Equations 3.2 and 3.3 into Equation 3.7, we get

$$\sigma_t = \frac{P}{A_0} \exp(\varepsilon_t). \tag{3.8}$$

Engineering (or nominal) stresses and strains are commonly used in tensile tests, with the double objective of avoiding complications in the computation of σ and ε and obtaining values that are more significant from an engineering point of view. Indeed, the load-bearing ability of a beam is better described by the engineering stress, referred to the initial area A_0. It is possible to correlate engineering and true values.

From Equations 3.4 and 3.8, the following relationship is obtained:

$$\boxed{\varepsilon_t = \ln(1 + \varepsilon_e)} \tag{3.9}$$

All of the preceding curves, as well as other ones, are represented schematically by simple equations in various ways. Figure 3.4 shows four different idealized shapes for stress–strain curves. Note that these are true-stress–true-strain curves. When we have a large amount of plastic deformation, the plastic strain is large with respect to the elastic strain, and the latter can be neglected. If the material does not work-harden, the plastic curve is horizontal, and the idealized behavior is called perfectly plastic. This is shown in Figure 3.4(a). If the plastic deformation is not so large, the elastic portion of the curve cannot be neglected, and one has an ideal elastoplastic material (Figure 3.4(b)). A further approximation to the behavior of real materials is the ideal elastoplastic behavior depicted in Figure 3.4(c); this is a linear curve with two slopes E_1 and E_2 that represent the material's elastic and plastic behavior, respectively. One could represent the behavior of the steels in Figure 3.3 fairly well by this elastoplastic, linear work-hardening behavior. It can be seen that $E_2 \ll E_1$. For example, for annealed steel, $E_2 \cong 70$ MPa, while $E_1 = 210$ GPa. However, a better representation of the work-hardening behavior is obtained by assuming a gradual decrease in the slope of the curve as plastic deformation proceeds (shown in Figure 3.4(d)). The convex

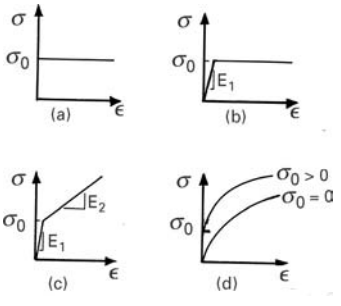

Fig. 3.4 Idealized shapes of uniaxial stress–strain curve. (a) Perfectly plastic. (b) Ideal elastoplastic. (c) Ideal elastoplastic with linear work-hardening. (d) Parabolic work-hardening ($\sigma = \sigma_o + K\varepsilon^n$).

shape of the curve is well represented by an equation of the type

$$\sigma = K\,\varepsilon^n, \tag{3.10}$$

where $n < 1$. This response is usually called "parabolic" hardening, and one can translate it upward by assuming a yield stress σ_0, so that Equation 3.10 becomes

$$\boxed{\sigma = \sigma_0 + K\,\varepsilon^n.} \tag{3.11}$$

The exponent n is called the work-hardening coefficient.

These equations that describe the stress–strain curve of a polycrystalline metal are known as the Ludwik–Hollomon equations.[1] In them, K is a constant, and the exponent n depends on the nature of the material, the temperature at which it is work-hardened, and the strain. The exponent n generally varies between 0.2 and 0.5, while the value of K varies between $G/100$ and $G/1{,}000$, G being the shear modulus. In Equation 3.11 ε is the true plastic strain, while in Equation 3.10 ε is true total strain. Equations 3.11 and 3.10 describe parabolic behavior. However, such a description is valid only in a narrow stretch of the stress–strain curve. There are two reasons for this. First, the equations predict a slope of infinity for $\varepsilon = 0$, which does not conform with the experimental facts. Second, the equations imply that $\sigma \to \infty$ when $\varepsilon \to \infty$. But we know that this is not correct and that, experimentally, a saturation of stress occurs at higher strains.

Voce[2] introduced a much different equation,

$$\boxed{\frac{\sigma_s - \sigma}{\sigma_s - \sigma_0} = \exp\left(-\frac{\varepsilon}{\varepsilon_c}\right),} \tag{3.12}$$

where σ_s, σ_0, and ε_c are empirical parameters that depend on the material, the temperature, and the strain rate. This equation says that the stress exponentially reaches an asymptotic value of σ_s at higher strain values. Furthermore, it gives a finite slope to the stress–strain curve at $\varepsilon = 0$ or $\sigma = \sigma_0$.

It should be noted that the parameters in the preceding equations (3.10 to 3.12) depend on the choice of the initial stress and/or strain. For instance, if one prestrained a material, one would affect K in the Ludwik–Hollomon equation.

The fact that some equations reasonably approximate the stress–strain curves does not imply that they are capable of describing the curves in a physically satisfactory way. There are two reasons for this: (1) In the different positions of stress–strain curves, different microscopic processes predominate. (2) Plastic deformation is a complex

[1] See P. Ludwik, *Elemente der Technologischen Mechanik* (Berlin: Springer, 1909), p. 32; and J. H. Hollomon, *Trans. AIME*, 162 (1945) 268.

[2] E. Voce, *J. Inst. Met.*, 74 (1948) 537.

physical process that depends on the path taken; it is not a thermodynamic state function. That is to say, the accumulated plastic deformation is not uniquely related to the dislocation structure of the material. This being so, it is not very likely that simple expressions could be derived for the stress–strain curves in which the parameters would have definite physical significance.

Some alloys, such as stainless steels, undergo martensitic phase transformations induced by plastic strain. This type of transformation alters the stress–strain curve. (See Chapter 11.) Other alloys undergo mechanical twinning beyond a threshold stress (or strain), which affects the shape of the curve. In these cases, it is necessary to divide the plastic regimen into stages. It is often useful to plot the slope of the stress–strain curve vs. stress (or strain) to reveal changes in mechanism more clearly.

In spite of its limitations, the Ludwik–Hollomon Equation 3.11 is the most common representation of plastic response. When $n = 0$, it represents ideal plastic behavior (no work-hardening). More general forms of this equation, incorporating both strain rate and thermal effects, are often used to represent the response of metals; in that case they are called *constitutive equations*. As will be shown in Chapter 6, the flow stress of metals increases with increasing strain rate and decreasing temperature, because thermally activated dislocation motion is inhibited.

The Johnson-Cook equation

$$\boxed{\sigma = (\sigma_0 + K\,\varepsilon^n)\left(1 + C\ \ln\frac{\dot{\varepsilon}}{\dot{\varepsilon}_0}\right)\left[1 - \left(\frac{T - T_r}{T_m - T_r}\right)^m\right]} \tag{3.13}$$

is widely used in large-scale deformation codes. The three groups of terms in parentheses represent work-hardening, strain rate, and thermal effects, respectively. The constants K, n, C, and m are material parameters, and T_r is the reference temperature, T_m the melting point, and $\dot{\varepsilon}_0$ the reference strain rate. There are additional equations that incorporate the microstructural elements such as grain size and dislocation interactions and dynamics: they are therefore called "physically based." The most common ones are the *Zerilli–Armstrong*[3] and the *MTS* (materials threshold stress, developed at Los Alamos National Laboratory) equations. The basic idea is to develop one equation that represents the mechanical response of a material from 0 K to 0.5 T_m and from very low strain rates ($\sim 10^{-5}$ s^{-1}) to very high strain rates ($\sim 10^{5}$ s^{-1}). Nevertheless, three factors throw monkey wrenches into these equations: creep (see Chapter 13), fatigue (Chapter 14), and environmental effects (Chapter 16). The effects of these factors are very complex and cannot be simply "plugged into" the equations.

[3] See F. Zerilli and R. W. Armstrong, *J. Appl. Phys.*, 68 (1990) 1580.

Example 3.1

For the stress–strain curve shown in Figure E3.1.1 (tantalum tested at strain rate of 10^{-4} s^{-1}), obtain the parameters of the Ludwik–Hollomon equation. Estimate the duration of the test in seconds.

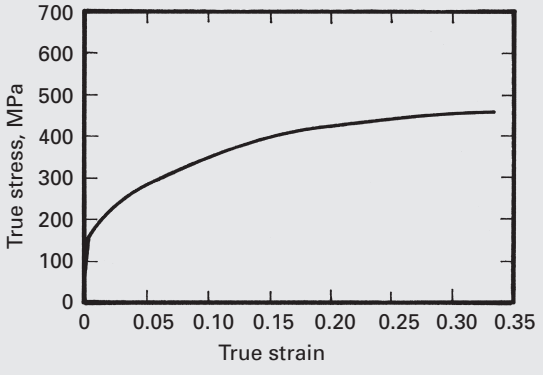

Fig. E3.1.1

Solution: From the $\sigma - \varepsilon$ curve, we have

$$\sigma_0 = 160\,\text{MPa}.$$

We use the Ludwik–Hollomon equation

$$\sigma - \sigma_0 = K\varepsilon^n,$$

so that

$$\log(\sigma - \sigma_0) = \log K + n \log \varepsilon,$$

which is a linear equation. We then make a plot of log $(\sigma - \sigma_0)$ vs log ε (shown in Figure E3.1.2) from the following table of values.

σ	ε	$\log(\sigma - \sigma_0)$	$\log \varepsilon$
280	0.05	2.08	–1.3
345	0.1	2.27	–1
385	0.15	2.35	–0.82
415	0.2	2.41	–0.70
435	0.25	2.44	–0.60
455	0.3	2.47	–0.52

From the new plot, we have

$$\log K = 2.75,$$
$$K = 589,$$
$$n = \text{slope} \approx 0.5.$$

Substituting K and n into the Ludwik–Hollomon equation yields

$$\sigma = 160 + 589\varepsilon^{0.5}\,(\text{in MPa}).$$

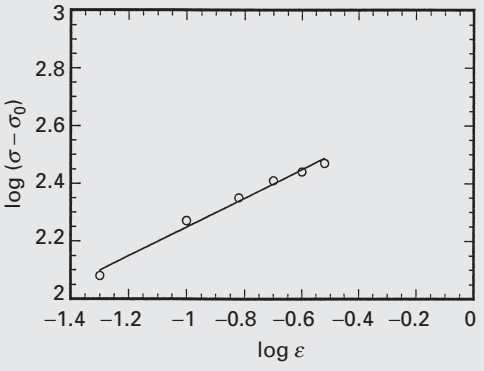

Fig. E3.1.2

The duration of the test, given that

$$\dot{\varepsilon} = 10^{-4}\text{s}^{-1} = \frac{d\varepsilon}{dt} \approx \frac{\Delta\varepsilon}{\Delta t},$$

is

$$\Delta t = \frac{\Delta\varepsilon}{\dot{\varepsilon}} \approx \frac{0.33}{10^{-4}} = 3.3 \times 10^3\text{s}.$$

The volume of a material is assumed to be constant in plastic deformation. It is known that such is not the case in elastic deformation. As was shown in Section 2.5 , the constancy in volume implies that

$$\varepsilon_{11} + \varepsilon_{22} + \varepsilon_{33} = 0$$

or

$$\varepsilon_1 + \varepsilon_2 + \varepsilon_3 = 0 \tag{3.14}$$

and that Poisson's ratio is 0.5. Figure 3.5 shows that this assumption is reasonable and that ν rises from 0.3 to 0.5 as deformation goes from elastic to plastic.

However, prior to delving into the plasticity theories, we have to know, for a complex state of stress, the stress level at which the body starts to flow plastically. The methods developed to determine this are called *flow criteria* (see Section 3.7). Figure 3.6 shows engineering- and true-stress–strain curves for the same hot-rolled AISI 4140 steel. In the elastic regimen the coincidence is exact, because strains are very small (~0.5%). From Equation 3.9, we can see that we would have $\varepsilon_e \approx \varepsilon_t$. As plastic deformation increases, ε_t and ε_e become progressively different. For $\varepsilon_t = 0.20$ (a common value for metals), we have $\varepsilon_e = 0.221$. For this deformation, the true stress is 22.1% higher than the nominal one. It can be seen that these differences become greater with increasing plastic deformation. Another *basic* difference between

Fig. 3.5 Change in Poisson's ratio as the deformation regimen changes from elastic to plastic.

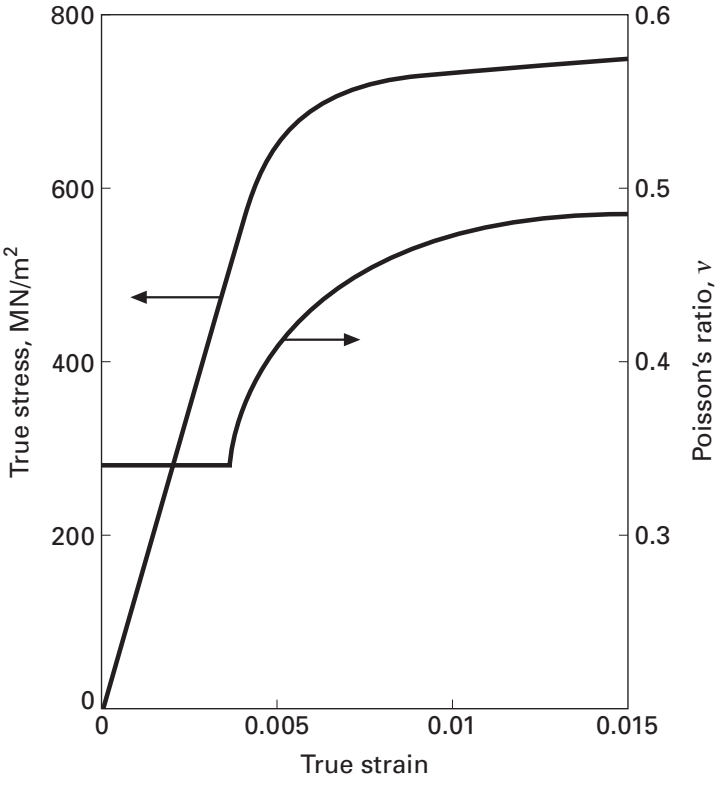

Fig. 3.6 True- and engineering-stress–strain curves for AISI 4140 hot-rolled steel. R. A. is reduction in area.

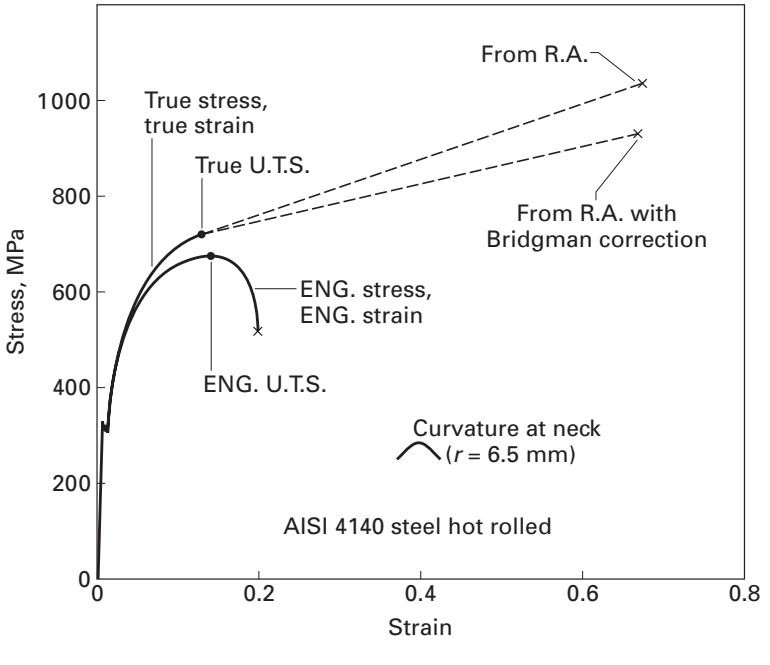

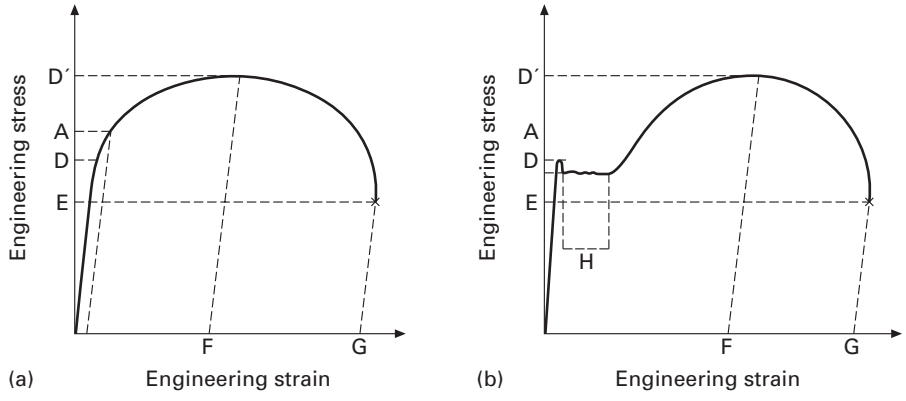

Fig. 3.7 Engineering- (or nominal-) stress–strain curves (a) without and (b) with a yield point.

the two curves is the decrease in the engineering stress beyond a certain value of strain (∼0.14 in Figure 3.6). This phenomenon is described in detail in Section 3.2.2.

3.2.1 Tensile Curve Parameters

Figure 3.7 shows two types of engineering stress–strain curves. The first does not exhibit a yield point, while the second does. Many parameters are used to describe the various features of these curves. First, there is the elastic limit. Since it is difficult to determine the maximum stress for which there is no permanent deformation, the 0.2% offset yield stress (point *A* in the Figure 3.7(a) is used instead; it corresponds to a permanent strain of 0.2% after unloading. Actually, there is evidence of dislocation activity in a specimen at stress levels as low as 25% of the yield stress. The region between 25 and 100% of the yield stress is called the *microyield* region and has been the object of careful investigations. In case there is a drop in yield, an *upper* (*B*) and a *lower* (*C*) *yield point* are defined in Figure 3.7(b). The lower yield point depends on the machine stiffness. A *proportional limit* is also sometimes defined *(D)*; it corresponds to the stress at which the curve deviates from linearity. The maximum engineering stress is called the *ultimate tensile stress* (UTS); it corresponds to point *D′* in Figure 3.7. Beyond the UTS, the engineering stress drops until the *rupture stress* (*E*) is reached. The *uniform strain* (*F*) corresponds to the plastic strain that takes place uniformly in the specimen. Beyond that point, necking occurs. Necking is treated in detail in Section 3.2.2. *G* is the *strain-to-failure*. Additional parameters can be obtained from the stress–strain curve: (1) The elastic energy absorbed by the specimen (the area under the elastic portion of the curve) is called *resilience*; (2) the total energy absorbed by the specimen during deformation, up to fracture (the area under the whole curve), is called *work of fracture*. The strain rate undergone by the specimen, $\dot{\varepsilon}_e = d\varepsilon_e/dt$, is equal to the crosshead velocity, divided by the initial length L_0 of the specimen.

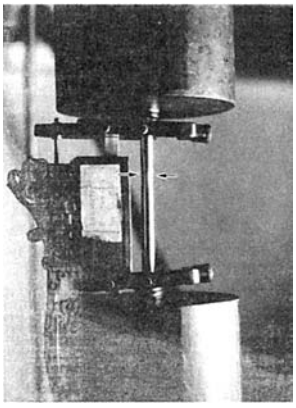

Fig. 3.8 Tensile specimen being tested; arrows show onset of necking.

The *reduction in area* is defined as

$$q = \frac{A_0 - A_f}{A_0}, \tag{3.15}$$

where A_0 and A_f are the initial area and cross-sectional area in the fracture region, respectively. The true strain at the fracture is defined as

$$\varepsilon_f = \ln \frac{A_0}{A_f}. \tag{3.16}$$

The true uniform strain is

$$\varepsilon_u = \ln \frac{A_0}{A_u}, \tag{3.17}$$

where A_u is the cross-sectional area corresponding to the onset of necking (when the stress is equal to the UTS).

3.2.2 Necking

Necking corresponds to the part of the tensile test in which instability exists. The neck is a localized region in the reduced section of the specimen in which the greatest portion of strain concentrates. The specimen "necks" down in this region. Figure 3.8 shows the onset of necking in a tensile specimen; arrows show the region where the cross section starts to decrease.

Several criteria for necking have been developed. The oldest one is due to Considère.[4] According to Considère, necking starts at the maximum stress (UTS), when the increase in strength of the material attributed to work-hardening is less than the decrease in the load-bearing ability owing to the decrease in cross-sectional area. In other words, necking starts when the increase in stress due to the reduction in cross-sectional area starts to exceed the increase in load-bearing ability because of work-hardening. We have, at the onset of necking,

$$\frac{d\sigma_e}{d\varepsilon_e} = 0 \tag{3.18}$$

Substituting Equations 3.4 and 3.9 into 3.18 yields

$$\frac{d\left(\frac{\sigma_t}{1+\varepsilon_e}\right)}{d(e^{\varepsilon_t} - 1)} = \frac{d\left(\frac{\sigma_t}{e^{\varepsilon_t}}\right)}{d(e^{\varepsilon_t} - 1)} = 0.$$

Making the transformation of variables

$$e^{\varepsilon_t} - 1 = Z, \quad e^{\varepsilon_t} = Z + 1$$

yields

$$\frac{d\left(\frac{\sigma_t}{Z+1}\right)}{dZ} = \sigma_t \frac{d(Z+1)^{-1}}{dZ} + (Z+1)^{-1}\frac{d\sigma_t}{dZ} = 0,$$

$$-\sigma_t(Z+1)^{-2} + (Z+1)^{-1}\frac{d\sigma_t}{dZ} = 0,$$

[4] A. Considère, *Ann. Ponts. Chaussèes*, Ser. 6. (1885) 574.

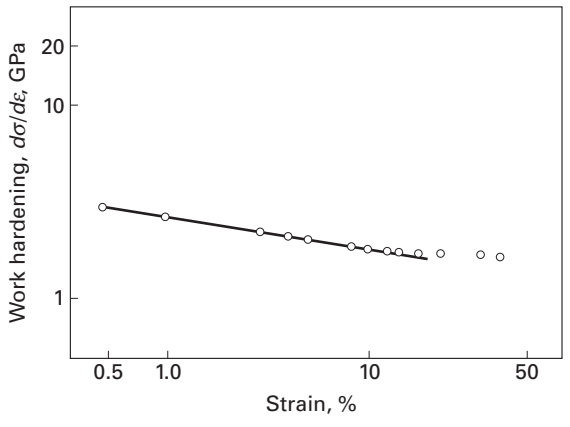

Fig. 3.9 Log $d\sigma/d\varepsilon$ versus log ε for stainless steel AISI 302. (Adapted with permission from A. S. de S. e Silva and S. N. Monteiro, *Metalurgia-ABM*, 33 (1977) 417.)

or

$$-\sigma_t e^{-2\varepsilon_t} + e^{-\varepsilon_t} = \frac{d\sigma_t}{d(e^{\varepsilon_t} - 1)} = 0,$$

$$\frac{d\sigma_t}{d(e^{\varepsilon_t} - 1)} = \sigma_t e^{-\varepsilon_t},$$

$$\frac{d\sigma_t}{\sigma_t} = e^{-\varepsilon_t} d(e^{\varepsilon_t} - 1) = d\varepsilon_t.$$

Using Equation 3.10, we obtain

$$d\sigma_t = nK\,\varepsilon^{n-1} d\varepsilon_t, \text{ or } \frac{d\sigma}{d\varepsilon_t} = \sigma_t \tag{3.19}$$

and it follows from Equation 3.19 that $\sigma_t = nK\varepsilon^{n-1}$. Finally, applying Equation 3.10 again results in $K\varepsilon^n = nK\varepsilon^{n-1}$, so that

$$\varepsilon_u = n.$$

This is an important result. The work-hardening coefficient is numerically equal to the true uniform strain and can be easily obtained in this way.

It is sometimes useful to present results of tensile tests in plots of $d\sigma/d\varepsilon$ versus σ or $d\sigma/d\varepsilon$ versus ε. An example of a plot of log $(d\sigma/d\varepsilon)$ versus log ε for AISI 302 stainless steel is given in Figure 3.9. It can be seen that $d\sigma/d\varepsilon$ decreases with ε, indicating that the necking tendency steadily increases. For metals that do not exhibit any work-hardening capability, necking should start immediately at the onset of plastic flow. Under certain conditions (predeformation at very low temperature or very high strain rate) some metals can exhibit this response, called *work-softening*.

The formation of the neck results in an accelerated and localized decrease in the cross-sectional area. Figure 3.6 shows how the true-stress–true-strain curve continues to rise after the onset of necking. It can also be seen that the true strain at fracture is much higher than the "total strain." The correct plotting of the true-stress–true-strain curve beyond the UTS requires determination of the cross-sectional area in the neck region continuously after necking. This is difficult to do, and the simplest way is to obtain one single point on the

plot, joining it to the point corresponding to the maximum load. For this reason, a dashed line is used in Figure 3.6. The deformation in the neck region is much higher than the one uniformly distributed in the specimen. It can be said that the neck acts as a second tensile specimen. Since its length is smaller than that of the specimen, and the crosshead velocity is constant, the strain rate is necessarily higher.

The onset of necking is accompanied by the establishment of a triaxial state of stress in the neck; the uniaxial stress state is destroyed by the geometrical irregularity. After studying flow criteria (see Section 3.7), we will readily see that the flow stress of a material is strongly dependent on the state of stress. Hence, a correction has to be introduced to convert the triaxial flow stress into a uniaxial one. If we imagine an elemental cube aligned with the tensile axis and situated in the neck region, it can be seen that it is subjected to tensile stresses along three directions. (The external boundaries of the neck generate the tensile components perpendicular to the axis of the specimen.) The magnitude of the transverse tensile stresses depends on the geometry of the neck, the material, the shape of the specimen, the strain-rate sensitivity of the material, the temperature, the pressure, and so on. Bridgman[5] introduced a correction from a stress analysis in the neck. His analysis applies to cylindrical specimens. The equation that expresses the corrected stress is

$$\sigma = \frac{\sigma_{\text{av}}}{(1 + 2R/r_n)\ln(1 + r_n/2R)}, \tag{3.20}$$

where R is the radius of curvature of the neck and r_n is the radius of the cross section in the thinnest part of the neck. Thus, one has to continuously monitor the changes in R and r_n during the test to perform the correction.

Figure 3.10 presents a plot in which the corrections have already been computed as a function of strain beyond necking. There are three curves, for copper, steel, and aluminum. The correction factor can be read directly from the plot shown. ε_u is the true uniform strain (the strain at onset of necking). In Figure 3.6, the true-stress–true-strain curve that was corrected for necking by the Bridgman technique lies slightly below the one determined strictly from the reduction in area at fracture and the load at the breaking point. This is consistent with Figure 3.10; σ is always lower than σ_{av}.

Necking is a characteristic of tensile stresses; compressive stresses are not characterized by necking. Barreling is the corresponding deviation from the uniaxial state in compressive tests. Hence, metals will exhibit necking during deformation processing only if the state of stress is conducive to it (tensile). Figure 3.11 shows plainly how the work-hardening capacity of a metal greatly exceeds that in an individual tensile test. Wire was drawn to different strains: drawing the

[5] P. W. Bridgman, *Trans. ASM*, 32 (1974) 553.